# Dithiafulvene and Catechol as Organic Molecular Building Blocks for Applied Materials



A thesis submitted to the School of Graduate Studies in partial fulfillment of the requirements for the degree of Master of Sciences

Department of Chemistry

Memorial University of Newfoundland

November 2014

St. John's, Newfoundland

# Abstract

This thesis reports the synthesis a series of novel dithiafulvenyl (DTF) compounds, and their characterization. This entails an investigation into their unique electronic properties, as well as their response to both chemical and electrochemical oxidation. This work expands upon previous work within the Zhao group to prepare bis-spiro compounds from DTFs, and works toward a mechanistic explanation for this process. Additionally, examination of DTF species unreactive to typical oxidative dimerization to tetrathiafulvalene (TTFV) using density-functional theory (DFT) optimization has elucidated the effect of resonance delocalization on the reactivity of the radical cation DTF toward TTFV formation.

This thesis also reports the synthetic efforts toward a catechol-functionalized polysiloxane material for anticorrosion and antifouling marine coating additives. Several routes have been explored in attempts to obtain the target compound, including the Hiyama and Kumada coupling reactions. The difficulties faced in synthesis and the potential new avenues to pursue are discussed.

# Acknowledgements

First and foremost, I have to thank my supervisor. Dr. Zhao has been incredibly supportive of me in all my endeavours throughout university. He provided me with goals and inspiration when I had none, and had patience with me when I encountered difficulties. His open and friendly demeanour meant a lot to a nervous undergrad just figuring out that chemistry was fun, and his knowledge and encouragement helped when chemistry became a source of frustration. I will always be grateful to him for his mentorship and the excellent example he set as a scientist.

I would like to thank my supervisory committee member and co-supervisor, Dr. Qiu, for his advice and support over my graduate program, and my committee member Dr. Flinn for his comments and suggestions to aid my progress.

I would also like to thank Jinghan Feng and Dr. Guang Chen for their collaboration on the anticorrosion additives project. They did everything in their power to help me succeed, and helped me considerably.

I want to thank Julie Collins and Dr. Hilary Jenkins (McMaster) for their work solving my single crystal X-ray structures, Linda Winsor for her considerable knowledge and assistance in my mass spectroscopic analyses, and Nick Ryan for his IR help.

I must also thank my labmates, who've been with me through it all, and who've listened to me and put up with me for all this time. Most especially, I want to thank Dr. Guang Chen, who instructed me when I first got in the lab, up until I was almost done my

Masters. Lab neighbours in the organic department also taught me a great deal over the course of my research, and I owe them my appreciation.

I have tremendous gratitude to all the staff and faculty of the chemistry department, and could not imagine doing my graduate work in another place or with better people. This place has sheltered me for 5 years, between my undergraduate and graduate work, and I still struggle with the idea that I won't get to see these people every day anymore.

Lastly, I have to thank my family and friends. I don't think I could have done this without the laughs, the love, and the patience I've received from those closest to me. There aren't enough thanks in the world for the peace of mind I got outside of the lab when the stresses inside were too much.

# Contents

# List of Figures

# List of Tables

# List of Schemes

# List of Abbreviations and Symbols

AC: Alternating current

AFM: Atomic force microscopy

APCI: Atmospheric pressure chemical ionization

ATR: Attenuated total reflectance

BINAP: 2,2’-bis(diphenylphosphino)-1,1’-binaphthyl

C: Celsius

CBPQT: Cyclobis(paraquat-*para*-phenylene)

CD: Circular dichroism

cm: Centimeter

CV: Cyclic voltammetry

d: Doublet

DDQ: 2,3-dichloro-5,6-cyano-1,4-benzoquinone

DFT: Density-functional theory

DMF: *N*, *N*-Dimethyl formamide

dmit: dimercaptoisotrithione

DTF: Dithiafulvene

ee: Enantiomeric excess

EIS: Electronic impedance spectroscopy

EI-TOF: Electrospray ionization- time of flight

eV: Electron-volt

FT-IR: Fourier transform infrared

g: gram

GC-MS: Gas column- mass spectroscopy

GPa: GigaPascal

h: hour

hfdt: bis(trifluoromethyl)tetrathiafulvalenedithiolate

HRMS: High resolution- mass spectroscopy

Hz: Hertz

ICT: Intramolecular charge transfer

*J*: Coupling constant

K: Kelvin

L: Litre

LC-MS: Liquid column- mass spectroscopy

M. P.: Melting point

*m*: meta

m: multiplet

Me: Methyl

mg: milligram

MHz: MegaHertz

mL: Millilitre

mmol: Millimole

MO: Molecular orbital

mol: Mole

MS: Mass spectroscopy

mV: Millivolt

nm: Nanometer

NMR: Nuclear magnetic resonance

*o*: ortho

ORTEP: Oak Ridge thermal ellipsoid probability

*p*: para

PDMS: Poly(dimethyl)siloxane

PMHS: Poly(methylhydro)siloxane

ppm: Parts per million

q: Quartet

rt: Room temperature

s: second

s: singlet

satd: saturated

SBF: Simulated body fluid

SCE: Saturated calomel electrode

SRB: Sulfate-reducing bacteria

t: Triplet

TBAB: Tetrabutylammonium bromide

TBAF: Tetrabutylammonium fluoride

TCNQ: 7,7,8,8-tetracyano-p-quinodimethane

terpy: Terpyridine

*tert*: tertiary

THF: Tetrahydrofuran

TLC: Thin-layer chromatography

TTF: Tetrathiafulvalene

TTFV: Tetrathiafulvalene vinylogues

UV: Ultraviolet

UV-Vis: Ultraviolet-visible

UV-Vis-NIR: Ultraviolet-visible-near infrared

V: Volt

XRD: X-Ray diffraction

δ: chemical shift

μλ: microwave

Ω: Ohm

# Chapter 1

# Introduction

### 1.1 Tetrathiafulvalene

Tetrathiafulvalene (TTF), a small π-electron rich organic molecule, was first discovered accidentally in 1970 by the Wudl group.[1] The initial investigations of TTF were focused on its crystallographic properties; however, it took very little time for progress to be made to assess its electrical and conductive properties, spring boarding into modern research work on its applicability in molecular electronics and exploration of the other fascinating molecular properties of its derivatives, such as tetrathiafulvalene vinylogues (TTFV). Indeed, TTF and related compounds have been found in organic syntheses since the 1930s, often as undesired byproducts,[2] but when Wudl reported that a chlorine salt of oxidized TTF acted as a conductor, more serious investigations began into TTF and its properties. Cowan and coworkers performed unrelated work in the same year, preparing a charge transfer complex of TTF and TCNQ (7,7,8,8-tetracyano-*p*quinodimethane), taking electrons from the TTF and achieving conduction through an charge transfer to the TCNQ.[3] This milestone in new conducting organic materials triggered vast interest in TTF, with the many opportunities to fine tune its conductive properties via manipulation of the length of the π-system and incorporation of additional more heteroatoms into the molecule. Initially, the synthesis of TTFV was executed through a tedious route, taking eight synthetic steps to obtain TTF in poor purity and yields.[4]

TTF is derived from two units of dithiafulvene (DTF) through oxidative coupling, mediated by chemical oxidants, such as iodine or DDQ, or through applied potential. The reactivity of DTF is very complex and significantly dependent on factors such as steric hindrance around the vinylidene carbon and resonance delocalization of the radical cation species. As a result, the fundamentals of DTF chemistry are still a challenging research topic that awaits further investigation.

TTF can be sequentially oxidized to form a radical cation and a dication. During the oxidation process, the non-aromatic dithiole unit of TTF loses an electron to form an aromatic dithiolium ring. For this reason, each of the oxidized states of TTF is stabilized by a gain of aromaticity at the cationic dithiolium ring. However, the most stable state is the dicationic ($TTF^{2+}$) species, as it maximizes aromaticity and π-conjugation. The stability of these compounds is highly appealing, because it allows the TTF to be used as a reversible π-electron donor. π-Electron donors have numerous uses in materials chemistry, such as oligothiophenes present in electroactive thin films,[5] the use of carbon nanotubes as absorbants for environmental cleanup via π-electron donor-acceptor interactions,[6] and fluorescent sensors,[7] to name a few. Although there are many potential sources of electron donors already available, the ease of oxidation of the TTF molecule, as well as the straightforward synthetic routes available to prepare it, make it a potential star in applied physical organic research.

### 1.1.1 π-Extended TTFs (exTTFs)

Simple TTF is a relatively small and uncomplicated molecule, but research has expanded the complexity and versatility of its derivatives for many years. One type of TTF is the family of π-extended TTFs (π-exTTFs), which extend conjugation either through fused aromatic rings on the dithiole ring (Figure 1.1, compounds **1**-**3**),[8-9] or by adding conjugated bridges in between the rings (Figure 1.1, compounds **4**-**6**)[10-12].

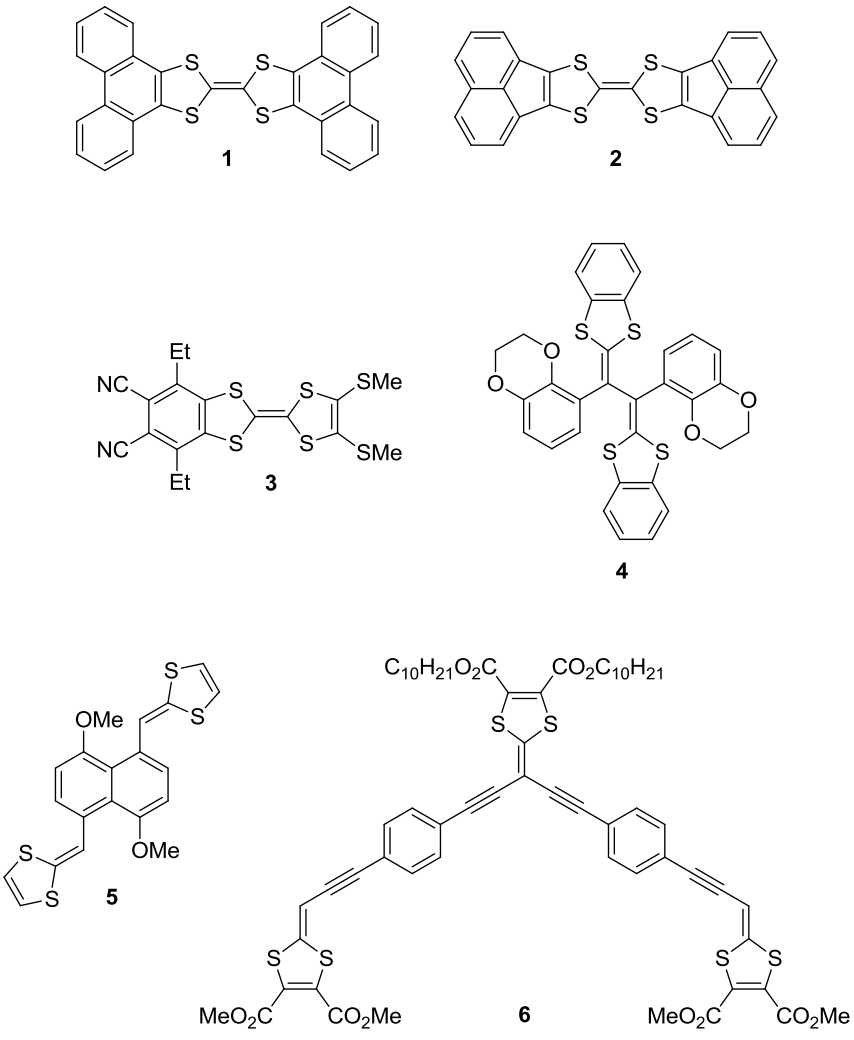


Figure 1.1 Selected examples of π-exTTFs.

The extension of the conjugated moieties around the dithiole rings reduces oxidation potentials. The formation of dicationic TTF derivatives can be considerably enhanced by the separation and delocalization of the positive charges across the extended π-frameworks of exTTFs. As a consequence, the Coulombic repulsion between the two dithiolium rings is attenuated, exerting a significant stabilizing effect on the dications. The increased degree of conjugation in exTTFs also modifies the electronic absorption behaviour of the compound, and can effectively change conformational properties and reactivity.

For most of the known exTTFs, this second oxidation can become much easier than the first oxidation, as a compound tends to undergo a simultaneous two-electron oxidation rather than stepwise single-electron transfers. This has been generally referred to as the "inverted potential" scenario in the electrochemistry of TTFs. Consider compound **7**,[13] Figure 1.2, which undergoes its first oxidation at +0.03 V, and its second oxidation at +0.46 V (vs. $Ag/Ag^{+}$). These oxidations may be made more difficult by the electron-withdrawing substituents **7** bears, a common trend seen in TTFs.[14] In comparison, compound **8**,[15] which is an exTTF carrying quinoid and polyaromatic units bridging the two dithiole rings, undergoes a two-electron transfer oxidation at +0.50 V (vs. SCE). The markedly different electrochemical behavior can be ascribed to the central π-units of compound **8**, which stabilize the dication of **8** to a great extent.

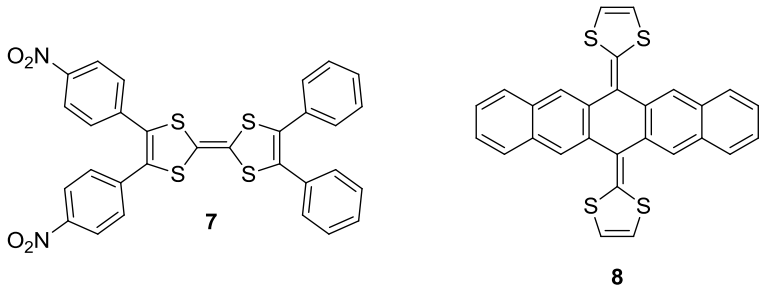


Figure 1.2 Comparison of redox-activities for π-exTTFs.

### 1.1.2 Applications

#### 1.1.2.1 Organic conductors and superconductors

The initial appeal of TTF was its potential use as the first organic conductor, wherein charge-transfer salts of the TTF oriented themselves in the solid state such that the central double bonds stacked, permitting intermolecular orbital interactions, and resulting in unidirectional conductivity.[1] In more recent investigations, TTF has been used as a superconductor, and found to have very high transition temperatures compared to other materials.[16] As a strong electron donor, it is easy to produce electron flow through materials composed of salts or complexes bearing TTF. Maximising charge carrier generation is the key to enhancing conductivity, which is best achieved with TTF by reducing the energy gap between the TTF and its electron acceptor counterpart.

In 2007, a simple amide-functionalized TTF was developed by the Amabilino group to investigate the effect of hydrogen bonding in the formation of conducting nanowires in the solid state.[17] This entailed the synthesis and irreversible heat treatment at 350 K of compound **9** xerogels (Figure 1.3) to yield a new phase of material. This new phase possessed a room temperature resistivity of roughly 20–30 Ω·cm, and conductive AFM

found a fibre-like morphology of the converted xerogels on graphite, with some regions even having parallel nanofibres. The more highly conducting regions of the gel, where these fibres were observed, were easily saturated with current, exhibited metallic character. In the less easily saturated regions, a wider band gap was observed, consistent with semiconductor character. It can be ascertained from this work that the structure of TTF-conductors can be enhanced by the presence of a hydrogen-bonding system, which directs assembly of the gels and improves their stability.

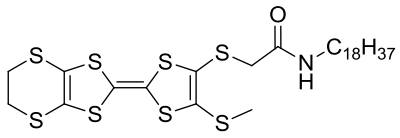


**9**

Figure 1.3 Structure of compound **9**.

In the recent work by Cui and coworkers, a TTF ligand was used to coordinate with nickel to create a superconductor (compound **10**, Figure 1.4).[18] The behaviour of this complex was assessed on several fronts, evaluating the effect of temperature, pressure, and applied magnetic field. Crystal structure determinations of compound **10**, $[Ni(hfdt)_2]$ (hfdt=bis(trifluoromethyl)tetrathiafulvalenedithiolate), at 12, 100, 200, and 250 K, indicated that the compound was structurally stable at all temperatures, a characteristic essential to a functional superconductor. Using a four-probe resistivity system, small crystal samples of **10** were subjected to high pressures at room temperature. Initially, at ambient pressure, **10** was at the very least a functional semi-conductor with a resistivity of 60 Ω cm and a calculated band gap of 0.12 eV, but as the pressure was increased to 7.3

GPa, the resistivity dropped down to 0.003 Ω cm, while the band gap similarly shrank. At 8 GPa, **10** became a semimetal, with no calculated band gap. With constant pressure studies at 7.6 GPa, the resistivity dropped until 85 K, at which point it increased sharply. Superconductivity was confirmed with the presence of a strong resistivity decrease at 8.1 GPa, with temperature onset at 5.5 K.**10**, subject to a pressure range of 7.3 to 8.6 GPa and a temperature range above 3.3 K, is a highly effective superconducting material for new applications.

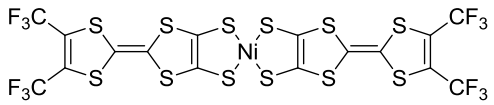


**10**

Figure 1.4 Superconductor **10** ([Ni(hfdt)$_2$]).

### 1.1.2.2 Sensors

Thanks to its reversible oxidization, during which TTF undergoes a conformational change, TTF is a very useful switchable material, with applications such as reversible sensors and selectively solubilizing materials.[19-21] It has drawn great attention in biological and enzymatic chemistry as an electron mediator for other redox sensitive sensing materials, although this is a niche application for TTF.[22-23] It can operate as a ligand, binding to metal cations with varying degrees of selectivity, or an anion sensor, likewise with varying degrees of selectivity.

An excellent example of a TTF derivative functioning as a metal ion sensor would be that of compound **11** (Figure 1.5), a ligand prepared using TTF as a chromophore.[24] Upon

binding to nickel(II) in solution, an immediate change in UV-Vis absorption is observed, with a new band developing at 318 nm, from a pure ligand absorption at 283 nm. This new band, found in the region indicative of ligand-centered $\pi \rightarrow > \pi^*$ and $n \rightarrow \pi^*$ transitions, is likely due to a conformational change from *trans* to *cis* upon complexation. It is reasonable to attribute this change in absorption to the electron donation of TTF through the 2,2',6',2''-terpyridine (terpy) moiety of the ligand into the nickel(II) upon binding. It is evident that a significant change in the electronic character of **11** has taken place, supported by a redshift of more than 100 nm for the intramolecular charge transfer band, typical behaviour for strong metal complexation. The behaviour associated with nickel(II) was also observed upon titration with zinc(II) and cadmium(II) solutions, and observed with minor differences in the case of iron(II). This indicates, as one would expect, that a simple ligand such as **11** is not a selective sensor, but useful as a non-specific reagent for the detection of a number of metal cations. Compound **11** was investigated at a concentration of $1.25 \cdot 10^{-5}$ mol $L^{-1}$, and found to respond to as little as 0.25 equivalents of metal ion solution, presenting a poor threshold of sensitivity for analytical purposes. However, this issue can be disregarded, as it is unlikely that **11** would be used as an analytical reagent, but rather, it would find purpose with multifunctional molecular materials, such as those related to optics or magnetism.

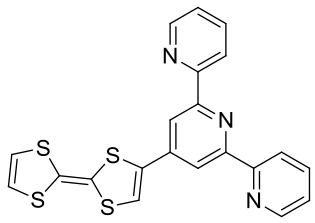

**11**

Figure 1.5 Compound **11** that acts as a colorimetric metal sensor.

Another example of TTF acting as a metal ion sensor is when a TTF is bonded to a calixarene. Compounds **12** and **13** (Figure 1.6) were prepared by Zhao and coworkers using simple starting materials and click chemistry.[25] In this case, **12** and **13** displayed changes in their UV-Vis spectra for only copper(II) and mercury(II) salt solutions, out of thirteen different metals ions tested. It is reported that these changes are simply due to progressive oxidation of the TTF in the presence of these metals, but not attributed to their binding to the host as such. Nevertheless, the compounds are still regarded as a type of chemosensor system for metal ions. In the presence of *p*-chloranil, a large excess of lead(II), and slightly less scandium(III), lead(II), and zinc(II) result in changes in the UV-Vis spectra, attributable to the intermolecular electron transfer between TTF-calixarene and the *p*-chloranil, but the significant amounts of metals needed to mediate these transfers suggest that the binding is weak. There is some slight improvement in transfer for **13** compared to **12** with respect to lead(II), which may be accounted for by the flexibility of the TTF arms, allowing the metal to better interact with the *p*-chloranil oxygen, the triazolyl nitrogen and the dithiafulvenyl sulfur atoms, which in turn enhances electron transfer.

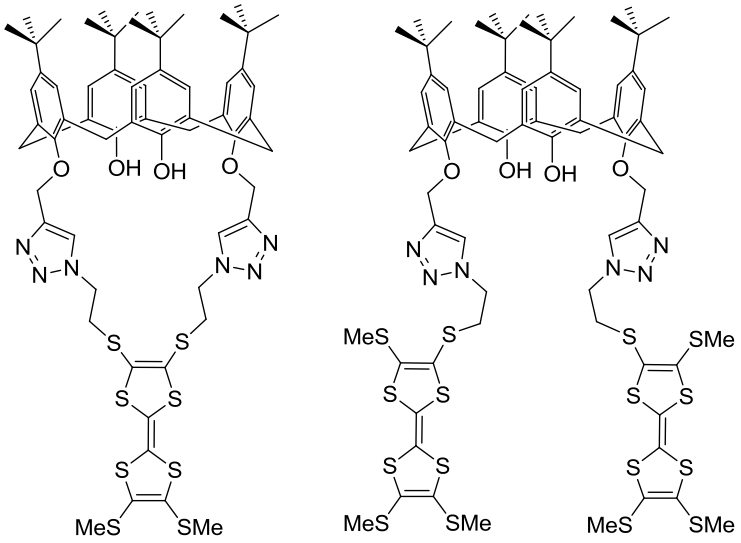


Figure 1.6 TTF-calixarene metal sensors **12** and **13**.

Another use for TTF-based sensors is anion detection. Even simple structures can undergo significant changes in UV-Vis or electrochemical responses upon analyte addition. One prime example of this is compound **14** (Figure 1.7), a fluoride sensor, which showed an enormous change in UV-Vis upon addition of fluoride ion which, according to the authors, deprotonated the hydrazone –NH (realistically, it is more likely that the fluoride hydrogen-bonds to the hydrazone hydrogen).[21] In the UV-Vis, the $\pi \rightarrow \pi^*$ band of the sensor shrank upon fluoride addition and the ICT band grew. This is, as one would expect, because the fluoride-induced deprotonation or hydrogen bond at the nitrogen site increases its electron pushing effect, raising the $\pi^*$ MO of the molecule and facilitating intramolecular charge transfer (ICT). Compound **14** also presented a huge difference in cyclic voltammograms after fluoride addition, with a positive shift of 395 mV for the first anodic potential observed after 4 equivalents of fluoride were added. The

fact that a large anodic shift was observed is generally uncommon, as anion binding tends to stabilize the oxidized state, and result in a cathodic shift. With compound **14**, the deprotonation improves the ICT of the sensor, as discussed with respect to the UV-Vis, and the electron donation from either the TTF or the deprotonated hydrazone nitrogen to the electron-withdrawing 2,4-dinitrophenyl takes place more readily.

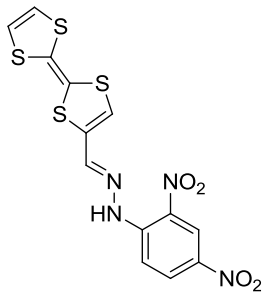


**14**

Figure 1.7 Fluoride sensor **14**.

### 1.1.2.3 Molecular switches

TTFs are popular choices as components of redox-controlled molecular switches, owing once again to their excellent tuneable redox and structural properties. Because their oxidations are readily reversible, they are inherently appealing as “triggers” in a molecular switch, with more than one electronic state, or switch stop, available. Furthermore, because TTF can be oxidized by chemical or electrochemical methods, it offers versatility in diverse applications and research fields. As well, its color changes upon change of oxidation state are usually significant, which allow easy monitoring and interpretation of the switching activity by UV-Vis spectral analysis and even simple visual inspection. The changes in fluorescence and cyclic voltammetric behaviours also

serve as excellent investigative tools, providing even further means to study a system. TTF can be incorporated for diverse purposes, such as the development of molecular machines,[26-28] or to work towards molecular computers through logic gates.[29-30]

Investigations into molecular switches tend to involve very rational design, to anticipate the changes in stimuli required to effect new states. This often leads to careful development of synthetic methodologies, sometimes involving template synthesis for larger structures, while other times requiring extensive application of coupling reactions. A more basic example would be compound **15** (Figure 1.8), which alternates between a *vase* and *kite* conformer based on the oxidation states of the incorporated TTFs.[31] The change in conformation is dramatic and can be easily examined by the behaviour of **15** in a cyclic voltammogram. The oxidations are more difficult for **15** than the parent TTF, especially the first two-electron oxidations, as the generated $\mathbf{15}^{2+}$ bears two radical cations in close proximity to one another, which experience some electronic coupling and Coulombic repulsions. This instability, as well as the presence of electron-withdrawing alkylsufanyl and quinoxaline substituents, increase the potential required for the first oxidation, and result in a broad oxidation peak, as well as conformational change. The second two-electron oxidation takes place relatively readily, as the cationic regions of the molecule are no longer interacting, and causes no further conformational change.

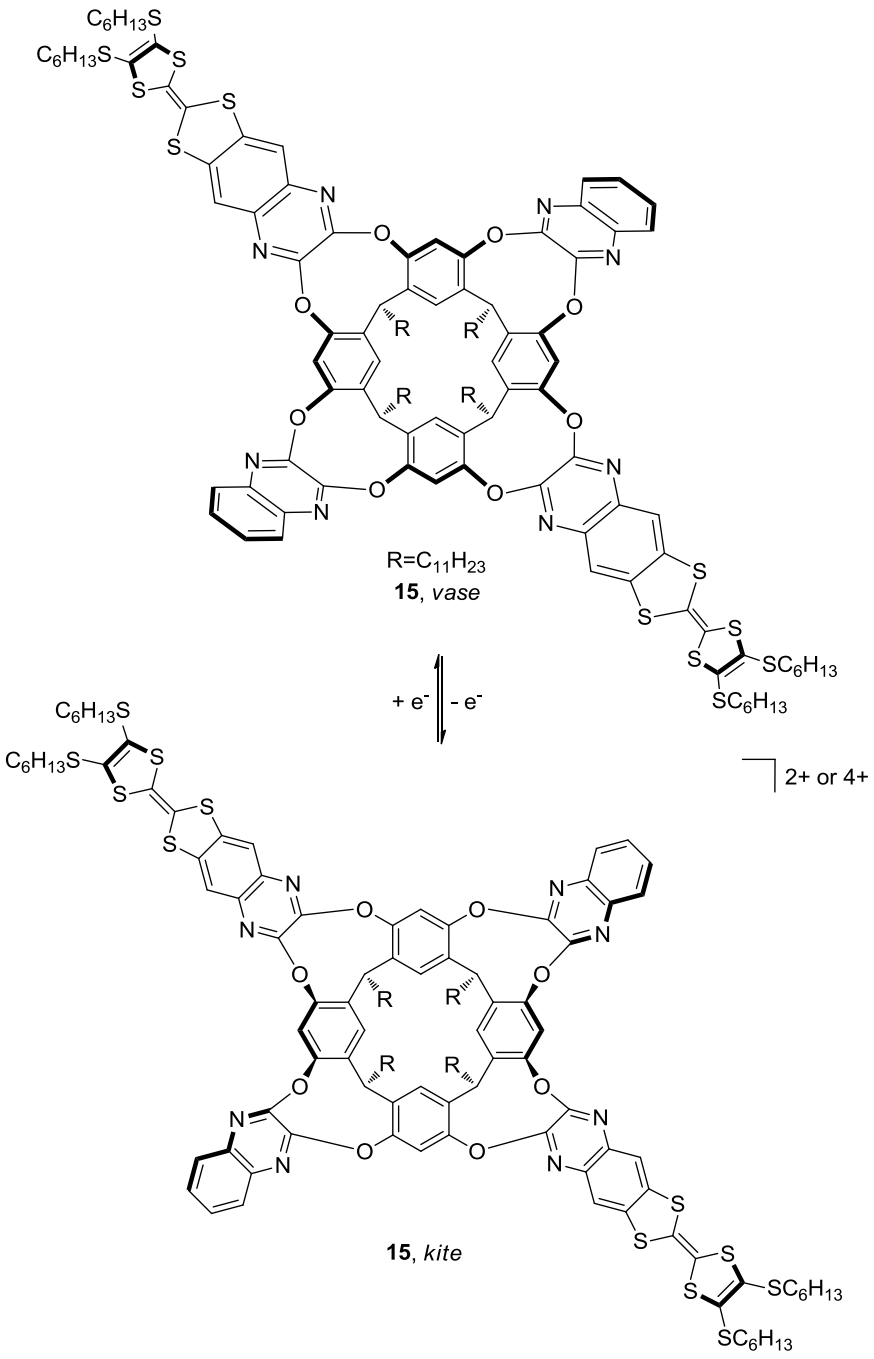


Figure 1.8 Conformational switching of **15**.

Another simple example is the compound series in Figure 1.9, designed as chiral molecular switches to be driven by TTF oxidation and cationic repulsions.[32] Molecules,

such as **16**, possessed of short *o*-alkylthio- linkers to TTF on the 2,2'-positions of the BINAP, formed a cation radical dimer ($TTF_2^{2+}$) upon the first oxidation of both moieties, stabilizing the Coulombic repulsions, but with the second oxidation, they repelled each other further, increasing the dihedral angle of the BINAP considerably, as observed in the CD spectrum. Furthermore, when further TTFs were linked on the 6,6'- positions, as in compound **17**, more significant changes were observed, even in the first oxidation, as the 6,6'-TTFs are incapable of forming the cation radical dimer to stabilize themselves.

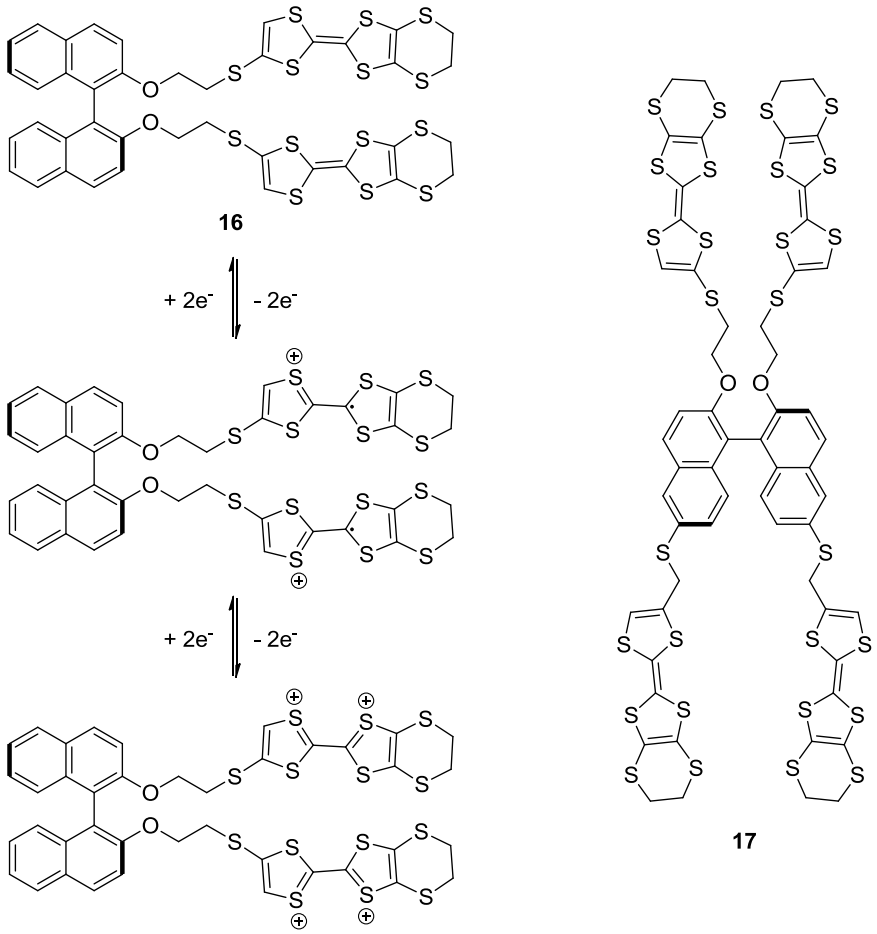


Figure 1.9 Chiral molecular switches **16** and **17**.

The interactions between supramolecular assemblies will obviously change if some property within one molecule is changed, giving rise to the notion of molecular machines. As seen in Figure 1.10, a system to mimic natural skeletal muscle was developed, based on affinities for different groups and interactions in different oxidation states.[33] In the neutral state, assembly **18** has two tetracationic cyclophanes, cyclobis(paraquat-*para*-phenylene) ($CBPQT^{4+}$) residing around the TTF moieties of a [3]rotaxane, thanks to TTF's electron donating ability and π-π stacking interactions. However, upon chemical or electrochemical oxidation, the $CBPQT^{4+}$s' movement to the naphthalene could be monitored by $^{1}H$ NMR, CV, and UV-Vis spectroelectrochemistry. This movement was triggered through repulsions between the dicationic TTFs and pyridiunium groups, as well as attractive π-π interactions between the naphthyl and pyridinium groups.

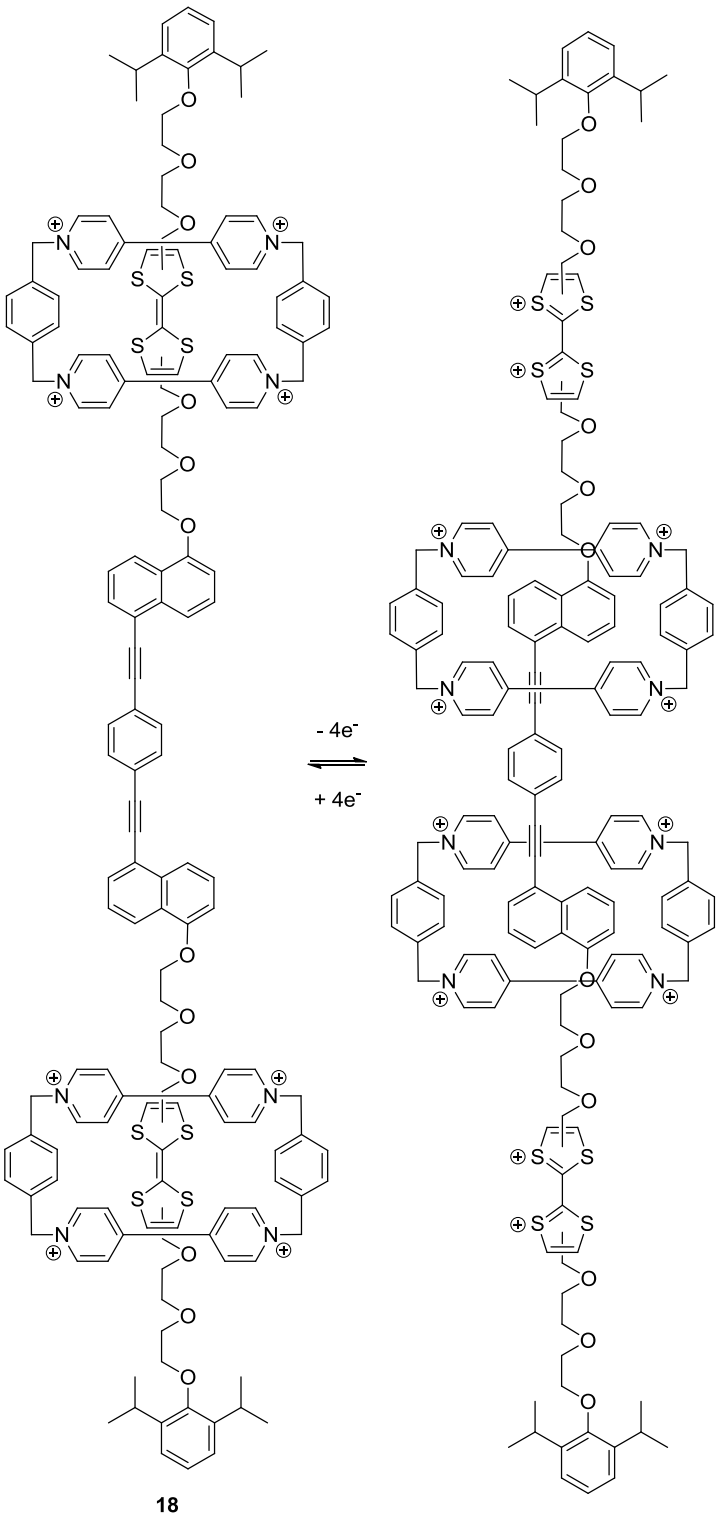


Figure 1.10 Neutral and oxidized rotaxane assembly **18**.

An excellent example of a molecular logic gate can be seen with compound **19** (Figure 1.11).[34] This molecule responds to diverse stimuli (inputs) to offer different outcomes (outputs), demonstrating varying logic gate performances. While **19** cannot be thought of as selective, it acts as a logic gate, from either an initial neutral or initial oxidized state, in several capacities. In the presence of certain inputs neutral **19** can act as an AND, OR, and INHIBIT logic gates, going from non-fluorescent to fluorescent, with measured fluorescence as the output (truth table for AND Table 1.1). For NOT, NAND, NOR, and XNOR logic gates, the initial state is that of $\mathbf{19}^{2+}$, which will change the output to the loss of fluorescence, instead of its growth or initialization (truth table for NAND Tables 1.2).

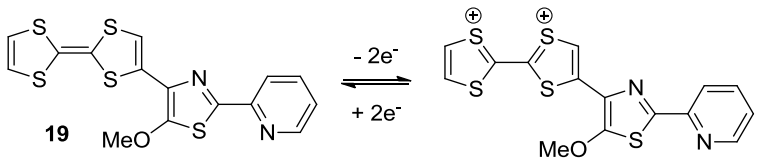


Figure 1.11 Oxidation of logic gate **19**.

| Input 1: $Ce^{4+}$ | Input 2: $H^+$ | Normalized fluorescence intensities (PL) |
|---|---|---|
| 0 | 0 | 0 (0.08) |
| 1 | 0 | 0 (0.06) |
| 0 | 1 | 0 (0.30) |
| 1 | 1 | 1 (1.00) |

Table 1.1 Truth table for **19** as AND logic gate, with inputs $(NH_4)_2Ce(NO_3)_6$ ($Ce^{4+}$) and $CF_3COOH$ ($H^+$).

| Input 1: $Fe^{2+}$ | Input 2: $NOBF_4$ | Normalized fluorescence intensities (PL) |
|---|---|---|
| 0 | 0 | 1 (1.00) |
| 1 | 0 | 1 (0.90) |
| 0 | 1 | 1 (1.00) |
| 1 | 1 | 0 (0.07) |

Table 1.2 Truth table for **19**$^{2+}$ as NAND logic gate, with inputs $Fe(ClO_4)_2$ ($Fe^{2+}$) and $NOBF_4$.

### 1.1.3 Synthetic methodologies

#### 1.1.3.1 TTF

Initially, synthesis of TTF was executed through a tedious route, taking eight synthetic steps to obtain TTF in poor purity and yields.[4] Due to recent research to find better synthetic routes for TTFs, numerous excellent methods have been developed to readily access a wide variety of simple and complex TTFs. In addition to the final step in preparation of TTF, there are many common precursor steps found throughout the literature. Presented in Scheme 1.1 are a series of synthetic routes to TTF (modified from reference **35**).[35]

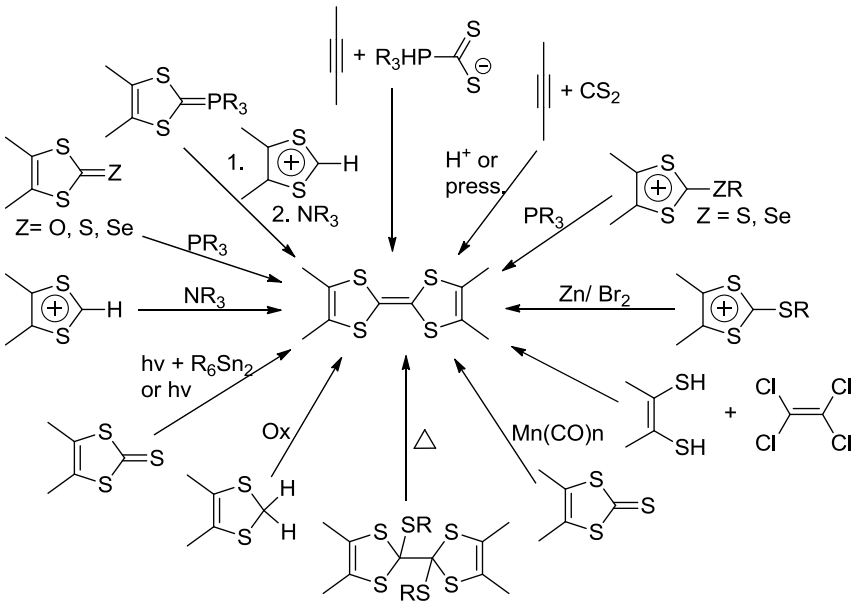


Scheme 1.1 Synthetic methods for constructing the TTF skeleton.

As shown above, there are many precursors that can be used to make TTF. However, these precursors themselves have many synthetic routes available for their preparation. Scheme 1.2 (modified from reference **35**) shows the various methods to make a typical thione compound, a key precursor to TTF.

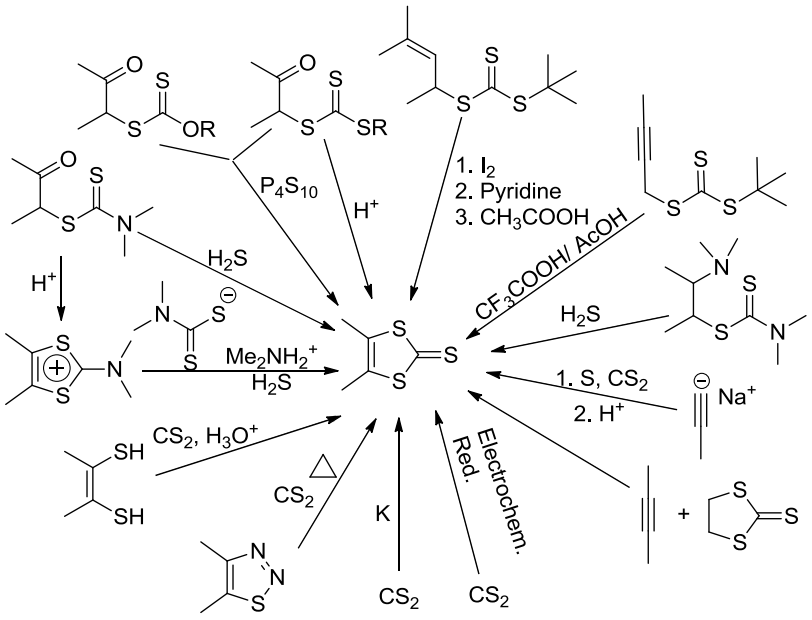


Scheme 1.2 Synthetic methods for thione.

As shown in Scheme 1.1, there are also many uses for a dithiolium salt in the preparation of TTF. There are several straightforward chemical methods by which a dithiolium salt can be prepared (Scheme 1.3, modified from reference **35**).

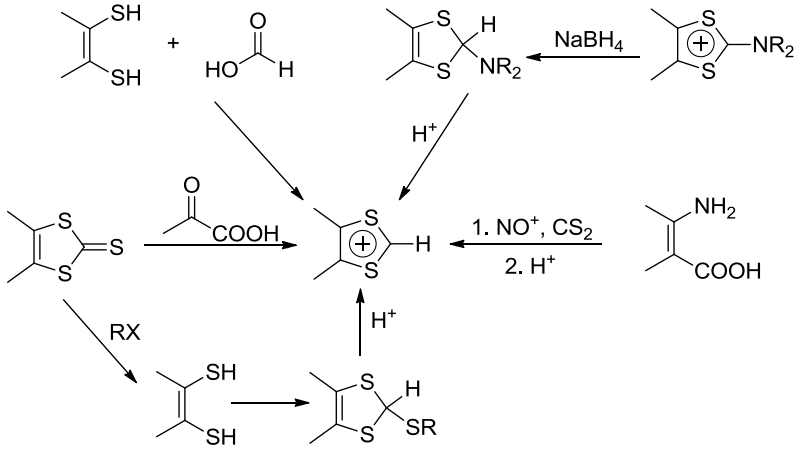


Scheme 1.3 Synthetic methods for dithiolium salt.

Among all the methods available to make TTF, there are three that are the most popular. As demonstrated in Scheme 1.4, the first, (a), is the base-promoted coupling of dithiolium salts or dithiole-2-chalcones; the second, (b), is the phosphite-promoted coupling of the same. These two are the best options for the synthesis of symmetric TTFs. The third method in Scheme 1.4, (c), the base-promoted coupling of a Wittig reagent and a dithiolium salt, is a highly efficient choice for the generation of asymmetric TTFs.

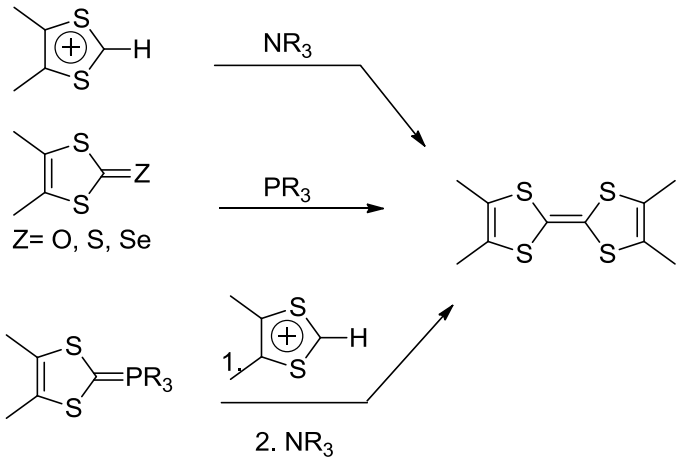


Scheme 1.4 The major routes to TTF.

The thione precursor, used for TTF synthesis in Scheme 1.2, is easily prepared on a bulk scale through the use of carbon disulfide and an alkali metal, such as sodium or potassium.[36] The reduction of carbon disulfide is performed readily by the alkali metal, and the reaction mechanism is described in Scheme 1.5. The resultant dithiolate ion is isolated as the tetraethylammonium salt of its zinc chelate. Substitution reactions between the dithiolate-zinc complex and appropriate electrophiles, such as alkyl halides, acyl halides, alkynyl halides, and alkenyl halides, yield thione products with the desired substituents (Scheme 1.6).

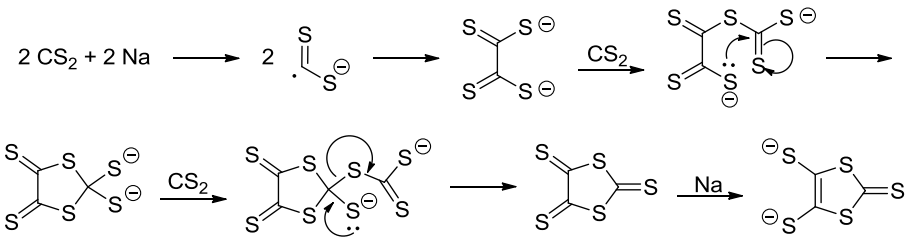


Scheme 1.5 Mechanism of 1,3-dithiole-2-thione-4,5-dithiolate (dimercaptoisotrithione, dmit) formation by sodium reduction.

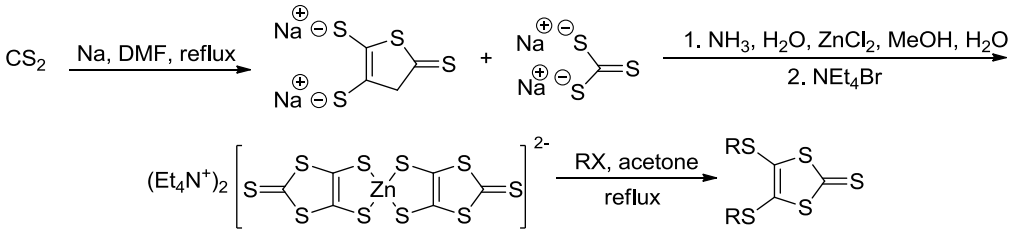


Scheme 1.6 Synthetic preparation methodology of thione precursor by sodium reduction of carbon disulfide.

From the thione precursor, a dithiazolium salt can be prepared. This requires an addition-reduction-elimination series of reactions, resulting in a cationic and an aromatic dithiole ring. This process entails the alkylation of the thione, and is generally favorable thanks to the aromaticity developed, but strong alkylating reagents are still required to overcome the π-bond. Dimethyl sulfate at 100 °C is a popular choice for reaction conditions (Scheme 1.7), and can be followed by addition of fluoroboric acid to yield the dithiolium tetrafluoroborate salt by precipitation (Scheme 1.8).[37]

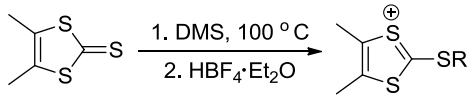


Scheme 1.7 Methylation of thione using dimethyl sulfate.

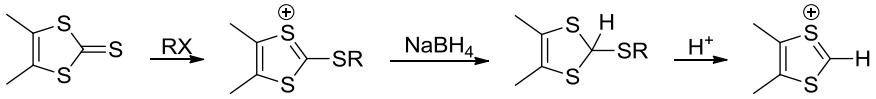


Scheme 1.8 Synthesis of dithiolium salts.

Dithiolium salts are functional TTF precursors, as they can be reacted with a phosphine to yield a Wittig reagent, or reacted with phosphite to yield a phosphonate ester (Scheme 1.9). These can be used to make a variety of TTFs: direct coupling with a dithiolium salt can produce a simple TTF, while the use of either as a precursor to a Horner–Wadsworth-Emmons reaction can yield π-exTTFs, which can be composed of large and extended conjugated structures.

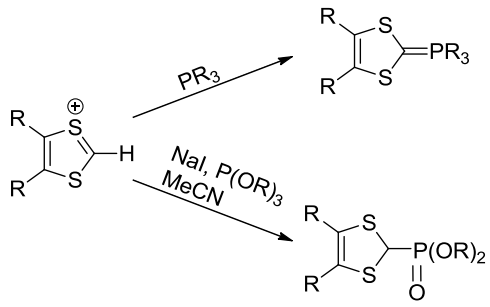


Scheme 1.9 TTF precursor preparations.

It is worth noting that, in dilute conditions, the thione can react with an excess of trialkylphosphites to produce the phosphonate ester in good yield. However, while this

one-step process is very efficient, the excess of trialkylphosphites makes purification very difficult and limits the applicability beyond the laboratory scale.

Modification of the TTF skeleton follows several basic routes; a very common one is to lithiate TTF with an organolithium reagent at low temperature, and then add electrophiles to react further. A series of examples of this are presented in Scheme 1.10, all of which have synthetic significance of their own. The aldehyde product is particularly useful, as it can be subjected to an olefination reaction to extend the chain of conjugation. The lithiation can be controlled by electron donating substituents on the dithiole ring. The presence of an electron donor reduces the acidity of the proton adjacent to it, and vice versa for electron withdrawing substituents, permitting the preparation of multisubstituted TTFs.[38]

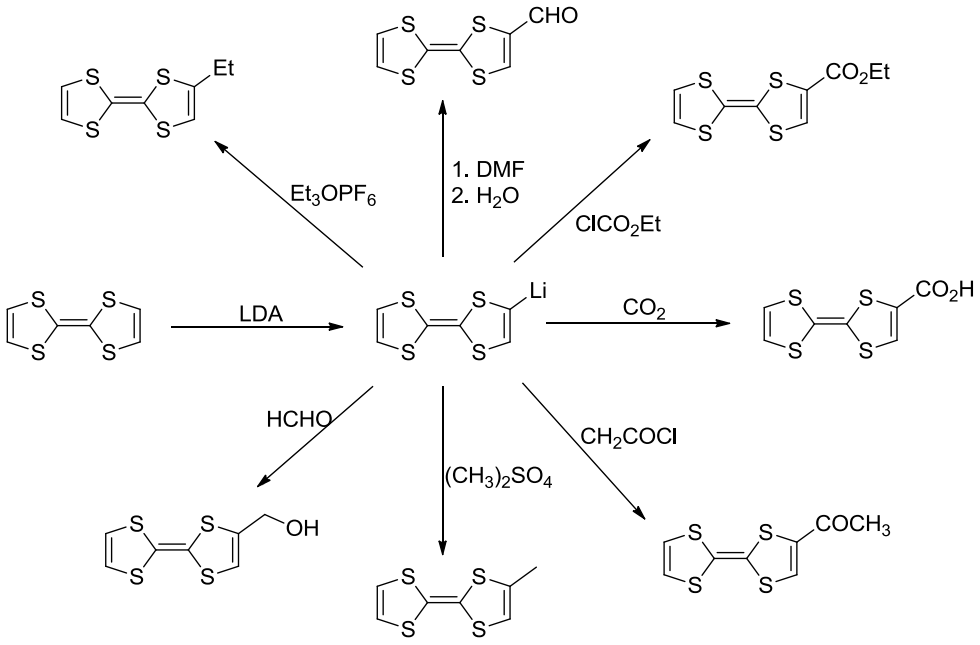


Scheme 1.10 Lithiation of TTF and selected further reactions. (modified from reference **38**)

### 1.1.3.2 π-exTTFs

In order to prepare π-exTTFs, the conjugated chain must be extended. As previously discussed, this can be accomplished by increasing the amount of conjugation between the dithiole rings, or by extending it by the addition of substituents to the rings. A common way to extend the amount of conjugation using substituents bonded to the dithiole rings is to use perform a Diels–Alder reaction,[39] requiring the generation of the reactive diene with a desired dienophile *in situ*, in order to prevent its decomposition and side reactions. The biggest issue with the Diels–Alder reaction is that it usually requires high temperature, which can cause the product to undergo decomposition if it is not thermally stable.

There are two popular methods used in order to increase the conjugation between the dithiole rings using π-conjugated spacers. The first is to prepare a diketone or dialdehyde to be used as the spacer, and then either couple it with thione or convert it to the target by a Wittig reaction. The first method is quick and efficient, but has the previously discussed issues of reactions with trialkylphosphites, as well as the risk of decomposition due to the high temperatures required to perform the reaction. The Wittig olefination utilizes phosphonium salts and mild conditions, with little byproduct formation, but it requires reagents to be base-stable, and the phosphonate preparation is tedious and expensive. The second method by which π-exTTFs are prepared is through reactions of dithiole monomers to extend conjugation. This offers a great deal of variety in methods, as just about anything can be self-coupled to produce a target. Scheme 1.11 presents a summary of these two methods.

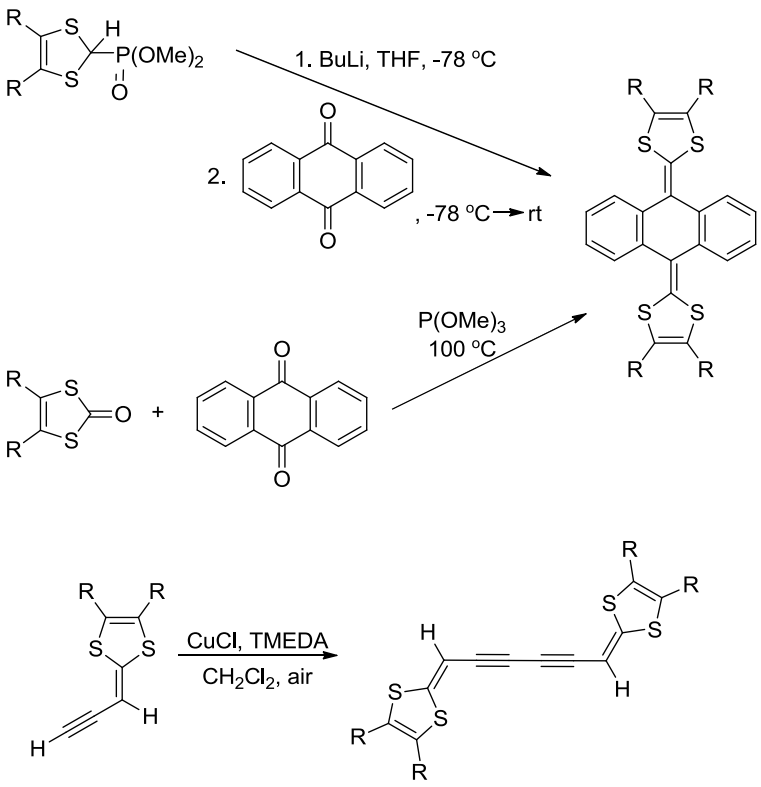


Scheme 1.11 Synthetic methods to extend the π-chain in TTF.

### 1.1.4 TTFV

Tetrathiafulvalene vinylogues (TTFVs) are a specific subset of π-exTTFs, which bear two vinyl groups between the dithiole rings. As can be seen from Figure 1.12 below, the oxidation of dithiafulvene (DTF) to TTFV follows a very straightforward radical dimerization mechanism.

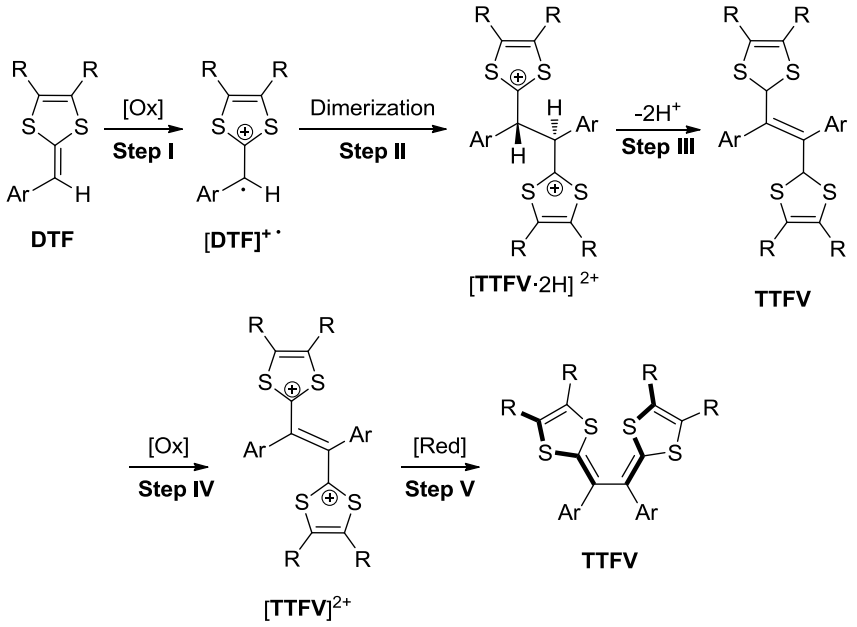


Figure 1.12 Mechanism of DTF oxidation.

In the dimerization reaction, oxidation of the DTF takes place at first by a chemical oxidant or applied potential. The oxidation yields an aromatic and stable radical cation, $[DTF]^{+\cdot}$, which dimerizes to yield a dicationic intermediate, $[TTFV{\cdot}2H]^{2+}$. In this intermediate, the Coulombic forces between the two nearby cationic dithiolium rings are significant. As a result, the molecule favors a *trans* conformation. Deprotonation of the first TTFV alleviates this repulsive stress, and further oxidation of TTFV takes place to restore the $[TTFV]^{2+}$. This is then reduced by a reducing agent, such as sodium thiosulfate, to yield a cisoid conformer product.

### 1.1.4.1 TTFV Synthesis

The stereotypical preparation of TTFV requires the oxidation of an appropriate dithiafulvene (DTF), followed by its radical homocoupling, and subsequent reduction.

This task can be accomplished using a chemical oxidant, such as iodine or 2,3-dichloro-5,6-dicyano-1,4-benzoquinone (DDQ), or electrochemically. TTFV macrocycles and polymers are attainable through the oxidation of monomers bearing more than one DTF unit by whatever means is preferred. Bulk electrolysis is a highly efficient means of producing large quantities of TTFVs from DTF precursors, and tends to proceed well, except in rare cases.

TTFVs can, of course, be prepared from a DTF bearing an aldehyde, which can be subjected to either a Wittig or Horner–Wadsworth–Emmons olefination; however, this is a less common choice, as it increases the synthesis time, but it offers reasonable access to an asymmetric TTFV. An example is shown in Scheme 1.12,[40] wherein a Vilsmeier–Haack reaction generated the second aldehyde, which was then reacted with a phosphonate ester in a Horner–Wadsworth–Emmons reaction to produce the desired target, compound **20**.

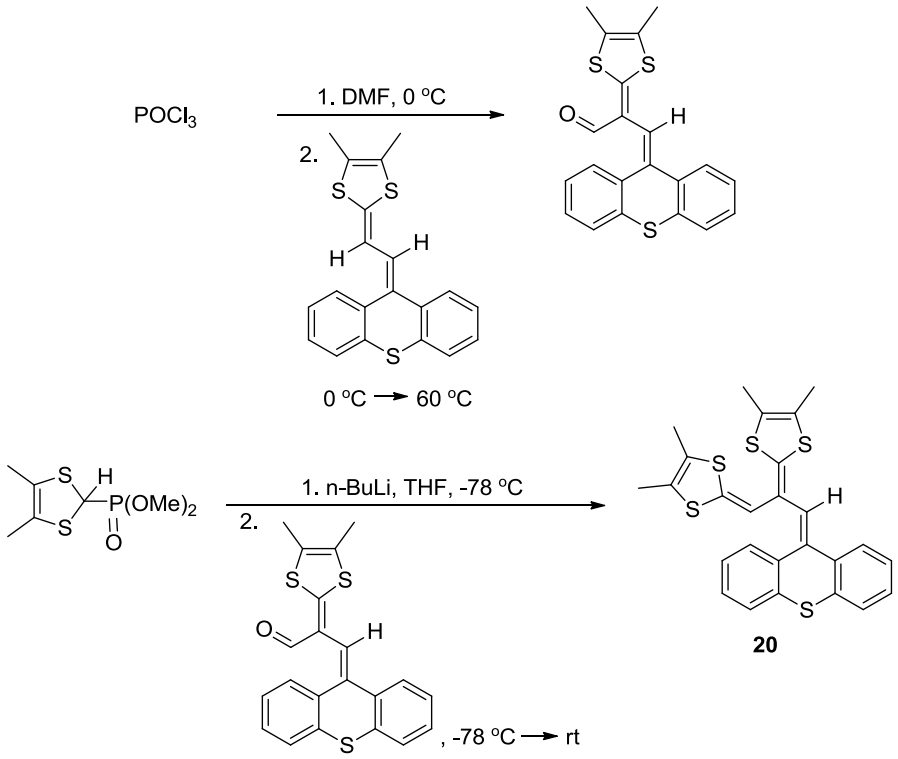


Scheme 1.12 Stepwise synthesis of an asymmetric TTFV, compound **20**.

## 1.2 Recent Progress in Anticorrosive Materials

While part of this thesis pertains to fundamental study, a brief foray into applied research was undertaken involving corrosion, its mechanism, and marine anticorrosion coatings, as well as bioinspiration for new coating additives. It is known that marine corrosion has presented a considerable challenge to humanity's maritime endeavours since time immemorial. The destruction and replacement of metal components, not the mention the costs associated with preventative and restorative maintenance, loss of efficiency, and loss of productivity all combine to create barriers to be overcome. The marine environment provides especially harsh conditions in which to combat corrosion, as it

offers an infinite supply of electrolytes, and is refreshed at the surface with oxygen through wave-action mixing.

In order to effectively prevent, or at least reduce, corrosion, the mechanisms it follows must be well understood. Once a solid grasp of corrosion mechanisms is attained, it becomes a much simpler task to prevent the process in the first place.

### 1.2.1 The Mechanism of Corrosion

Galvanic corrosion requires a surface to behave as an electrochemical cell. This entails the presence of an anode, a cathode, and two bridges between the two-one being an electrolyte solution, the other being metallic conductor. Assuming there is a potential difference between the anode and the cathode, and suitable materials for oxidation and reduction, respectively, at each, corrosion will take place. The potential difference is formed when there are different conditions at different sites on the surface, such as differing concentrations of electrolytes (e.g., sodium chloride in seawater) or dissolved oxygen.

The anode is the metal surface, generally iron, although there are often inclusions of other metals, or metal sulfides, such as manganese(II) sulfide in steel, contaminating the substrate. Upon oxidation, the metal can be converted to water-soluble ions, or it can form a protective (and insoluble) oxide coating on the metal surface. In any case, the region where the metal is oxidized alters the consistency of the metal surface, resulting in further oxidation at that site. This reaction is paired with a cathodic reduction of dissolved

oxygen to hydroxide. Overall, the processes of galvanic corrosion constitute an electrochemical cell.

There are many environmental factors encouraging corrosion processes. The “splash zone” best exemplifies the problems that increase the rate and severity of marine corrosion. The constant wetting ensures a water-film on the surface (a water-film can also be formed atmospherically at greater than 80% humidity), creating the chance for a salt bridge to form. Furthermore, this wetting is with saltwater, which is itself an electrolyte, and guarantees a good connection between anodic and cathodic sites. The re-mixing of the water with fresh air ensures a high dissolved oxygen concentration, thus enabling the cathode to perform its counterpart reduction to the oxidation of the metal by the anode. The mixing at the water surface as compared to sites either lower or higher on the metal surface creates differences in the concentrations of electrolytes and oxygen, forming the necessary potential difference for galvanic corrosion to take place.

The “splash zone” is also relatively warm, as it is near the surface, increasing the rate of corrosion, while also encouraging microorganisms, such as sulfate-reducing bacteria (SRB), to flourish and impact the strength of the substrate. Wave-action can stress the metal, while changes in temperature are also likely to exist throughout the metal, which also impacts its mechanical performance.

Other problems that can enhance corrosion include existing pits and crevices. Pitting corrosion tends to start at defects in the metal, such as the previously-mentioned manganese(II) sulfide inclusions. The small manganese sulfide areas become anodic, and

are oxidized, generating micropits. These pits experience different electrochemical conditions compared to the bulk metal surface due to poorer mixing. This allows further oxidation to occur resulting in growth of pits through galvanic corrosion. The presence of SRB rapidly converts the sulfide to hydrogen sulfide, a gas which leaves the metal surface around the site unprotected. The presence of SRB has been demonstrated in the literature to have a significant impact on the rate and degree of pitting observed.[41] Again, this relates to the water temperature, as the activity of SRB is reduced at low temperatures. For instance, it has been observed that pitting corrosion is diminished in polar waters as opposed to more temperate conditions. Crevice corrosion is very similar to pitting corrosion, only it begins in sites where surfaces meet, such as metal-metal or metal-non-metal parts adhered to one another by some means. The presence of these pieces offers a shelter from currents, restricting mixing and creating different concentrations of dissolved oxygen and electrolyte as compared to other areas on the metal surface. This gives the needed potential difference for galvanic corrosion to commence and, from this starting point, it spreads. It is reasonable to assume that SRB continue to have an influence in crevice corrosion, and may even have a greater impact in crevices, as there is an immediately available protected site for colonization.

### 1.2.2 Protective Coatings

The application of protective coatings, known as “barrier protection”, shields corrodible substrates from corrosion by preventing the passage of dissolved oxygen and electrolyte solution to the substrate, thus blocking the formation of the galvanic cell and its resulting damage. There are two means by which a barrier can be applied upon a surface; firstly, in

a process called passivation, the simple by-products of corrosion, insoluble metal oxides, create an impermeable barrier (for example, the atmospheric corrosion of copper(0) creates a green copper(II) oxide, known as patina, which shields the bulk of the copper from further corrosive action); secondly, a coating can be applied, composed of parts such as binders, pigments, extenders, solvents, and additives. While binders and pigments make up the bulk of an organic coating and its performance, the other components each have specialized purposes. Extenders can be added to increase the volume and thus surface coverage, while solvents dictate the film formation behaviour and ease of processability. Additives are added in small amounts to fine tune and enhance specific properties of the coating.[42]

In pigment-centred coatings, inert pigments are mixed in with the other components, which align within the organic binders in the film to create layers and slow the passage of oxygen and other corrosive substances. The resultant reduced concentrations slow the rate of corrosion and protect the substrate.[42] By comparison, binder-centred coatings operate with organic polymers, relying on the organic binders to act as an impenetrable barrier. This demands a strong grasp of structure-property relationships in molecules, as the organic binders must be able to bind to the metal substrate, as well as provide a protective barrier, and offer a good mechanical performance.[42]

Amongst binder-centred coatings, the most popular choices for marine anticorrosion applications are epoxy resins. These combine bisphenol A and epichlorohydrin, and are then crosslinked with either polyamines or polyamides. These resins offer good adhesion to metal substrates, and are resistant to chemical attack. However, they are subject to

damage and degradation due to UV exposure, demanding a secondary topcoat to be applied to protect the basecoat from this condition (generally polyurethane).[42] A second widely used type of polymer binder is acrylic. Polymerization of acrylic acid or ester yields the bulk binder, while isocyanates or amine resins are added to enhance crosslinking and to cure the coating. Pure acrylics tend to be disfavored, as they do not offer great corrosion protection, but modifications can be performed to augment their performance.[42] Polyurethanes themselves are also often chosen, as they have good mechanical strength, gloss and color retention, and are resistant to scratching and mechanical harm, all attributable to the hydrogen bonds formed between the isocyanate groups in the coatings and compounds bearing active hydrogens. One major drawback to these types of coatings is that they are weak against mechanical strains, but they can be improved with modifications.[42] Polysiloxanes are another type of organic coating, utilizing the strength of silicon-oxygen bonds to protect their substrate. They offer excellent color and gloss retention, but have poor mechanical properties and miscibility with more common coatings.[42] Furthermore, because polysiloxane is bio-inert, it is safe for diverse applications, including medical implants, and, because its hydrophobic nature offers a strong barrier to charged species (such as those of an electrolyte solution) reaching a metal surface, it can inhibit corrosion.[43]

### 1.2.3 Bioinspired Design of Anticorrosion and Antifouling Materials

The organisms that survive and thrive in harsh marine environments can offer clues toward enhancing materials in those same conditions. One prime example of this is the Atlantic blue mussel, which adheres itself for life to marine substrates such as rocks,

wharves, or any other stable footing. From here, these simple filter feeders can live for many years. The mechanism by which these animals hang on is well worth investigation into its applicability in human endeavours and industrial pursuits.

The adhesive feet of blue mussels are essentially protein chains secreted by the mussel. What is intriguing about these chains is that, at the foot-substrate interface, the chains are composed of 21 and 27 mole percent dopamine (compound **21**, Figure 1.13),[44] whose R group is the organic moiety catechol (bolded group of compound **21**).

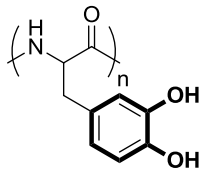


**21**

Figure 1.13 Structure of dopamine, compound **21**; bolded structure is catechol.

This molecule has drawn attention from the scientific community, especially from chemists interested in using catechol-functionalized molecules to achieve surface modifications,[45-47] but also from the medical field, as a potential scaffold for hydroxyapatite (the material in bones),[48] wet adhesives that do not trigger significant inflammation,[49] and for biologically degradable adhesive hydrogels that do not induce inflammation.[50]

The mechanism of the adhesive action of catechol has yet to be fully elucidated, but there are several proposed mechanisms. One proposed mechanism is co-ordination bonding, wherein a deprotonated catechol can replace a ligand on the surface to create a stable

bond.[51] Another is bidentate chelation bonding, wherein both oxygens play a role in bonding to a surface atom,[52] possibly improving the stability of the surface atom by filling more sites and improving the coordination environment of the central atom. A third possible mechanism for the adhesive nature of catechol could be a bridged bidentate model, where each oxygen atom bonds to a different surface atom.[53] A final proposed mechanism requires a mixture of either monodentate bonding with some hydrogen bonding through the hydrogen of the hydroxyl groups on catechol, or monodentate-bidentate bonding, varying over the surface.[54] Of course, the mechanism of binding varies depending on the surface composition,[45] and is also likely to change based on the macromolecular structure upon which the catechol is functionalized.

This moiety holds great promise in marine research, as it is functionally adhesive in wet conditions, but can still be modified to perform other tasks, such as antifouling.[55] The potential to prepare materials with multiply defined functions is highly intriguing, and could be used to remove flaws from other compounds, such as polysiloxanes, while leaving the strengths.

### 1.2.4 Polysiloxanes in Chemistry

#### 1.2.4.1 Hydride Sources

Polysiloxanes, especially polymethylhydrosiloxane (PMHS) (**22**, Figure 1.14), have been investigated as gentle and environmentally friendly hydride sources for many years.[56-57] They are cheap and straightforward to prepare, as well as highly stable, and can be used as hydride transfer reagents (from the weak silicon-hydrogen bond) to prepare expensive

reagents such as organotin hydrides (e.g., one of the best ways to prepare $Bu_3SnH$ is from $(Bu_3Sn)_2O$ and PMHS), demonstrating that the low cost of PMHS and its stability toward multiple functional groups do not affect its applicability.

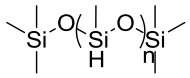

**22**

Figure 1.14 General structure of compound **22** (PMHS).

In recent work by Chandrasekhar and coworkers, PMHS was utilized as a hydride transfer reagent to cleave allyl ethers, esters, and amines to generate alcohols (up to 94% yield), acids (up to 87% yield), and primary amines (up to 92% yield) respectively (Scheme 1.13).[58] Simply by combining PMHS, $ZnCl_2$, and $Pd(PPh_3)_4$ in THF at room temperature, their work has served to expand the usefulness of the allyl protecting group, relying on the gentle and one-step PMHS approach, rather than the use of harsh potassium *tert*-butoxide and acid workup. Furthermore, this work studied the selectivity of the PMHS hydride for the allyl-X bond in the presence of other alcohol protecting groups, and it was found that benzyl, *p*-methoxybenzyl, tosyl, tetrahydropyranyl, methoxy methyl, *tert*-butyldimethylsilyl, and acetyl were all stable under these conditions, providing researchers with another avenue for selective deprotection of diols.

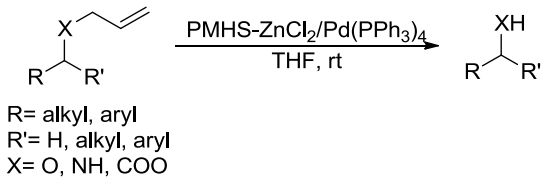


Scheme 1.13 Deallylation of allyl ethers, esters, and amines using PMHS.

In more recent work, the Beller group developed a system to reduce aldehydes to alcohols through the use of iron(II) acetate, tricyclohexylphosphine, and PMHS at low temperature, followed by a mildly basic workup (Scheme 1.14).[59] This work is highly appealing for several reasons: firstly, iron(II) acetate is either cheaply made, using iron metal and hot glacial acetic acid, or readily purchased from bulk suppliers, and secondly, these salts are much less toxic to the environment than the tin by-products of Stille-type reductions. Their investigations assessed the tolerance of other functionalities, such as halides, nitro groups, esters, and nitriles, and found that all were unaffected during the reduction of the aldehyde. In this regard, a wide range of aldehydes were successfully reduced to the corresponding primary alcohols, with isolated yields ranging from 72 to 99% in some cases. This work further demonstrated the large scope of applications of polysiloxanes as hydride sources, and offered a cheaper alternative to more established methods.

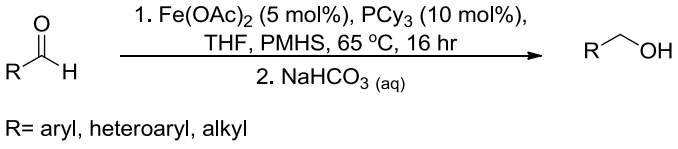


Scheme 1.14 Iron-mediated reduction of aldehydes using PMHS as hydride source.

### 1.2.4.2 Catalyst/ Ligand Scaffold; General Scaffold

As synthetic chemistry advances, it has become essential to take a green approach, and ensure high recovery yields of any unreacted materials or catalysts, to reduce waste, costs, and potential environmental impacts. As polysiloxanes can be prepared in any chain size, they can be produced bearing a large number of ligand sites, enhancing activity, and may be recoverable, as either insoluble catalyst supports, or recovered following simple workups (soluble supports). This, alongside the fact that polysiloxane can be readily functionalized, makes for an appealing scaffold for catalysis, or for an unreactive and neutral stationary phase or alternative support, hence opening the door to uses in chromatography or biomedical chemistry.

The functionalization of polysiloxane with an appropriate ligand system can provide a valuable support for catalysts, making them quantitatively recoverable, often without significant loss of activity. A prime example of this is the 2004 work by DeClue and coworkers, wherein two polysiloxane-ligand structures (compounds **23** and **24**, Figure 1.15) were prepared and evaluated for activity in the Sharpless asymmetric dihydroxylation reaction.[60] Compound **23** was insoluble in common solvents used for this type of reaction (reported solvents used were *tert*-butyl alcohol: water (1:1, v/v) and acetone: water (10:1, v/v)), while **24** produced a homogeneous reaction mixture under experimental conditions. Through a battery of experiments, testing a large scope of olefins for dihydroxylation using osmium tetraoxide and a secondary oxidant, either 4-methylmorpholine *N*-oxide or potassium ferricyanide in either *tert*-butyl alcohol water (1:1, v/v) or acetone water (10:1, v/v), respectively, at 0 to 4 °C, it was observed that,

although both ligands produced similar yields and enantiomeric excesses (ee), compound **24** could react much more rapidly, as expected given its solubility.

However, when recovering the ligands, **23** could be obtained by simple filtration, while **24** was precipitated out of the reaction mixture by addition of excess water and then isolated by filtration. **24** could be reused directly, with all reagents but the metal oxide, to yield similar quantities and ee from the reaction (although it took considerably longer), while **23** could be left to react without addition of extra osmium tetraoxide for a week and no noticeable reaction would take place.

Compound **23** is suspected to have captured some trace amounts of the metal through the filtration, while the slow precipitation of **24** likely did not collect any, as the metal would be both soluble and dilute in the aqueous solution. Nearly quantitative amounts of both ligands could be recovered and reused, and in the presence of added osmium tetraoxide, both retained high catalytic activities with similar yields, stereoselectivity, and almost identical reaction times to the first experiment. The ligands were recovered and reused for five iterations of the experiment, and found to be consistently effective. The preparation of these ligands, particularly the soluble ligand **24**, offers a unique solution to industrial operations requiring these processes, controlling costs and still offering an excellent system.

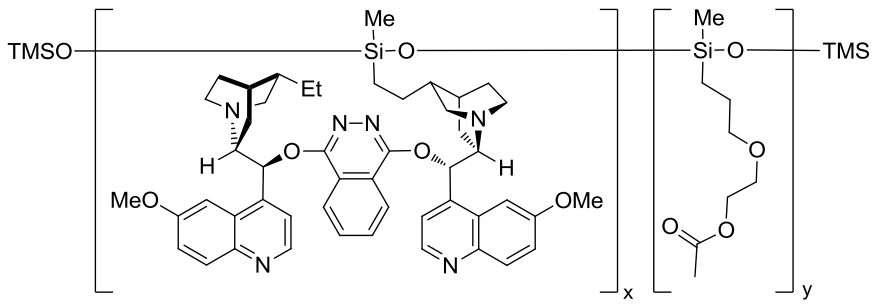


| Compound | x:y | Solubility |
|---|---|---|
| **23** | 1:0 | No |
| **24** | 5:7 | Yes |

Figure 1.15 Structures of polysiloxane ligand-supports, compounds **23** and **24**.

An example of polysiloxane acting as a neutral support can be found in the preparation of a poly(L-lactic acid)-polysiloxane carbonate hybrid membrane, to be used as a biodegradable and non-toxic substrate for hydroxycarbonate-apatite formation and bone regeneration.[61] The membrane was prepared by dipping a small circular glass substrate into a solution of poly(L-lactic acid)-polysiloxane (prepared by the researchers from poly(L-lactic acid) and aminopropyltriethoxysilane monomer and calcium carbonate, followed by drying at room temperature. The dried sample was evaluated by FT-IR, and it is apparent that a strong new band has formed at approximately 1600 $cm^{-1}$, which is reasonable for the formation of a new bond between the amino functionality of the silane and the carboxyl functionality of the acid. The membrane sample was then soaked in simulated body fluid (SBF) at 37 °C for 3 days, after which apatite-specific peaks can be seen in the thin film-XRD, suggesting the presence of silicon supports and the beginnings of bone-like structure. After the soak, silicon could be detected in the hydroxycarbonate apatite layer that had formed on the sample, suggesting that the silicon was solubilized in

the SBF, but promptly re-integrated into the new structure as either siloxane or silicate. *In vitro* experiments using osteoblasts (bone-forming cells) were undertaken, using some samples that had been soaked in SBF and some samples that were used directly after drying. While both membranes could support cell proliferation and were non-toxic, the soaked samples bearing the hydroxycarbonate-apatite layer supported cell growth much better, and possessed a statistically significant increase in cell numbers over the dipped and dried membrane. Although this work is only in very early stages, advancement could provide new bone regrowth techniques to aid both active and aging populations with superior medical care, while reducing costs and expenses in increased surgeries and patient recovery times.

#### 1.2.4.3 Hydrosilylation

In their crude form, polysiloxanes are not ideal as anticorrosion coating materials. Their good qualities are negated by their immiscibility and weak mechanical properties, making them unappealing for industrial-scale application. To this end, diverse methods for the modification of polysiloxane have been developed, in order to enhance their performance. Although there are a multitude of possible catalyst systems available for hydrosilylation, the two most common catalysts used are Speier's catalyst and Karstedt's catalyst (Figure 1.16, compounds **25** and **26**, respectively). Based around a platinum core, they can be used in small mole percentages to offer high yields of silylated products.

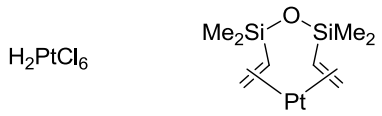


**25** **26**

Figure 1.16 Common catalysts for hydrosilylation.

The most typical approaches utilize an alkene and a metal catalyst bearing somewhat labile ligands, and which follow a Chalk–Harrod mechanism (Scheme 1.15) proposed in 1965 and which is based on Speier's catalyst.[62] In this mechanism, oxidative addition bonds the silane to a metal-alkene complex, usually with a $d^8$ or $d^{10}$ configuration, which is then followed by insertion of the alkene into the metal-hydride bond, and then reductive elimination to produce the silyl product and regenerate the metal complex.[63]

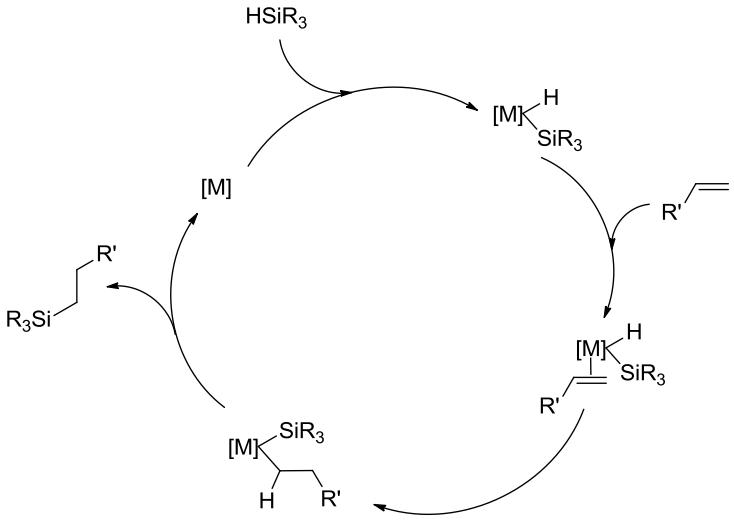


Scheme 1.15 Chalk–Harrod mechanism of hydrosilylation.

A modified Chalk–Harrod mechanism has been developed (Scheme 1.16) to account for certain oddities such as the formation of vinylsilanes. This follows a path where the

alkene insertion into the metal-silyl bond occurs, followed by reductive elimination of the carbon-hydrogen bond. The Chalk–Harrod mechanism is expected to be followed over the modified mechanism, though, as the modified mechanism has a considerably higher energy of activation for the rate-determining step, according to calculations.[64]

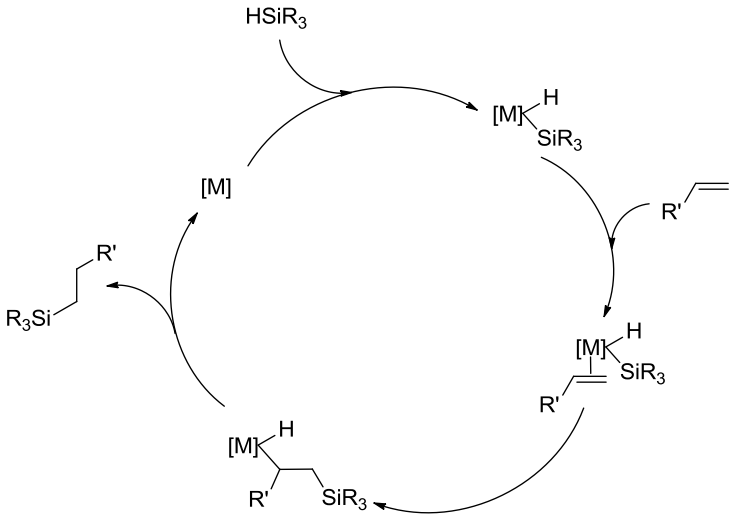


Scheme 1.16 Modified Chalk–Harrod mechanism of hydrosilylation.

A recent example of Speier's and Karstedt's catalysts can be found in the work of the Safa group.[65] This work entailed the preparation of new poly(methylalkoxy)silanes through hydrosilylation with simple alcohols in the presence of trace catalyst (Scheme 1.17). Although both catalysts worked, Karstedt's catalyst took less time, required a lower temperature, and provided higher yields than Speier's catalyst. Furthermore, a lower relative concentration of Karstedt's catalyst ($[Pt^0]/[Si–H] = 15 \cdot 10^{-5}$) was used than Speier's catalyst ($[Pt^0]/[Si\text{-}H] = 34 \cdot 10^{-5}$), making it a significantly more economical option. It is plain to see that the differing structures of the two catalysts, from the very simple Speier's catalyst, to the somewhat more complex Karstedt's catalyst,

have a huge bearing on reactivity and greatly influence the transition state in the rate-determining step. The appropriate choice of catalyst is absolutely critical to industrial endeavours, as small differences in reactivities on the laboratory scale could drive costs to exorbitant heights based solely on this factor.

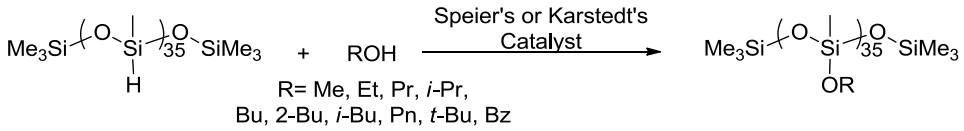


Scheme 1.17 Simple hydrosilylation of alcohols.

Hydrosilylation chemistry can also be used to prepare precursors for polysiloxane-backboned copolymers. In recent work by the Chisholm group, an epoxy-functionalized poly(dimethyl)siloxane (PDMS) copolymer was prepared for creating an antimicrobial surface coating.[66] This was accomplished by first adding the backbone to allyl glycidyl ether using Karstedt's catalyst. From there, levofloxacin was added to the terminal epoxide to yield the target (Scheme 1.18). Evaluation of the coating showed a uniform distribution of the levofloxacin, which resulted in a superior initial kill of applied microbes, and an improved longevity of activity, as compared to a control of polysiloxane mixed with levofloxacin. This simple and direct approach to coating preparation could offer rapid improvements in materials used for biomedical surfaces or even implants.

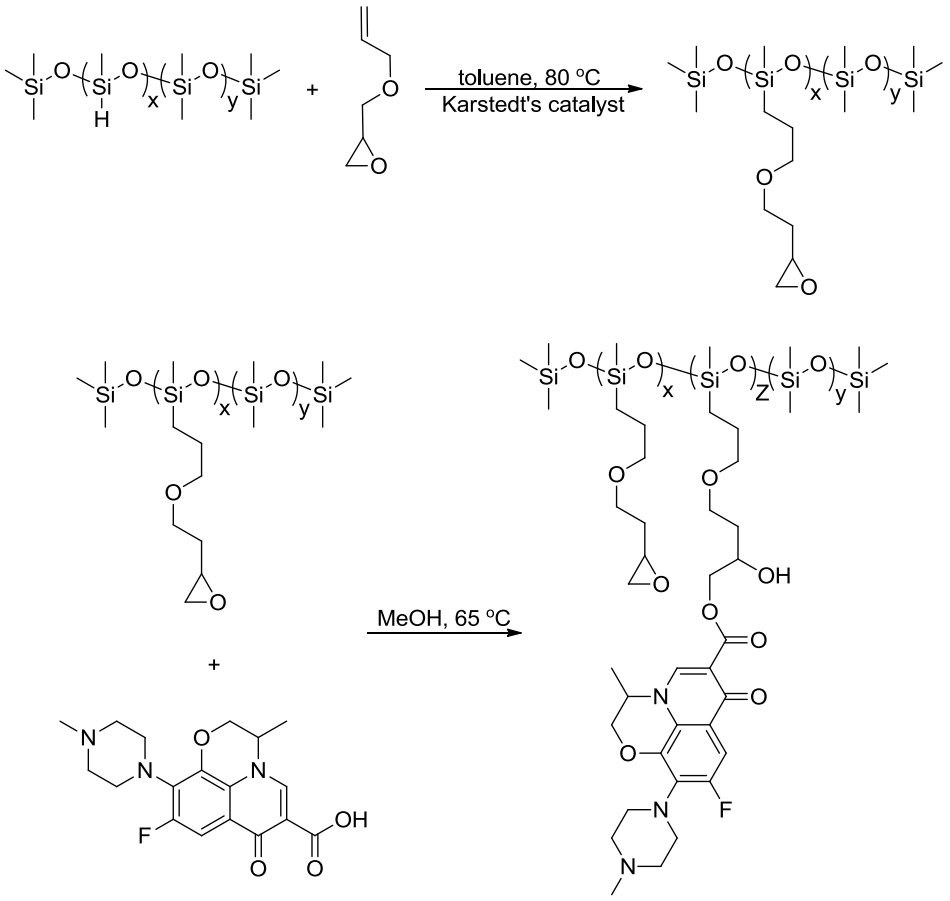


Scheme 1.18 Preparation of a levofloxacin-polysiloxane antimicrobial coating material.

## 1.3 Scope of Thesis

This M.Sc. dissertation has completed one major project in the synthesis and properties evaluation of DTFs and their reactivities toward oxidative dimerization, one major project in the development of a novel ex-TTF, and progressed towards one project on a TTFV cryptand, and one project toward catechol functionalized polysiloxane. Chapter 1 contains brief overviews on two topics: (i) TTF's properties, applications, syntheses, and its sub-groupings of exTTFs and TTFV, and (ii) corrosion and polysiloxanes, with a brief note on the molecule catechol.

Chapter 2 focuses on the synthesis and characterization of a series of DTF molecules, and their behaviour upon oxidation. Although many TTFVs have been prepared, there has yet to be a conclusive fundamental study of the reactivities of DTFs, permitting better predictions of possible targets, as well as byproducts.Utilizing standard olefinations and iodine-driven oxidations, as well as cyclic voltammetric techniques, several DTFs were studied and compared in order to determine trends in behaviour, and to find a basis for these trends in terms of structural differences. Certain compounds were successfully crystallized, and their structures confirmed by X-ray single crystallographic analysis.

Chapter 3 presents the progress toward a catechol-functionalized polysiloxane for anticorrosive coating additives. Such a coating has not yet been developed, and could provide accost-effective and environmentally friendly new material to protect against marine corrosion damages. The synthesis required investigation of the Hiyama coupling reaction, the Kumada coupling reaction, the Vilsmeier–Haack reaction, the Rieche reaction, and the Wittig reaction. Although this project is incomplete, the eventual results will provide great insight into anticorrosion additives, and may yield a marketable product.

Chapter 4 is a summary, and the conclusions of this thesis are given. This includes possible solutions to challenges encountered during this work, and proposes future directions for further study, as well as a brief discussion of a prepared but under-explored compound relevant to this thesis.

## 1.4 References


1. Wudl, F.; Wobschall, D.; Hufnagel, E. J., *J. Am. Chem. Soc.* **1972,** *94*, 670-672.

2. Prinzbach, H., *Angew. Chem. Int. Ed.* **1965,** *4*, 435.

3. Ferraris, J.; Cowan, D. O.; Walatka, V. V.; Perlstein, J. H., *J. Am. Chem. Soc.* **1972,** *94*, 3372.

4. Melby, L. R.; Hartzler, H. D.; Sheppard, W. A., *J. Org. Chem.* **1974,** *39*, 2456-2458.

5. Shirota, Y., *J. Mater. Chem.* **2000,** *10*, 1-25.

6. Chen, W.; Duan, L.; Zhu, D., *Environ. Sci. Technol.* **2007,** *41*, 8295-8300.

7. Pourghaz, Y.; Dongare, P.; Thompson, D. W.; Zhao, Y., *Chem. Commun.* **2011,** *47*, 11014-11016.

8. Ćavara, L.; Gerson, F.; Cowan, D. O.; Lerstrup, K., *Helv. Chim. Acta.* **1986,** *69*, 141-151.

9. Kimura, T.; Watanabe, D.; Namauo, T., *Heteroatom Chem.* **2011,** *22*, 605-611.

10. Yamashita, Y.; Tomura, M., *J. Solid State Chem.* **2002,** *168*, 427-432.

11. González, S.; Martín, N.; Sánchez, L.; Segura, J. L.; Seoane, C.; Fonseca, I.; Cano, F. H.; Sedó, J.; Vidal-Gancedo, J.; Rovira, C., *J. Org. Chem.* **1999,** *64*, 3498-3506.

12. Nielsen, M. B.; Petersen, J. C.; Thorup, N.; Jessing, M.; Andersson, A. S.; Jepsen, A. S.; Gisselbrecht, J.-P.; Boudon, C.; Gross, M., *J. Mater. Chem.* **2005,** *15*, 2599-2605.

13. Ueno, R.; Fujino, D.; Yorimitsu, H.; Osuka, A., *Chem.- Eur. J.* **2013,** *19*, 7156-7161.

14. Roncalli, J., *J. Mater. Chem.* **1997,** *11*, 11-23.

15. Martín, N.; Sánchez, L.; Seoane, C.; Fernández, C., *Synthetic Met.* **1996,** *78*, 137-141.

16. Williams, J. M.; Kini, A. M.; Wang, H. H.; Carlson, K. D.; Geiser, U.; Montgomery, L. K.; Pyrka, G. J.; Watkins, D. M.; Kommers, J. M., *Inorg. Chem.* **1990,** *29*, 3272-3274.

17. Puigmartí-Luis, J.; Laukhin, V.; Pérez del Pino, Á.; Vidal-Gancedo, J.; Rovira, C.; Laukhina, E.; Amabilino, D. B., *Angew. Chem. Int. Edit.* **2007,** *46*, 238-241.

18. Cui, H.; Kobayashi, H.; Ishibashi, S.; Sasa, M.; Iwase, F.; Kato, R.; Kobayashi, A., *J. Am. Chem. Soc.* **2014,** *136*, 7619-7622.

19. Liang, S.; Chen, G.; Zhao, Y., *J. Mater. Chem.* **2013,** *1*, 5477-5490.

20. Rivadehi, S.; Reid, E. F.; Hogan, C. F.; Bhosale, S. V.; Langford, S. J., *Org. Biomol. Chem.* **2012,** *10*, 705-709.

21. Xiong, J.; Cui, L.; Liu, W.; Beves, J. E.; Li, Y.-Y.; Zuo, J.-L., *Tetrahedron Lett.* **2013,** *54*, 1998-2000.

22. Henao-Escobar, W.; Domínguez-Renedo, O.; Asunción Alonso-Lomillo, M.; Julia Arcos-Martínez, M., *Talanta* **2013,** *117*, 405-411.

23. Jia, W.; Bandodkar, A. J.; Valdés-Ramírez, G.; Windmiller, J. R.; Yang, Z.; Ramírez, J.; Chan, G.; Wang, J., *Anal. Chem,* **2013,** *85*, 6553-6560.

24. Belhadj, E.; El-Ghayoury, A.; Mazari, M.; Sallé, M., *Tetrahedron Lett.* **2013,** *54*, 3051-3054.

25. Zhao, B.-T.; Zhu, X.-M.; Chen, X.-H.; Yan, Z.-N.; Zhu, W.-M., *Chinese Chem. Lett.* **2013,** *24*, 573-577.

26. Saha, S.; Flood, A. H.; Stoddart, J. F.; Impellizzeri, S.; Silvi, S.; Venturi, M.; Credi, A., *J. Am. Chem. Soc.* **2007,** *129*, 12159-12171.

27. Fahrenbach, A. C.; Zhu, Z.; Cao, D.; Liu, W.-G.; Li, H.; Dey, S. K.; Basu, S.; Trabolsi, A.; Botros, Y. Y.; Goddard, W. A.; Stoddart, J. F., *J. Am. Chem. Soc.* **2012,** *134*, 16275-16288.

28. Barin, G.; Coskun, A.; Friedman, D. C.; Olson, M. A.; Colvin, M. T.; Carmielli, R.; Dey, S. K.; Bozdemir, O. A.; Wasielewski, M. R.; Stoddart, J. F., *Chem.- Eur. J.* **2011,** *17*, 213-222.

29. Magri, D. C., *New J. Chem.* **2009,** *33*, 457-461.

30. Canevet, D.; Salle, M.; Zhang, G.; Zhang, D.; Zhu, D., *Chem. Commun.* **2009,** *17*, 2245-2269.

31. Frei, M.; Diederich, F.; Tremont, R.; Rodriguez, T.; Echegoyen, L., *Helv. Chim. Acta.* **2006,** *89*, 2040-2057.

32. Zhou, Y.; Zhang, D.; Zhu, L.; Shuai, Z.; Zhu, D., *J. Org. Chem.* **2006,** *71*, 2123-2130.

33. Liu, Y.; Flood, A. H.; Bonvallet, P. A.; Vignon, S. A.; Northrop, B. H.; Tseng, H.-R.; Jeppesen, J. O.; Huang, T. J.; Brough, B.; Baller, M.; Magonov, S.; Solares, S. D.; Goddard, W. A.; Ho, C.-M.; Stoddart, J. F., *J. Am. Chem. Soc.* **2005,** *127*, 9745-9759.

34. Fang, C.-J.; Zhu, Z.; Sun, W.; Xu, C.-H.; Yan, C.-H., *New J. Chem.* **2007,** *31*, 580-586.

35. Schukat, G.; Richter, S. M.; Fanghaenel, E., *Sulfur Reports* **1987,** *7*, 155-240.

36. Steimecke, G.; Sieler, H. J.; Kirmse, R.; Hoyer, E., *Phosphorus and Sulfur* **1979,** *7*, 49-55.

37. Moore, A. J.; Bryce, M. R., *Tetrahedron Lett.* **1992,** *33*, 1373-1376.

38. Zheng, P.; Guo, Y.-J.; Liu, W.; Li, Y.-Z.; Zuo, J.-L.; You, X.-Z., *Transition Met. Chem.* **2008,** *33*, 767-777.

39. Gorgues, A.; Hudhomme, P.; Sallé, M., *Chem. Rev.* **2004,** *104*, 5151-5184.

40. Amriou, S.; Perepichka, I. F.; Batsanov, A. S.; Bryce, M. R.; Rovira, C.; Vidal-Gancedo, J., *Chem.- Eur. J.* **2006,** *12*, 5481-5494.

41. Melchers, R. E. *Corrosion*, **2004**, *60*, 824-837.

42. Sørensen, P. A.; Kiil, S.; Dam-Johansen, K.; Weinell, C. E., *J. Coat. Technol. Res.* **2009,** *6*, 135-176.

43. Hansal, W. E. G.; Hansal, S.; Pölzler, M.; Kornherr, A.; Zifferer, G.; Nauer, G. E., *Surf. Coat. Tech.* **2006,** *200*, 3056-3063.

44. Lee, H.; Scherer, N. F.; Messersmith, P. B., *Proc. Natl. Acad. Sci.* **2006,** *103*, 12999-12003.

45. Ye, Q.; Zhou, F.; Liu, W., *Chem. Soc. Rev.* **2011,** *40*, 4244-4258.

46. Lee, B. P.; Messersmith, P. B.; Israelachvili, J. N.; Waite, J. H., *Ann. Rev. Mater. Res.* **2011,** *41*, 99-132.

47. Kang, S. M.; Hwang, N. S.; Yeom, J.; Park, S. Y.; Messersmith, P. B.; Choi, I. S.; Langer, R.; Anderson, D. G.; Lee, H., *Adv. Funct. Mater.* **2012,** *22* , 2949-2955.

48. Ryu, J.; Ku, S. H.; Lee, H.; Park, C. B., *Adv. Funct. Mater.* **2010,** *20*, 2132-2139.

49. Brubaker, C. E.; Kissler, H.; Wang, L.-J.; Kaufman, D. B.; Messersmith, P. B., *Biomaterials* **2010,** *31*, 420-427.

50. Brubaker, C. E.; Messersmith, P. B., *Biomacromolecules* **2011,** *12*, 4326-4334.

51. Moser, J.; Punchihewa, S.; Infelta, P. P.; Gratzel, M., *Langmuir* **1991,** *7*, 3012.

52. Chen, L. X.; Liu, T.; Thurnauer, M. C.; Csencsits, R.; Rajh, T. J., *J. Phys. Chem. B* **2002,** *106*, 8539.

53. Dalsin, J. L.; Lin, L. J.; Tosatti, S. G. P.; Voros, J.; Textor, M.; Messersmith, P. B., *Langmuir* **2005,** *21*, 640.

54. Rodenstein, M.; Zurcher, S.; Tosatti, S. G. P.; Spencer, N. D., *Langmuir* **2010,** *26*, 16211.

55. Heo, S.-b.; Jeon, Y.-S.; Kim, Y.; Kim, S.; Kim, J.-H., *J. Coat. Technol. Res.* **2013,** *10*, 811-819.

56. Hayashi, K.; Iyoda, J.; Shiihara, I. J., *J. Organomet. Chem.* **1967,** *10*, 81.

57. Reding, M. T.; Buchwald, S. L., *J. Org. Chem.* **1995,** *69*, 7884-7890.

58. Chandrasekhar, S.; Raji Reddy, C.; Jagadeeshwar Rao, R., *Tetrahedron* **2001,** *57*, 3435-3438.

59. Shaikh, N. S.; Junge, K.; Beller, M., *Org. Lett.* **2007,** *9*, 5429-5432.

60. DeClue, M. S.; Siegel, J. S., *Org. Biomol. Chem.* **2004,** *2*, 2287-2298.

61. Maeda, H.; Kasuga, T.; Hench, L. L., *Biomaterials* **2006,** *27*, 1216-1222.

62. Chalk, A. J.; Harrod, J. F., *J. Am. Chem. Soc.* **1965,** *87*, 16-21.

63. Marciniec, B., *Hydrosilylation: a comprehensive review on recent advances.* Springer Science + Business Media: 2009; p 432.

64. Troegel, D.; Stohrer, J., *Coordin. Chem.Rev.* **2011,** *255*, 1440-1459.

65. Safa, K. D.; Tofangdarzadeh, S.; Hassanpour, A., *J. Organomet. Chem.* **2009,** *694*, 4107-4115.

66. Kugel, A.; Chisholm, B.; Ebert, S.; Jepperson, M.; Jarabek, L.; Stafslien, S., *Polym. Chem.* **2010,** *1*, 442-452.

# Chapter 2

# Synthesis and Characterization of DTFs, Their Properties and Reactivities

## 2.1 Introduction

TTFVs are a heavily researched subset of TTFs, owing to their switchable properties with respect to oxidation, and their unique electronic character. As discussed in Section 1.1.6, the interesting behaviours associated with TTFV have been attributed to their conformational switching upon oxidation. Many different TTFVs have been prepared in the literature, often to analyze this conformational change, or to assess dihedral angles in comparable structures, or even simply to investigate the changes in oxidation potential for different TTFVs. Often, TTFV is prepared as an applicable material, again, owing to the highly efficient switching, and potential task-oriented molecules that can be designed from it. However, as yet there has not been a full study on the fundamental behaviours of DTFs and their redox-properties. To this end, not much can be said with certainty when predicting DTF oxidations to TTFVs, or its other properties.

DTFs are oxidized to form TTFVs according to the mechanism shown in Figure 1.12, Section 1.1.6. However, little is known about the factors that affect this mechanism or reaction rate, or that change the pathway entirely. To this end, several different DTFs were designed, as shown in Figure 2.1, synthesized, and then characterized. Furthermore,

their oxidation behaviour was analyzed to determine what factors could be at play in the mechanism, and their voltammetric, UV-Vis absorption spectroscopic, and crystallographic analyses were also performed.

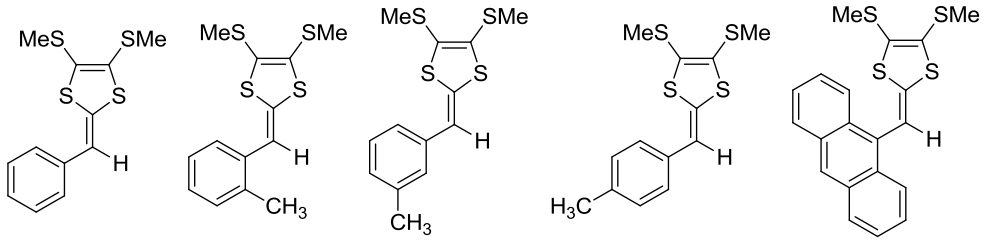


**27** **28** **29** **30** **31**

Figure 2.1 Chemical structures of target simple DTFs.

Previous work in the Zhao group has utilized an *ortho*-bromo DTF to prepare a novel spiro-compound (compound **32**, Figure 2.2).[1] Initially, it was suspected that the bromide might somehow hydrogen-bond to the cations, and inhibit deprotonation. However, as it is a very large atom, it is possible that the bromine could have a steric effect as well. To this end, the above series was devised. **27** should have no steric effects to impact the reaction mechanism, and is likely to proceed normally, but **28** through **30** move a methyl group around the ring, in order to evaluate whether steric interactions can play a role in the reaction mechanism. Finally, **31** may have some steric blocking effect, but is likely more significant that it possesses a large and delocalized electron system.

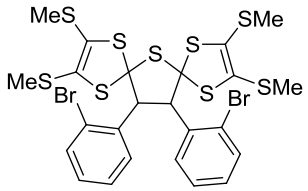


**32**

Figure 2.2 Novel spiro-TTF compound.

The goal of this work is to determine the effect of bulky groups on the aryl substituents, as well as the effect of conjugation and electron delocalization on the dimerization mechanism.

## 2.2 Results and discussion

### 2.2.1 Synthesis and Characterization of Simple DTFs 27-31

#### 2.2.1.1 Retrosynthetic Analysis

The retrosynthetic analysis of DTF **27** is outlined in Scheme 2.1. It is worth noting that this retrosynthesis is the same for all the simple DTFs, compounds **27** – **31**, as all are readily available as purchasable aldehydes from chemical suppliers.

Compound **27** can be broken into two synthons through an olefination reaction between s-methyl thione, **32**, and **33**. *S*-methyl thione **33** is readily accessible through established procedures reported in literature, and benzaldehyde can be purchased.

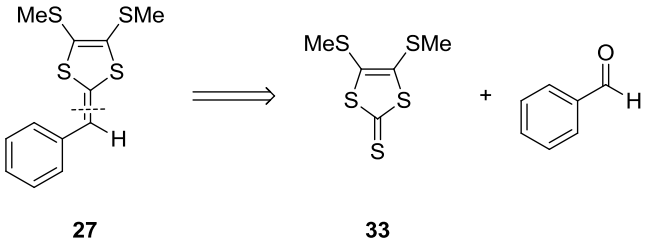


**27** **33**

Scheme 2.1 Retrosynthesis of simple DTF **27**.

### 2.2.1.2 Synthesis of *S*-methyl thione 33

*S*-methyl thione **33** was prepared using known procedures.[2] As presented in Scheme 2.2, the synthesis of *S*-methyl thione **33** began with a reaction in DMF between Na and $CS_2$. Chelation of the dithiolate ion with $Zn^{2+}$ using $ZnCl_2$ in concentrated $NH_3 \cdot H_2O$, followed by precipitation with tetraethylammonium bromide, afforded the red salt **34**, with an overall yield of 67%. The salt was then dissolved and dissociated into the dithiolate in acetone, and reacted with MeI to produce the *S*-methyl thione **33** in 67% yield.

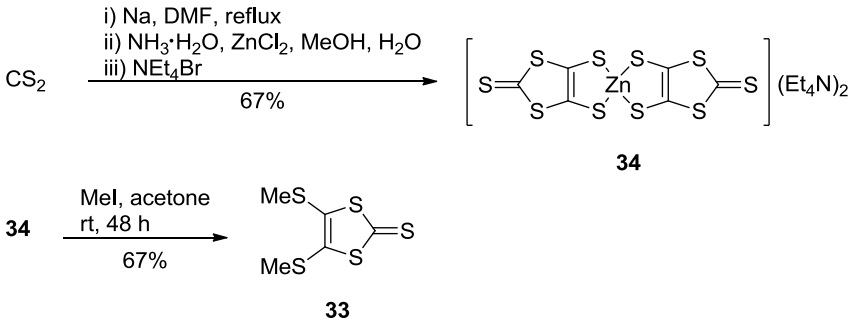


Scheme 2.2 Synthesis of *S*-methyl thione **33**.

#### 2.2.1.3 Synthesis of Simple DTFs 27-31, 35

Phosphite-mediated coupling was an ideal and straightforward means to obtain the target DTFs.[3] In the presence of refluxing trimethyl phosphite, *s*-methyl thione **33** was reacted with precursor aldehydes benzaldehyde, *o*-, *m*-, *p*-tolualdehydes, and 9-anthracenecarboxaldehyde to yield **27**, **28**, **29**, **30**, and **31**, in their respective yields following column chromatography on flash silica (**27, 29, 30, 31**) or recrystallization (**28**) (synthesis presented in Scheme 2.3, yields and times listed in Table 2.1).

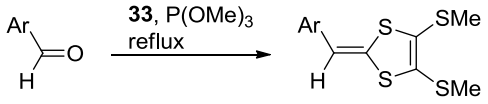


Scheme 2.3 Synthesis of simple DTFs **27**- **31**.

| | Ar | Time (h) | Yield |
|---|---|---|---|
| **27** | 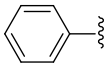 | 12 | 91 |
| **28** | 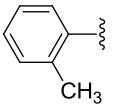 | 3 | 12 |
| **29** | 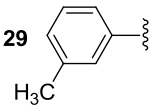 | 1.5 | 60 |
| **30** | 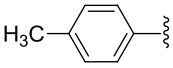 | 1 | 80 |
| **31** | 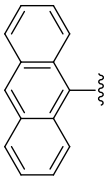 | 5 | 89 |

Table 2.1 Synthetic conditions and resultant yields for **27**- **31**.

Synthesis using mesitaldehyde to yield **35** was also attempted, however, refluxing in trimethyl phosphite only yield the tetra SMe TTF (Figure 2.3). This is likely due to the presence of the two *o*-methyl groups on mesitaldehyde, which restricted the reactivity of the thione carbon.

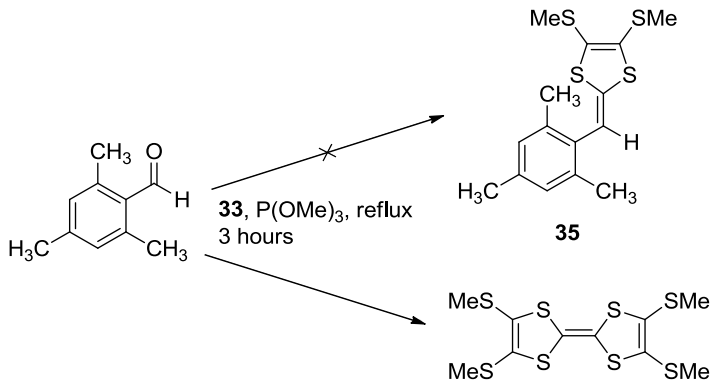


Figure 2.3 Synthetic efforts toward compound **35**.

### 2.2.1.4 Oxidation and Product Characterization of 27, 28 and 30

Iodine-mediated oxidation of **27**, **28** and **30** was attempted, in order to assess the resultant TTFV products. Although it resulted in a poor yield, oxidation of **27** did produce some TTFV (compound **36**, Scheme 2.4). The poor yield is likely attributable to the tedious purification process and the instability of the compound under laboratory conditions, as both **27** and **36** appear to decompose rapidly during purification, leaving little for characterization. This decomposition may be due to radical delocalization, especially to the open *para* site on the phenyl group, where many possible products could form.

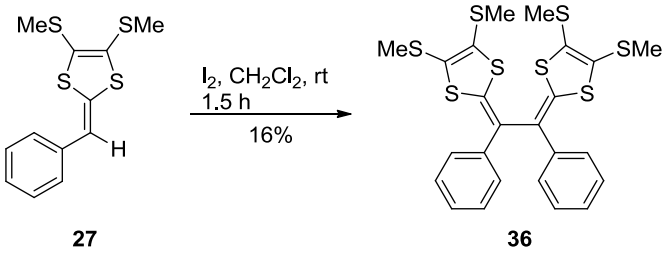


Scheme 2.4 Oxidation of **27**.

After examining the MS, $^{1}$H-NMR, and $^{13}$C-NMR data for the oxidation of **28**, it was clear that it formed a mixture of a TTFV and a spirocompound (Scheme 2.5). It is likely that, were **37** and **38** easily separable, a method could be developed to ascertain the effect of the methyl groups, to grow single crystals, and to assess bond angles and strains, as well as interatomic distances in the solid state.

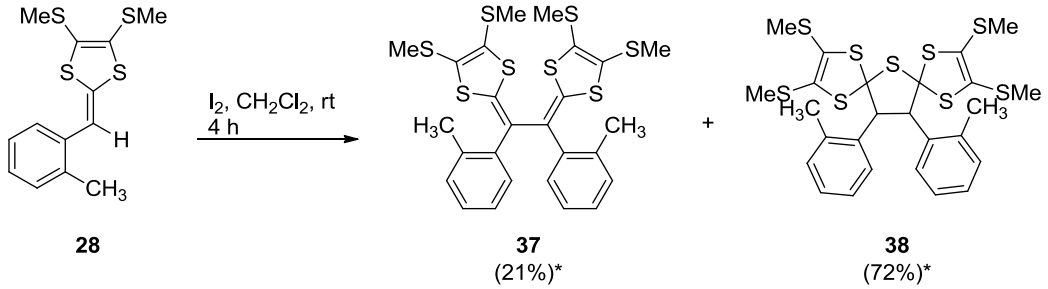


**28** **37** (21%)* **38** (72%)*

Scheme 2.5 Oxidation of **28**. *Yields based on SMe ratio in $^{1}$H NMR

The formation of this mixture is supported by the $^{1}$H NMR, as shown in Figure 2.4. The ratio of the aromatic region, from 7.20 to 6.83 ppm, integrates to 6 H, while the singlet at 4.63 ppm integrates as 1 H. Compound **38** should show 4 H in the aromatic region and 1 H as $H_a$ off the cycle in the centre, but 6 H are observed in the aromatic region, suggesting a rough 1: 2 ratio of **37: 38**. However, it is well-known that the signals of the aromatic region are less reliable for accurate integration due to relaxation time differences. Furthermore, it is not certain that the aromatic region shows protons of only these two compounds, and it may reflect some minute contamination of the sample. To obtain a more accurate estimate of relative distributions of **37** and **38**, the alkyl region is deemed more trustworthy, given that there is no significant signal overlap, and, in particular, the SMe region is considered diagnostic. With respect to the SMe peaks, the

ratio of products is 2.06: 7.19, which reduces to a ratio of 1:3.49 for **37**:**38**. Meanwhile, the *o*-tolyl Me protons show a 0.99: 3.26 ratio, reduced to 1: 3.29. These two ratios are in good agreement, and the aromatic region also somewhat agrees, supporting a roughly 1: 3.39 ratio of **38**:**37**. With this ratio, the estimated yields can be determind to be 21% for **37** and 72% for **38**. The GC-MS spectrum confirms the presence of *m/z* signals that match the molecular ions of **37** and **38**, but does not provide meaningful quantitative measurements.

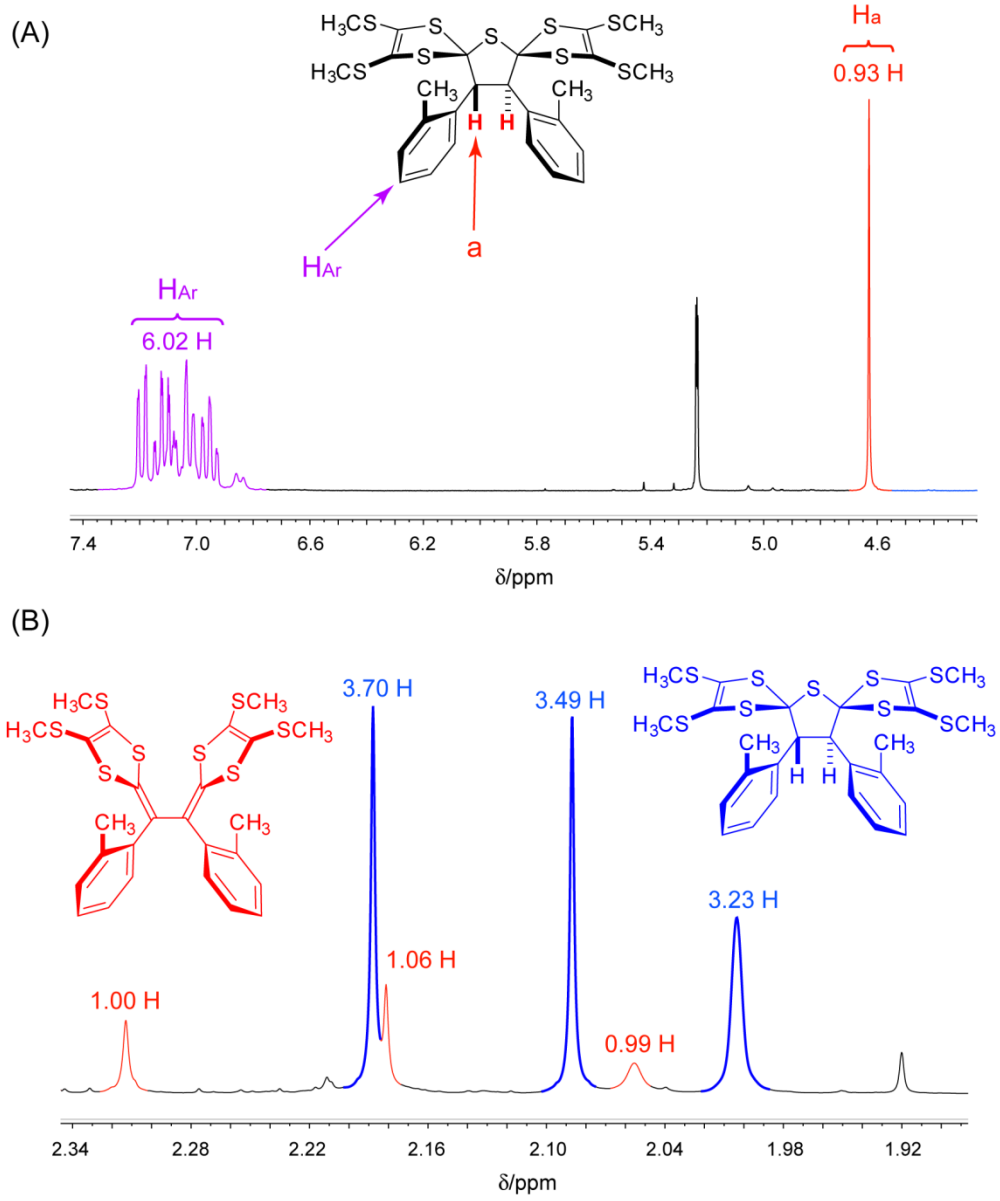


Figure 2.4 $^{1}$H NMR spectrum of **37** and **38** mixture; (a) aromatic region; (b) alkyl region.

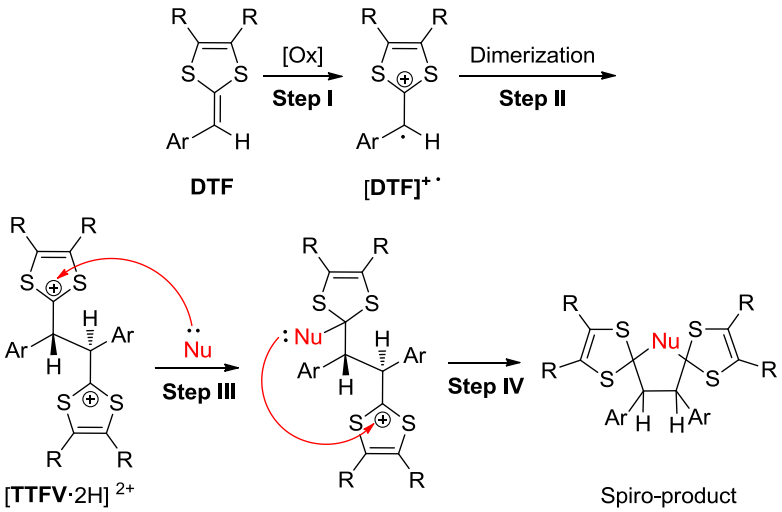


Figure 2.5 Proposed mechanism of spiro-compound formation.

A new possible mechanism that could explain the formation of these products is presented in Figure 2.5, as proposed by the Zhao group. Further experimentation with other *o*-modified aryl substituents on TTFV would enable the mechanism to be validated, or demand an appropriate correction. As can be seen, initially, the mechanism is the same as the typical TTFV formation (Figure 1.12), but at Step III, the paths diverge. While the typical TTFV will follow a radical dimerization and deprotonation pathway, in the case of the spiro-compound, there is likely some steric inhibition, limiting the ability of the base to act. In this case, a nucleophile (for **37**, thiosulfate added in workup) will attack each cation in a stepwise fashion, to create the final product. While still unexplored, this new avenue presents an intriguing methodology for synthesis, as spiro-compounds often possess significant biological activity,[4] and so could be of great interest to the biomedical and pharmaceutical fields.

Meanwhile, compound **30** produced the expected TTFV, **39**, based upon MS, $^{1}$H-NMR, and $^{13}$C-NMR data, in 39% yield (Scheme 2.6).

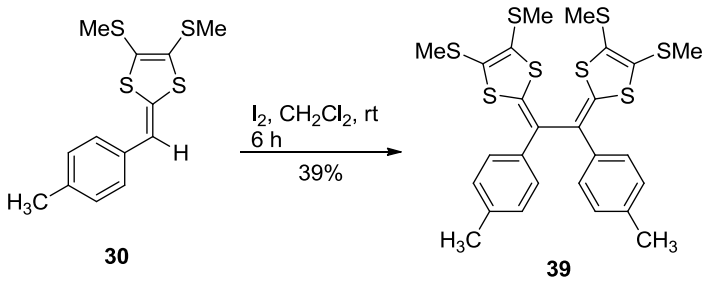


Scheme 2.6 Oxidation of **30**.

### 2.2.1.5 Structural Properties of DTFs 28, 30, 31, and 39; Calculated Geometries of DTFs and Real X-ray Structures of DTFs and a TTFV

Single crystals of DTFs **28**, **30**, and **31** were grown (**31** was grown by former Zhao group student Stephen Bouzan in a leftover sample after completion of his program). **28** was grown slowly in a mixed solvent solution of ethyl acetate and hexanes at 0 °C, and the X-ray crystal structure is presented in Figures 2.6a) and c). Figure 2.6b) shows the DTF-optimized geometries of **28**, with SMe groups omitted for ease of calculation.

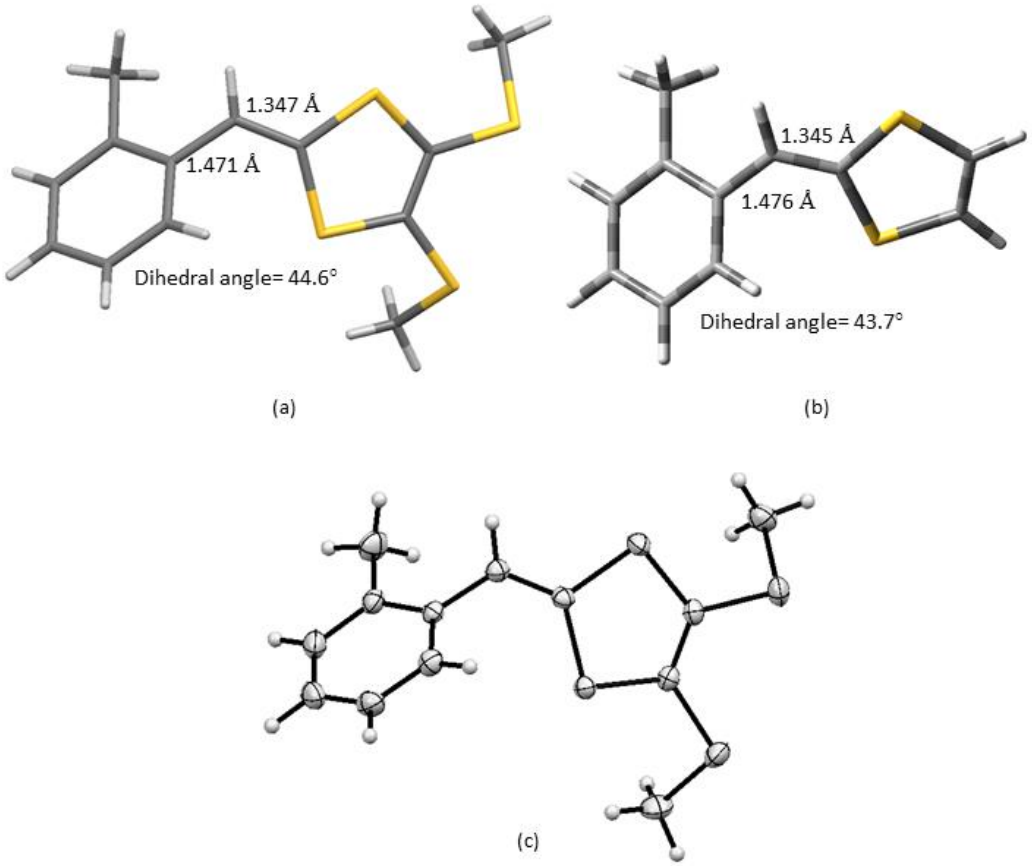


Figure 2.6 (a) Single crystal X-ray structure of **28**, (b) DFT-optimized structure of **28** (Calculations performed at the ω97BXD/6-31G(d,p) level of theory), (c) ORTEP drawing of **28** at 50% probability level.

Compound **28** shows a dihedral angle of 44.6°, as compared to the optimized angle of 43.7°, and the two indicated bond lengths are also very similar, suggesting that DFT can provide a reasonable means of predicting crystal structures of these molecules. In the X-ray structure of **28**, it can be seen that the methyl group of the *o*-tolyl substituent is directed outwards, away from the SMe of the dithiole moiety, as would be expected to minimize steric repulsion. It is likely that these steric restrictions would reduce the

number of available geometries for **28** to take, and thus narrow the possible results when performing calculations. The molecule takes monoclinic packing in the solid state.

Meanwhile, **30** was grown in a mixed solvent of dichloromethane and methanol at 0 °C, and Figures 2.7a) and c) shows the X-ray analysis of the single crystal structure, while Figure 2.7b) shows the DFT-optimized geometry for the molecule.

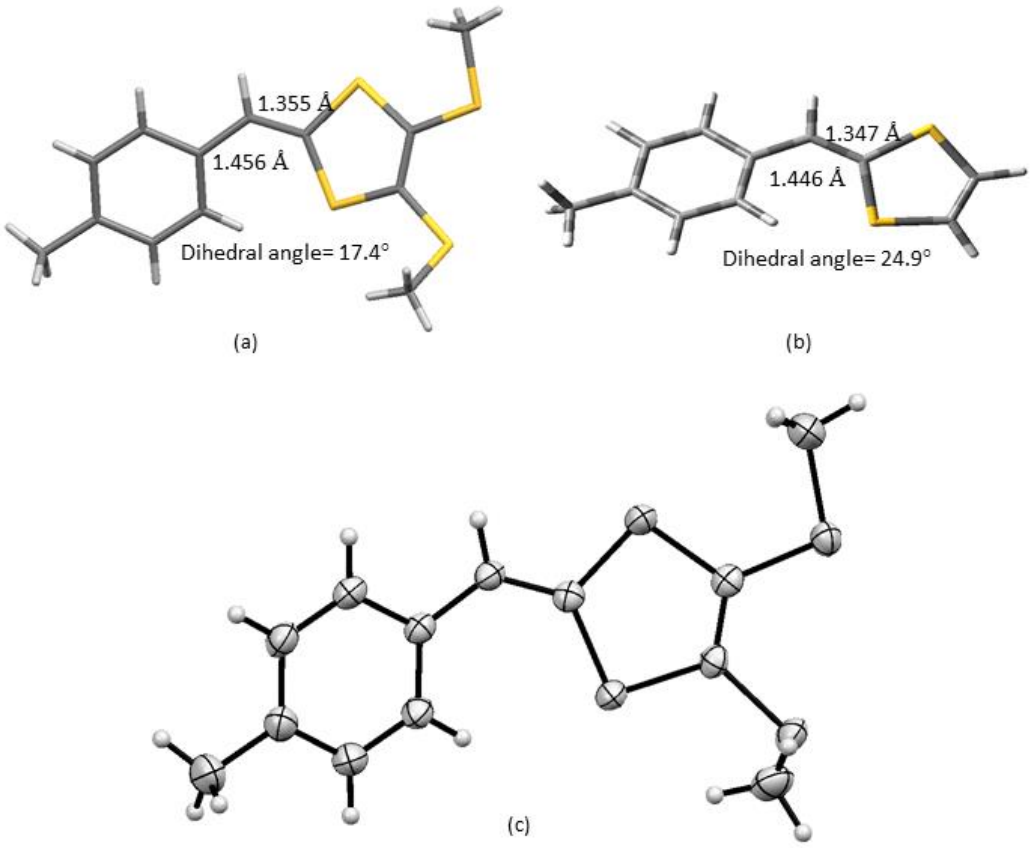


Figure 2.7 (a) Single crystal X-ray structure of **30**, (b) DFT-optimized structure of **30** (Calculations performed at the ω97BXD/6-31G(d,p) level of theory), (c) ORTEP drawing of **30** at 50% probability level.

On comparison, the DFT-optimized structure for **30** appears to fit the experimental data more poorly than did the pair for **28**, especially with respect to the dihedral angle, but it is still acceptable for simple predictive work. It is worth noting that this crystal grew rapidly, in less than 24 hours, and grew with a less than 3% weighted R value. Although this may be attributable to the ease of packing in the bulk solution, with all of the methyl groups on the *p*-tolyl substituent having only one place to go, it may be that the lack of large repulsive interactions between the tolyl protons, the vinylidene proton, and the dithiole moiety opened up more possible geometries for the molecule to take, and thus made the calculations that much less trustworthy. The molecule takes an orthorhombic crystal system.

Compound **31** was grown in dichloromethane at 4 °C by former group member Stephen Bouzan, and the resultant crystal was analyzed by X-ray crystal diffraction. Figures 2.8a) and c) show the single crystal structure of **31**, while Figure 2.8b) presents the DFT-optimized geometry for **31**.

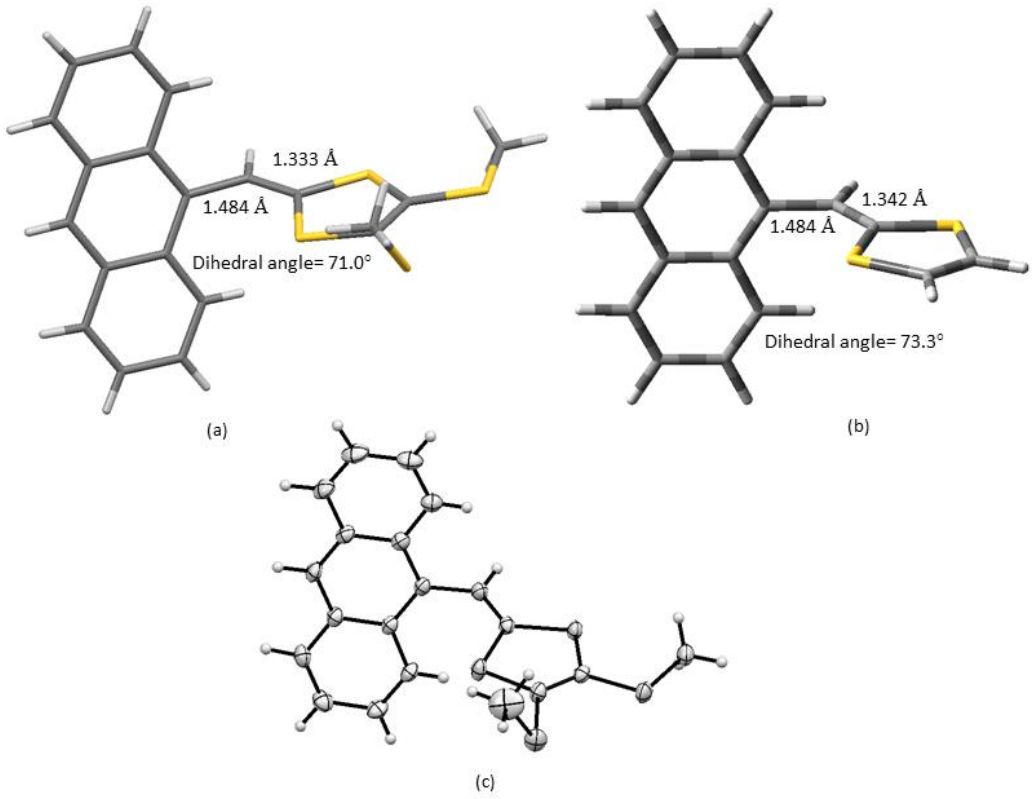


Figure 2.8 (a) Single crystal X-ray structure of **31**, (b) DFT-optimized structure of **31** (Calculations performed at the ω97BXD/6-31G(d,p) level of theory), (c) ORTEP drawing of **31** at 50% probability level.

As can be observed from the simple comparison of Figures 2.8a) and 2.8b), the DFT-optimization remains useful, even in molecules as complex as this. The calculated dihedral angle is very close to the actual one, and the bond lengths are also very close, with one being the same in both the predicted model and the real structure. It is not unimaginable to assume that the accuracy of the calculation on **31** could be due to the rigidity of the anthryl substituent, restricting rotation to around the vinylidene bond. Furthermore, because of the large π-electron cloud around the aromatic moiety, electron-

electron repulsion with the lone pairs of the sulfur could further limit the range of geometries available to **31**.

It is clear that more hindered and "stiff" molecules are more reliably evaluated by DFT-optimization, which may make planning of future targets simpler. In order to improve the theory available, it is necessary to increase the library of "flexible" molecules evaluated, to fully understand their properties in single crystals.

Finally, a crystal of **39** was grown in ethyl acetate and hexanes at 0 °C, and evaluated by X-ray diffraction (Figure 2.9).

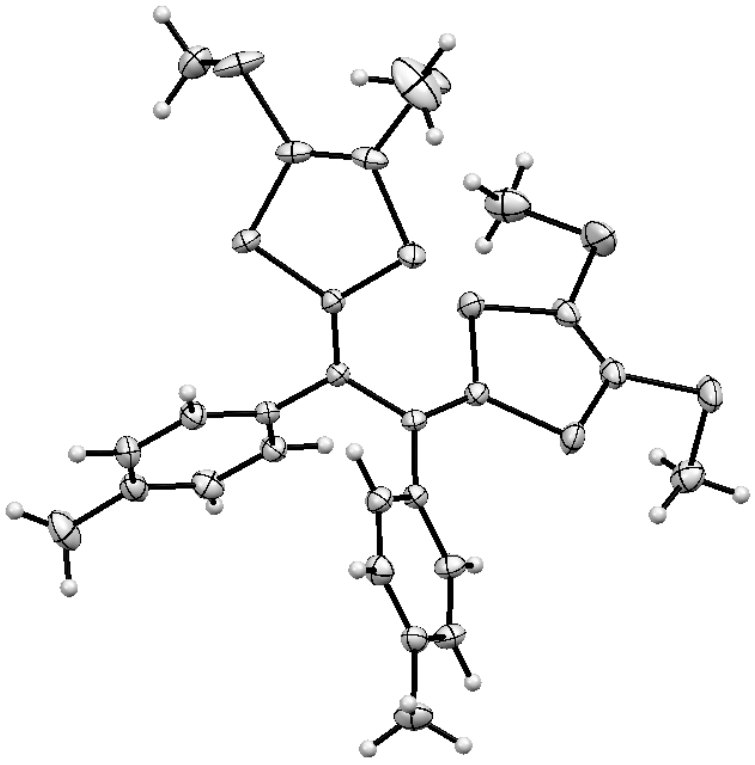

Figure 2.9 ORTEP drawing of **39** at 50% ellipsoid probability.

### 2.2.1.6 Electronic Properties of Simple DTFs 27, 28, 30, 31, and 40

UV-Vis absorption spectra of simple DTFs **27**, **28**, **30**, and **31** were measured, as well as compound **40**, prepared by former group member Guang Chen, and as yet unexplored in this regard (Figure 2.11).

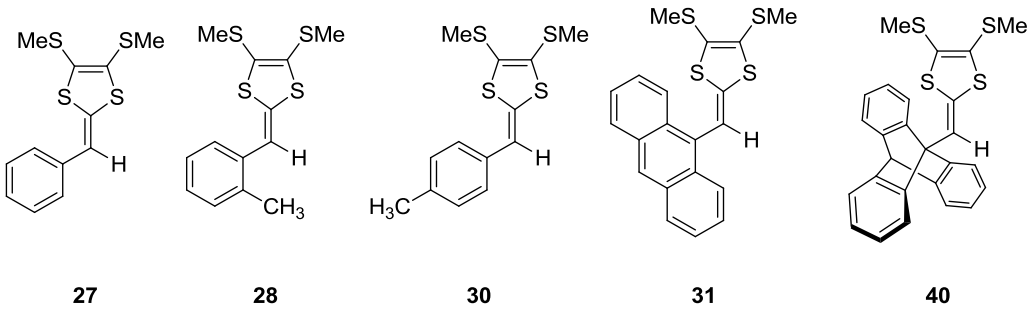


Figure 2.10 Structures of simple DTFs **27**, **28**, **30**, **31**, and **40**.

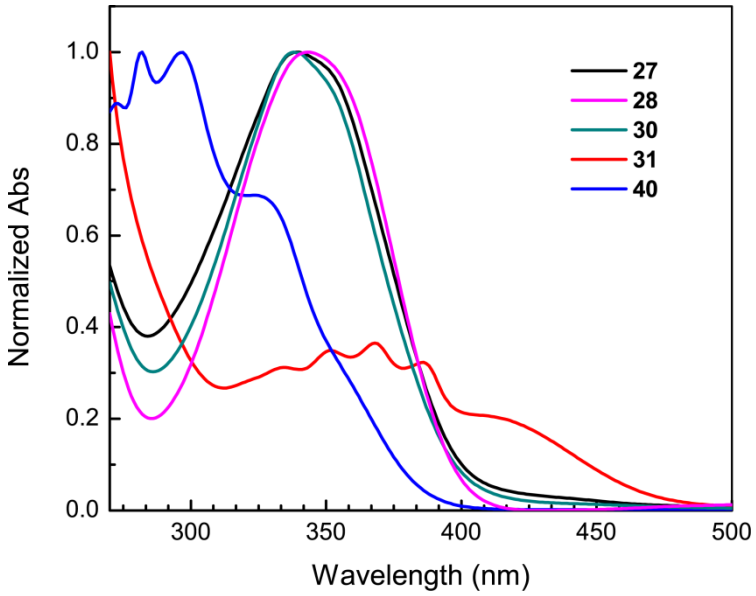


Figure 2.11 UV-Vis spectra of **27**, **28**, **30**, **31**, and **40** measured in $CH_2Cl_2$.

As would be expected, compounds **27**, **28**, and **30** show very similar UV-Vis absorptions. **27** shows an absorption maximum at 339 nm, **28** at 344 nm, and **30** at 338 nm, and all present only one band. When considering compounds **31** and **40**, things become more complicated. Compound **31** exhibits three absorption bands, at 386 nm, 368 nm, and 352 nm, as well as a small shoulder band on each side, at 334 nm and 415 nm. This increase in complexity is likely due to the presence of increased conjugation in the naphthyl moiety. Considering compound **39**, there are two prominent absorption bands at 282 nm and 297 nm, and two shoulders at 273 nm and 325 nm. Again, this is attributable to the complexity of the 9-tripticyl moiety, as compared to the more basic DTFs. The absorptions of the dimers of these DTFs were not considered, as a simple alkyl group like methyl does not impact the long-range conjugation, and thus will not impact the UV-Vis.[5]

#### 2.2.1.7 Electrochemical Redox Properties of 27, 28, 30, 31, and 40

Cyclic voltammetric analyses of **27**, **28**, **30**, **31**, and **40** were performed, and their voltammograms are presented in Figure 2.12.

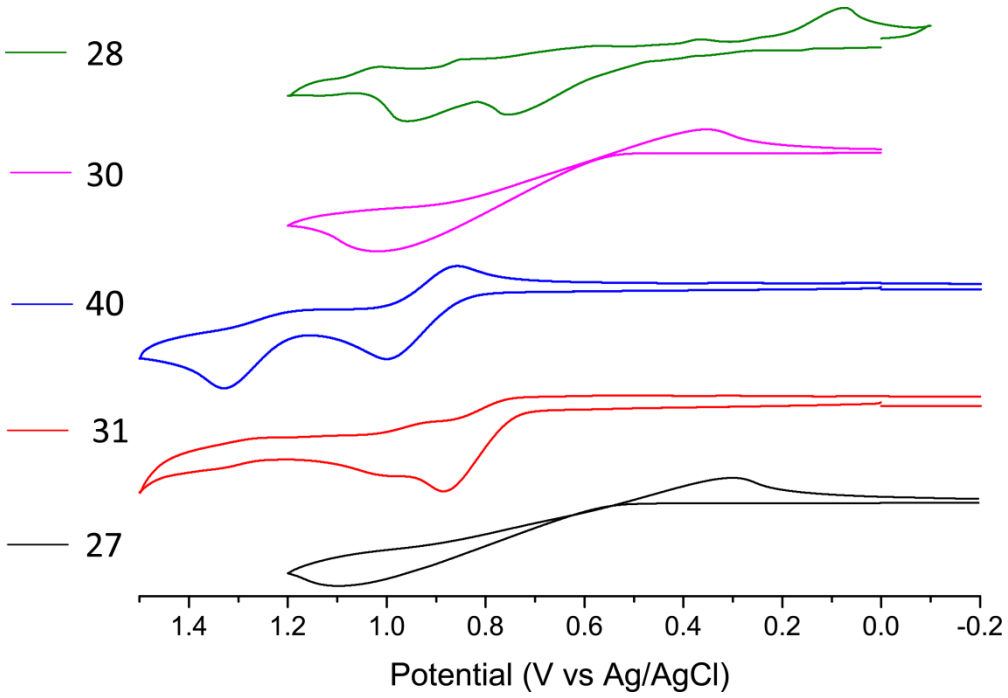


Figure 2.12 Cyclic voltammograms of **27**, **28**, **30**, **31**, and **40** in 1 mM $Bu_4NBF_4$ in $CH_2Cl_2$, glassy carbon as the working electrode, Pt wire as the counter electrode, and Ag/ AgCl as the reference electrode. Scan rate: 100 mV/s.

As can be seen from the above figure, **27** and **30** experience the simple redox couple of DTF – $TTFV^{2+}$, as the generated $DTF^{+\cdot}$ will dimerize to form the TTFV dication rapidly in solution. In comparison, the cylic voltammogram of **28** shows a two-step oxidation and a one-step reduction, suggesting that the initially formed $DTF^{+}$ may convert into another compound, which is again oxidized before being reversibly reduced back to DTF.

In the case of **40**, the first oxidation is the oxidation of DTF, while the second oxidation potential is for the oxidation of the triptycenyl moiety. The sole reduction potential observed is for the quasi-reversible reduction of the $TTFV^{2+}$, which is only quasi-reversible because it appears less intense than the oxidation peak.

Finally, for **31**, there is only an oxidation peak observed, and no paired reduction. This suggests that the radical cation is either unstable or highly reactive, and is consumed before it can form a $TTFV^{2+}$.

#### 2.2.1.8 Spin-density Mapping of Radical Cations of 27, 28, 29, 30, 31, 33, and 40

Spin-density mapping can be a helpful tool in evaluating the density of unpaired electrons on a molecule. To this end, the geometries of **27**, **28**, **29**, **30**, **31**, **33**, and **40** were optimized at the ω97BXD/6-31G(d,p) level of theory, and then spin-density maps prepared. As can be seen in Figure 2.13, while some DTFs carry the radical primarily on the vinylidene carbon, compound **31** has such strong resonance contributors that the radical travels to the *para* position of the ring. This could well account for the lack of further oxidation observed in the CV (Figure 2.12), and one possible cause of the irreversible oxidation may be a coupling between two radical cation **31** molecules to create an aryl-aryl bond.

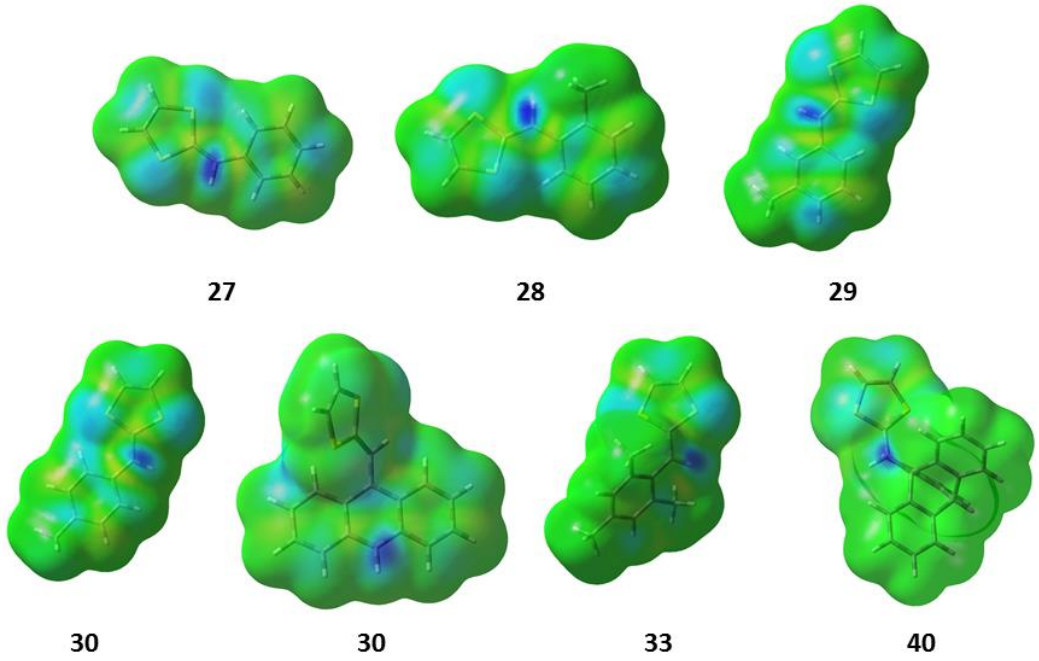


Figure 2.13 Spin-density maps of **27**, **28**, **29**, **30**, **31**, **33**, and **40**. (Optimized at the ω97BXD/6-31G(d,p) level of theory)

#### 2.2.1.9 Summary

A new method for the preparation of thia-spiro-compounds has been found, and an investigation into the key structural features driving such reasons was undertaken. It has been determined that both steric hindrance at the *ortho* site of the aryl substituent and resonance delocalization have an effect on the oxidation behaviours of DTFs, allowing future work to be tailored with this in mind.

## 2.3 Experimental

### General Procedures

Chemicals were purchased from commercial suppliers and used without further purification. All reactions were conducted in standard, dry glassware and under an inert atmosphere of nitrogen. Evaporation and concentration were carried out with a water aspirator, except in the case of vacuum distillation of trimethyl phosphite, in which case a high vacuum pump was used. Flash column chromatography was performed using 240-400 mesh silica gel obtained from SiliCycle. Thin-layer chromatography (TLC) was carried out with silica gel 60 F254 covered on plastic sheets and visualized by UV light. Melting points were measured on an Optimelt automated melting point system, manufactured by Stanford Research Systems. $^{1}$H NMR and $^{13}$C NMR were measured on a Bruker Avance III 300 MHz spectrometer. Chemical shifts are reported in ppm downfield from the signal of the internal reference $SiMe_4$. A single bounce diamond ATR accessory was used on a Bruker Alpha IR spectrometer to obtain all IR spectra. High-resolution mass spectrometric (HRMS) analyses were performed on a GTC Premier Micromass instrument (MS Technology) using atmospheric pressure chemical ionization (APCI). Low resolution LCMS-TRAP analyses were performed using an Agilent 110 series LC and an Agilent 1100 series MSD trap, model G2445D SL. Single crystal X-ray diffraction data for **30** were collected on a Rigaku Saturn CCD area detector equipped with a SHINE optic with $MoK_\alpha$ radiation ($\lambda$= 0.71075Å). Single crystal X-ray diffraction data for **28**, **31**, and **3** were collected in an X-ray facility using a Rigaku SMART6000 CCD detector equipped with a Cu anode generator at McMaster University. UV-Vis

spectra were measured on a Cary 6000i UV-Vis-NIR spectrophotometer. Cyclic voltammetric (CV) experiments were carried out in a standard three-electrode setup controlled by a BASi epsilon workstation.

***p*-Tolyl-TTFV (39).**

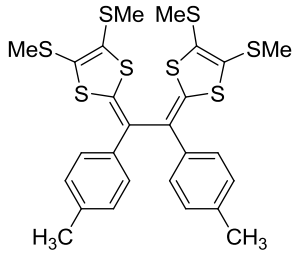


**39**

Compound **30** (86.4 mg, 0.289 mmol) was dissolved in $CH_2Cl_2$ (15 mL). To this, $I_2$ (220.2 mg, 0.860 mmol) was added. The resulting dark green solution was stirred at rt for 6 hours, then quenched with $Na_2S_2O_3$ (20 mL, satd). The contents was left to stir at rt overnight, then the yellow-brown organic layer was separated, washed with $Na_2S_2O_3$ (satd), $H_2O$, and dried over $MgSO_4$, and concentrated under reduced pressure. The residue was dissolved in EtOAc (10 mL) and filtered through a cotton plug, then hexanes (60 mL) was added, and the solution chilled at 0 °C for three weeks. Suction filtration using 0 °C hexanes washes yield **39** (33.4 mg, 0.0561 mmol, 39%) as small, cubic orange-brown crystals. $^1$H NMR (300 MHz, $CD_2Cl_2$) δ 7.38-7.30 (d, *J*=8.2 Hz, 2H), 7.20-7.13 (d, *J*= 8.0 2H), 2.46 (s, 3H), 2.44 (s, 3H), 2.35 (s, 3H); $^{13}$C NMR (75 MHz, $CD_2Cl_2$) δ 137.42, 135.05, 134.67, 129.65, 128.08, 126.91, 125.40, 125.37, 21.32, 19.10, 19.05; FTIR (pure) 3076.40, 3040.63, 3013.37, 2982.86, 2914.30, 1535.26, 1505.94, 1420.49, 1306.98, 1179.17, 1110.22, 955.31, 888.52, 807.65, 759.26, 725.74, 666.01, 534.52,

460.76 $cm^{-1}$ HRMS (EI-TOF, +eV) m/z calculated for $C_{26}H_{26}S_8$ 593.9800, found $M^+$ 593.9792.

**_o_-Tolyl-DTF (37) and _o_-tolyl-spiro-TTFV (38).**

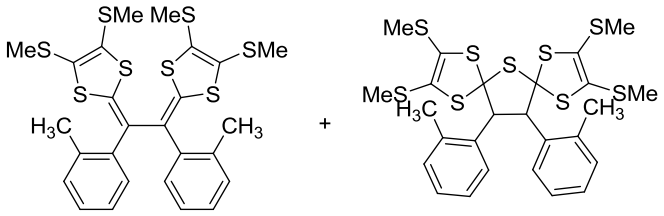


**37** **38**

$I_2$ (0.44 g, 1.72 mmol) was dissolved in $CH_2Cl_2$ (50 mL) and compound **28** (164.3 mg, 0.550 mmol), dissolved in $CH_2Cl_2$ (10 mL), was added dropwise over 30 minutes at rt (three rinses of **28** using $CH_2Cl_2$ (2 mL) were also added), then left to stir at rt for four hours. The resulting solution was then quenched with $Na_2S_2O_3$ (20 mL, satd) and left to stir at rt overnight. The yellow-brown organic layer was separated, washed with $Na_2S_2O_3$, $H_2O$, and dried over $MgSO_4$. Following concentration under reduced pressure, the crude mixture was purified by column chromatography, using 1% EtOAC in hexanes eluent. The fractions with the fewest spots on TLC (a mixture of two major spots and several minor tailing spots) were concentrated in vacuo to yield the mixture of **37** and **38** (0.16 g) as a brown liquid. $^1$H NMR (300 MHz, $CD_2Cl_2$) δ 7.22-6.92 (m, 6H), 4.63 (s, 1H), 2.31 (s, 1H), 2.19 (s, 3H), 2.18 (s, 1H), 2.09 (s, 3H), 2.06 (s, 1H), 2.00 (s, 3H); $^{13}$C NMR (75 MHz, $CD_2Cl_2$) δ 138.45, 133.54, 130.86, 130.75, 130.25, 130.13, 128.86, 128.62, 126.85, 126.77, 126.49, 125.79, 83.75, 60.99, 20.63, 91.57, 19.55, 19.01, 18.93; FTIR (neat) 3057.84, 3018.56, 2951.74, 2918.00, 2854.39, 1735.66, 1419.19, 1236.80, 1044.04,

966.18, 853.45, 730.67 $cm^{-1}$; LC-MS TRAP (APCI, +eV) 594.9 $(M_{37}+H)^+$, 628.9 $(M_{38}+H)^+$.

**Phenyl-TTFV (36).**

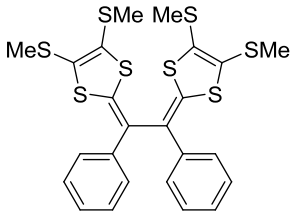


**36**

Compound **27** (246.5 mg, 0.866 mmol) was dissolved in $CH_2Cl_2$ (25 mL). To this, $I_2$ (670.5 mg, 2.62 mmol) was added. The resulting dark green solution was stirred at rt for 1.5 hours, then quenched with $Na_2S_2O_3$ (50 mL, satd). The contents was left to stir at rt overnight, then the yellow-brown organic layer was separated, washed with $Na_2S_2O_3$ (satd), $H_2O$, and dried over $MgSO_4$, and concentrated under reduced pressure to yield a crude product. This was purified by column chromatography in 5% EtOAc in hexanes to yield **36** (82.4 mg, 0.145 mmol, 16%) as a red oil. $^1H$ NMR (300 MHz, $CD_2Cl_2$) δ 7.35-7.30 (m, 2H), 7.23 (m, 2H), 7.11 (m, 1H), 2.33 (s, 3H), 2.31 (s, 3H); $^{13}C$ NMR (75 MHz, $CDCl_3$) δ 137.20, 135.95, 131.29, 128.63, 128.02, 126.93, 126.68, 124.87, 18.90; FTIR (neat) 3050.65, 3024.62, 2981.64, 2914.42, 2848.98, 2819.10, 1520.51, 1493.65, 1420.98, 1308.58, 1027.89, 963.39, 889.27, 754.06, 697.45, 576.17, 465.30 $cm^{-1}$; HRMS (EI-TOF, +eV) m/z calculated for $C_{24}H_{22}S_8$ 565.9487, found $M^+$ 565.9498.

**Anthryl-DTF (31).**

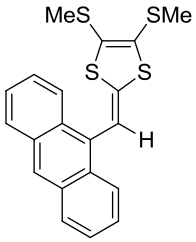


**31**

9-Anthracenecarboxaldehyde (262.9 mg, 1.27 mmol) and **33** (342.3 mg, 1.51 mmol) were dissolved in $P(OMe)_3$ (20 mL) and heated to reflux for 5 hours. At this point, excess $P(OMe)_3$ was removed by vacuum distillation, and the resulting red solution filtered directly through a silica plug (5% EtOAc in hexanes). The filtrate was concentrated under reduced pressure to yield a red syrup, which was further purified by a silica column (hexanes eluent), and concentrated under reduced pressure to yield **31** (434.6 mg, 1.13 mmol, 89%) as a red oil. $^1$H NMR (300 MHz, $CDCl_3$) δ 8.44-8.39 (s, 1H), 8.21 – 8.12 (d, *J*=8.4 Hz, 2H), 8.04 – 7.97 (d, *J*= 7.7 Hz, 2H), 7.53 – 7.42 (m, 4H), 7.10 (s, 1H), 2.48-2.45 (s, 3H), 2.16-2.13 (s, 3H); $^{13}$C NMR (75 MHz, $CDCl_3$) δ 137.35, 131.58, 131.08, 128.93, 128.90, 127.32, 125.96, 125.90, ; FTIR (neat) 3074, 3048, 2992, 2918, 2852, 2822, 1670, 1621, 1570, 1517, 1497, 1440, 1427, 1420, 1346, 1313, 1262, 1157, 1013, 969 $cm^{-1}$; HRMS (EI-TOF, +eV) *m/z* calculated for $C_{20}H_{16}S_4$ 384.0135, found $M^+$ 384.0139.

***p*-Tolyl-DTF (30).**

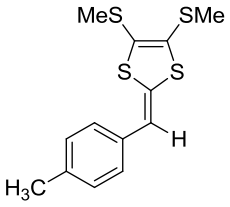


**30**

*p*-Tolualdehyde (300.8 mg, 2.50 mmol) and **33** (669.3 mg, 3.00 mmol) were dissolved in $P(OMe)_3$ (20 mL) and heated to reflux for 1 hour. At this point, excess $P(OMe)_3$ was removed by vacuum distillation, and the resulting orange-brown solution purified by column chromatography (5% EtOAc in hexanes eluent) and then concentrated under reduced pressure to yield **30** (597.5 mg, 2.00 mmol, 80%) as an orange oil. $^1$H NMR (300 MHz, $CDCl_3$) δ 7.19-7.08 (m, 4H), 6.47-6.43 (s, 1H), 2.44-2.42 (s, 3H), 2.41-2.40 (s, 3H), 2.34-2.32 (s, 3H) ; $^{13}$C NMR (75 MHz, $CDCl_3$) δ 135.87, 133.54, 130.53, 129.25, 127.01, 126.78, 124.22, 115.12, 21.26, 19.04, 18.93; FTIR (pure) 3119.30, 3074.05, 3042.40, 3018.17, 2990.55, 2916.62, 2852.61, 2823.58, 2729.66, 1576.33, 1554.53, 1507.56, 1419.46, 1310.59, 967.29, 891.63, 820.13, 510.57 $cm^{-1}$; HRMS (EI-TOF, +eV) m/z calculated for $C_{13}H_{14}S_4$ 297.9978, found $M^+$ 297.9982.

***m*-Tolyl-DTF (29).**

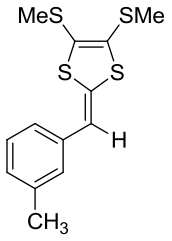


**29**

*m*-Tolualdehyde (0.7015 g, 5.84 mmol) and **33** (1.5597 g, 6.89 mmol) were dissolved in $P(OMe)_3$ (40 mL) and heated to reflux for 1.5 hours. At this point, excess $P(OMe)_3$ was removed by vacuum distillation, and the resulting red solution was purified by column chromatography using 5% EtOAc in hexanes eluent. Concentration under reduced pressure followed by purification by column using pure hexanes eluent yielded **29** (1.0460g, 3.50 mmol, 60%) as a clear yellow oil. $^{1}$H NMR (300 MHz, $CD_2Cl_2$) δ 7.33-7.26 (m, 1H), 7.10-7.02 (m, 3H), 6.53-6.50 (s, 1H), 2.49-2.48 (s, 3H), 2.47-2.46 (s, 3H), 2.42-2.40 (s, 3H) ; $^{13}$C NMR (75 MHz, $CD_2Cl_2$) δ 138.69, 136.59, 132.03, 128.79, 127.86, 127.73, 127.21, 124.46, 124.23, 115.26, 21.64, 19.24, 19.12 ; FTIR (neat) 3087.53, 3035.37, 2989.34, 2916.51, 2729.90, 1560.97, 1418.88, 1310.74, 96.47, 889.88, 805.49, 688.78,473.10 $cm^{-1}$; HRMS (EI-TOF, +eV) m/z calculated for $C_{13}H_{14}S_4$ 297.9978, found $M^+$ 297.9987.

***o*-Tolyl-DTF (28).**

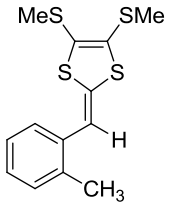


**28**

*o*-Tolualdehyde (2.50 g, 20.8 mmol) and **33** (5.59 g, 24.9 mmol) were dissolved in $P(OMe)_3$ (50 mL) and heated to reflux for 3 hours. At this point, excess $P(OMe)_3$ was removed by vacuum distillation, and the resulting red solution was purified by column chromatography using 5% EtOAc in hexanes eluent, followed by concentration under reduced pressure. The resulting red oil was further purified by column chromatography using 2.5% EtOAc in hexanes, and, following concentration under reduced pressure, the red oil was diluted in EtOAc (30 mL) and hexanes (175 mL) and chilled at 0 °C for five days. Suction filtration with 0 °C hexanes washes yielded **28** (0.7401 g, 2.45 mmol, 12%) as large orange needles. $^1$H NMR (300 MHz, $CD_2Cl_2$) δ 7.37-7.32 (m, 1H), 7.29-7.13 (m, 3H), 6.6.2 (s, 1H), 2.49-2.48 (s, 3H), 2.43-2.42 (s, 3H), 2.33-2.31 (s, 3H) ; $^{13}$C NMR (75 MHz, $CD_2Cl_2$) δ 135.85, 135.76, 133.19, 130.60, 127.09, 126.94, 126.29, 126.25, 124.57, 113.76, 20.10, 19.15, 19.13; FTIR (neat) 2992.57, 2967.67, 2942.42, 2915.41, 1575.57, 1456.16, 1105.82, 889.37, 819.42, 753.15, 501.73 $cm^{-1}$; HRMS (EI-TOF, +eV) m/z calculated for $C_{13}H_{14}S_4$ 297.9978, found $M^+$ 297.9984.

**Phenyl-DTF (27).**

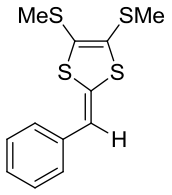


**27**

Benzaldehyde (0.3989 g, 3.76 mmol) and **33** (0.9356 g, 4.14 mmol) were dissolved in $P(OMe)_3$ (30 mL) and refluxed for 3 hours. At this point, excess $P(OMe)_3$ was removed by vacuum distillation, and the resulting red solution was purified by column chromatography using 5% EtOAc in hexanes eluent, followed by concentration under reduced pressure to yield **27** (0.97g, 3.41 mmol, 91%) as a red oil. $^1$H NMR (300 MHz, $CDCl_3$) δ 7.39-7.32 (m, 2H), 7.24-7.14 (m, 3H), 6.49-6.47 (s, 1H), 2.45-2.43 (s, 3H), 2.43-2.41 (s, 3H); $^{13}$C NMR (75 MHz, $CDCl_3$) δ 136.27, 131.95, 128.56, 127.14, 126.82, 125.98, 124.25, 114.91,19.04, 18.93; FTIR (neat) 3096.19, 3077.72, 3050.32, 3023.70, 2988.16, 2951.79, 2916.49, 2847.45, 2821.70, 1595.72, 1577.58, 1557.87, 1493.79, 1452.09, 1419.41, 1310.14, 1133.04, 1068.54, 966.55, 889.10, 831.45, 744.00, 687.97, 583.83, 508.51, 470.60 $cm^{-1}$; HRMS (TOF MS CI, +eV) m/z calculated for $C_{12}H_{12}S_4$ 283.9822, found $M^+$ 283.9834.

**4,5-Bis-(methylthio)-1,3-dithiol-2-thione (33).**

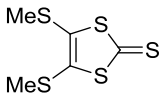

**33**

To a solution of **34** (20.02 g, 27.9 mmol) in acetone (300 mL) was added MeI (15 mL, 240 mmol). The mixture was left to stir at room temperature over 3 days, then suction filtered. The filtrate was concentrated under reduced pressure and dissolved in minimal boiling 25% MeCN in acetone. The resulting solution was chilled at 0 °C overnight, and then yellow-green needles were isolated via suction filtration. These needles were purified by column chromatography using 50% $CH_2Cl_2$ in hexanes eluent to yield a yellow solution, which was concentrated under reduced pressure to afford **33** (8.4817 g, 37.5 mmol, 67%) as large yellow needles. $^1$H NMR (300 MHz, $CDCl_3$) δ 2.50 (s, 1H). The data are consistent with the literature report.[6]

**Bis(tetraethylammonium) bis(1,3-dithiole-4,5-dithiolate)zincate (34).**

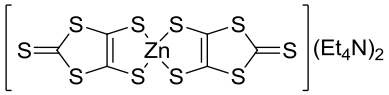

**34**

A mixture of Na (14.73 g, 640 mmol) and $CS_2$ (80 mL, 1.33 mol) was refluxed for 30 minutes. Dried DMF (100 mL) was added dropwise over a period of 30 minutes. The mixture was refluxed for 3 hours and then excess $CS_2$ was removed by vacuum distillation at 45 °C. The reaction was quenched in an ice-water bath with dropwise addition of MeOH (100 mL). After warming back to rt, a solution of $ZnCl_2$ (20.46 g, 150

mmol) in concentrated $NH_3 \cdot H_2O$ (100 mL) was added dropwise to the reaction mixture over 30 minutes. Following this, a solution of $Et_4NBr$ (40.40 g, 192 mmol) in $H_2O$ (40 mL) was added rapidly dropwise over 5 minutes. After 30 minutes of stirring, the mixture was left to stand overnight. Suction filtration with $H_2O$ washes afforded **34** (80.22 g, 0.112 mol) as a red powder. M. P. 203-204 °C. M. P. is consistent with reported data.[2]

### 2.4 References


1. Bouzan, S.; Dawe, L. N.; Zhao, Y., *Tetrahedron Lett.* **2013,** *54* (35), 4666-4669.

2. Steimecke, G.; Sieler, H. J.; Kirmse, R.; Hoyer, E., *Phosphorus and Sulfur* **1979,** *7*, 49-55.

3. Feng, J. M. Eng. Thesis. Memorial University, 2014.

4. Ivanov, A. V.; Svinareva, P. A.; Tomilova, L. G.; Zefirov, N. S., *Russ. Chem. Bull.* **2001,** *50* (5), 919-920.

5. Zhao, Y.; Chen, G.; Mulla, K.; Mahmud, I.; Liang, S.; Dongare, P.; Thompson, D. W.; Dawe, L. N.; Bouzan, S., *Pure Appl. Chem.* **2012,** *84*, 1005-1025.

6. Rathore, R.; Chebny, V. J.; Kopatz, E. J.; Guzei, I. A., *Angew. Chem. Int. Edit.* **2005,** *44* (18), 2771-2774.

# Chapter 3

# Toward Anticorrosive Marine Coating Additives

## 3.1 Introduction

As discussed in Section 1.2 of Chapter 1, corrosion is an important issue for any water-oriented tasks or endeavours. To this end, technology to inhibit that process has been developed, but the problem has not been resolved as yet. A coating layer can effectively resist the process of corrosion on metal surface, but it cannot completely eliminate corrosion, since water or electrolyte solution can still penetrate the coating layer at a slow rate. Once electrolyte solution reaches the metal surface underneath the coating, corrosion begins to take place and the coating loses the protective function. Therefore, one of the major tasks in current anticorrosion coating research is focused on how to increase the effectiveness of the coating protection.

Coating additives are a straightforward approach to augment the performance of a coating, utilizing only a small change in the existing procedures to effect a large improvement in the coating's properties. Additionally, additives are a cost-effective measure to modify coatings, as they can be used in very small amounts, relative to the bulk material. Generally, these additives are used to fine-tune a coating to a particular environment, optimizing the protection afforded for that circumstance.

Preliminary work in the Zhao group[1] has found that eugenol, a molecule related to catechol (compounds **41** and **42**, Figure 3.1), can be readily coupled onto polysiloxane using Speier's catalyst.

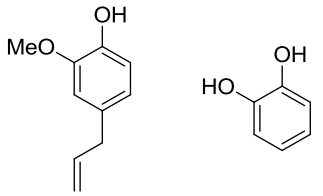


Figure 3.1 Eugenol (**41**) and catechol's (**42**) molecular structures.

The new polymer additives prepared have been analyzed, and found to offer a great improvement in corrosion protection, even with as little as a 1 wt% additive. Polymers **43** and **44** (Figure 3.2) were blended with a conventional epoxy resin, coated on steel test plates, and subjected to corrosion testing for 20 days in 3.5 wt% NaCl solution.

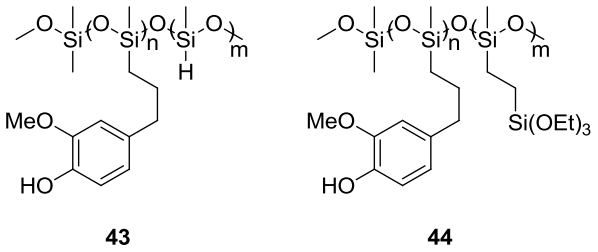


Figure 3.2 Polymers **43** and **44**.

Evaluation of anticorrosion properties was performed using electronic impedance spectroscopy (EIS), which measures the impedance of a surface (acting as a working electrode) in an electrochemical cell. The impedance is the resistance (real) and reactance (imaginary) of a real electrical circuit; only ideal circuits possess purely resistance. EIS

measures the circuit's ability to resist current flow by probing frequency responses to applied small amplitude AC voltages, or, more simply, EIS studies the frequency dependence of the impedance to the applied potential. Through circuit modeling and simulations, circuits can be designed to fit the data. In this way, the number of parts to an impedance signal can be determined, and the individual impedances and behaviours of those parts found.

Through EIS, it was determined from impedance Bode plots that the pure resin offers an impedance of $2.2 \times 10^6$ Ω at 0.1 Hz after 20 days of submersion in 3.5 wt % NaCl solution, while the addition of a 2.5 wt% of **43** has $4.4 \times 10^7$ Ω, and a 1 wt% addition of **44** to the resin shows $1.3 \times 10^8$ Ω. All started higher, but the pure resin started with the lowest initial impedance value, and it decreased the most. Additionally, examination of phase angle Bode plots suggests that electrolyte solution permeates the pure resin coating in just six days, while the coatings bearing additives do not develop new time constants over the course the experiment, and so appear to protect the surface for that time. Furthermore, at the start of the experiment with the **43** additive there are two time constants, possibly attributable to a complex coating with different functional parts. With the **44** additive, a second time constant can be seen, but there are few changes, and so the additive may make the coating more stable or water-resistant, perhaps due to crosslinking of the triethoxysilyl groups.

With these promising results, work must begin to investigate how more hydroxyl groups will affect the additive and coating. This is why this chapter sets out to prepare a polysiloxane additive functionalized with catechol groups. This will detail the progress

thus far to producing such a target (**45**, Figure 3.3), and list the challenges encountered, as well as attempt to explain synthetic difficulties.

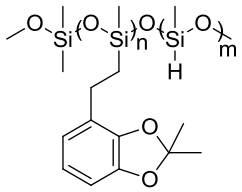

**45**

Figure 3.3 Target polymer molecule, **45**.

## 3.2 Results and Discussion

### 3.2.1 Synthesis toward 45

#### 3.2.1.1 Retrosynthetic Analysis

The retrosynthetic analysis of compound **45** can be found in Scheme 3.1. Polymer **45** can be prepared from vinyl-functionalized catechol (**46**) and PMHS through catalytic hydrosilylation. **46** can be generated using a metal-catalyzed coupling reaction on an iodo-functionalized protected catechol **47**. This, in turn, can be prepared by simple iodination of protected catechol **48**, which is readily produced by reaction of catechol and acetone in the presence of a Lewis acid.

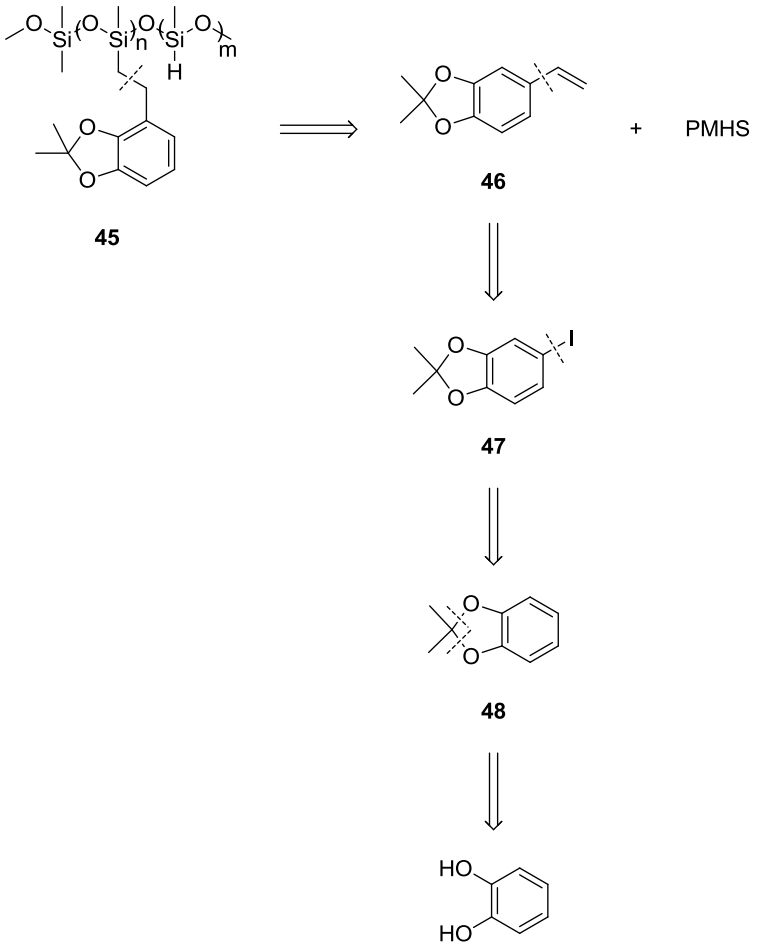


Scheme 3.1 Retrosynthesis of **45**.

### 3.2.1.2 Toward the Synthesis of Vinyl-Functionalized Protected Catechol 46

First, protected catechol **48** was prepared using known procedures.[2] As presented in Scheme 3.2, **48** was made in 75% yield by reaction of catechol with acetone and phosphorus trichloride in benzene. This was then reacted further with iodine in the presence of mercuric acetate as oxidant in dichloromethane to afford **47** in 75% yield.

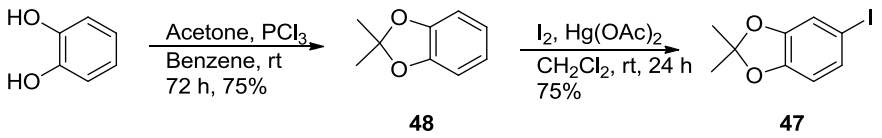


Scheme 3.2 Synthesis of **47**.

From **47**, it was anticipated that a direct Hiyama coupling with triethoxyvinylsilane should afford **46**. In advance of consuming the limited **47**, several test reactions were performed using iodobenzene and *p*-iodoanisole to determine the appropriate conditions. Unfortunately, none of the test reactions afforded any vinyl-functionalized products, as detailed in Scheme 3.3 and Table 3.1.

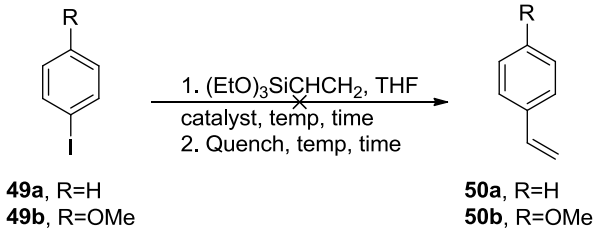


Scheme 3.3 Synthetic attempts toward **50a** and **50b**.

| Trial | **49a/ b** | 1.Temp | 1. h | Cat. (%) | Quench (eq.) | 2. Temp | 2. h | Result |
|---|---|---|---|---|---|---|---|---|
| 1 | **49a** | Reflux | 3.5 | $Pd(PPh_3)_4$ (5%) | NaOH (4) | Reflux | 16 | NMR mess |
| 2 | **49a** | Reflux | 3.5 | $PdCl_2(PPh_3)_2$ (5%) | NaOH (4) | Reflux | 16 | Insoluble product |
| 3 | **49b** | 120 °C (μλ) | 1/6 | $Pd(OAc)_2$ (0.1%) | TBAB (0.5) | Added TBAF at start | | Starting material |
| 4 | **49b** | Reflux | 18 | $PdCl_2$ (2%) | TBAF (1.2) | Added TBAF at start | | Trace, smear in TLC |
| 5 | **49b** | Reflux | 48 | $PdCl_2$ (2%) | TBAF (1/2) | rt | 72 | Starting material |

Table 3.1 Summary of Hiyama conditions attempted toward **50a** and **50b**.

In trials 1 and 2, either an uninterpretable $^1$H NMR spectrum or an insoluble mass resulted. In both cases, no delay was taken before the silane was added to the reaction, and 4 equivalents of sodium hydroxide were used to quench the aryl-silane intermediate, as it has been used in literature[3] and performs the same mechanistic function as fluoride does, by activating the silane for transmetallation. Although Pd(0) cannot enter the aryl-halide bond, some was freshly prepared on hand, so it was considered a worthwhile opportunity just to verify. Later trials with *p*-iodoanisole as the precursor also failed, although it is worth noting that in trial 5, a 30 minute delay was undertaken before the addition of the silane. One unfortunate limitation was the lack of dry diethyl ether, as it is another solvent commonly used for these types of reactions, and might have been able to stabilize any charges or partial charges in the solution. It is possible that if more catalyst systems and varied additions times and temperatures were attempted, the reaction might

proceed as desired, but given the lack of promise in these results, a new approach was required.

The Kumada reaction utilizes palladium(II) insertion into aryl-halide bonds like the Hiyama, however, it uses an aggressive Grignard reagent to add an alkyl, alkenyl, or aryl group in the place of the halide. In these experiments, **47** was used as a precursor, simply to offer more rapid results if the reactions were successful. A summary is presented in Scheme 3.4 and Table 3.2.

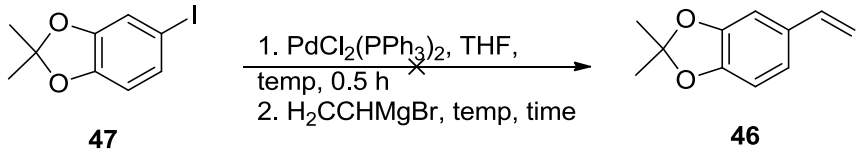


**47** **46**

Scheme 3.4 Synthetic attempts using the Kumada reaction toward **46**.

| Trial | 1.T | Cat. mol % | 2. T | 2. Time | Result |
|---|---|---|---|---|---|
| 1 | rt | 3 | rt | 3 hr | Inextractable water-soluble solid |
| 2 | Reflux | 3 | Reflux | 48 hr | Recovered **47**, possible trace of **46** in $^1$H NMR |
| 3 | rt | 5 | rt | 6 hr | Recovered starting material |

Table 3.2 Summary of Kumada conditions attempted toward **46**.

Again, the Kumada reaction was found to be unsuccessful. There was some promise in the $^1$H NMR for trial 2, but column chromatography could not separate the two products, and the experiment could not be repeated. Diethyl ether would have been an ideal

solvent, as it is well-known to stabilize Grignard reagents, but the anhydrous solvent is both tedious and dangerous to prepare, and costly to order. Both of these difficulties would make this synthesis cost-prohibitive on an industrial scale, and so another approach had to be taken.

Upon further consideration, a two-step process utilizing a formylation of the protected catechol **48** followed by a single Wittig reaction was conceived. Initially, direct attempts were made to formylate **48**, utilizing the Vilsmeier–Haack and Reiche reactions (presented in Schemes 3.5 and 3.6, respectively), to obtain **51**.

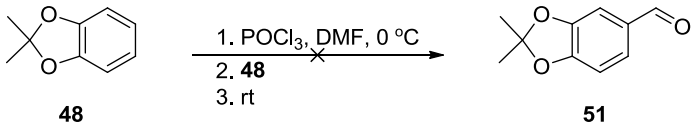


Scheme 3.5 Synthetic attempt toward **51** using Vilsmeier–Haack conditions.[4]

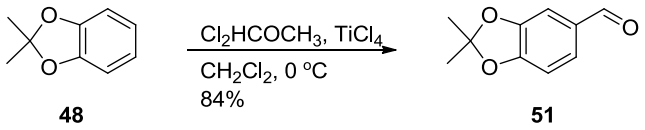


Scheme 3.6 Synthesis of **51** using Rieche conditions.[5]

The Vilsmeier–Haack reaction was unsuccessful in direct formylation of **48**, however, pleasantly, the Rieche reaction worked, with very simple workup to a pure product and excellent yield. Disappointingly, the dichloromethyl methyl ether was extremely expensive, and so other approaches were required to obtain **51** on large scale. At the least, the Rieche formylation provided **51** for characterization and TLC purposes for future experiments.

Few other direct methods are available for the formylation of an aryl compound, but there are many permutations of the butyl lithium formylation of an aryl halide. Bearing this in mind, **47** was readily converted to **51** using butyl lithium to generate a lithiated species, which then reacted with DMF (Scheme 3.7).

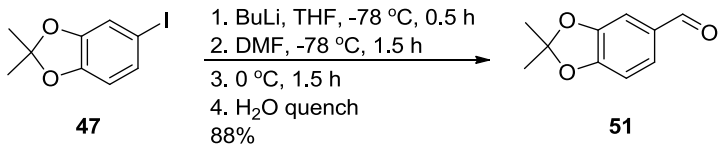


Scheme 3.7 Butyl lithium formylation of **47**.

Although the butyl lithium formylation offered a higher yield for that reaction than the Rieche reaction (88% versus 84%), the overall yield of the iodination and subsequent butyl lithium formylation is only 66%, and requires a tedious recrystallization to purify the iodocatechol, as well as the use of costly iodine and mercuric acetate. It is reasonable to assume the costs balance out, including the cost of labor, but this is an interesting note. In spite of efforts to reduce the cost of this synthesis for cheap anticorrosion coating additives, certain steps will unavoidably require expensive reagents or workup. In the event of scale-up for industry, it is probable that the Rieche reaction would be a better choice, as it would require less man hours and offer a higher yield, although it working with pure titanium(IV) chloride in large quantities would require special staff safety training.

Once **51** had been obtained successfully, the sole remaining intermediate before **45** was the vinyl-functionalized protected catechol, **46**. Preparation was attempted using a single

Wittig reaction, with butyl lithium and tetramethylphosphonium bromide in THF (Scheme 3.8, Table 3.3).

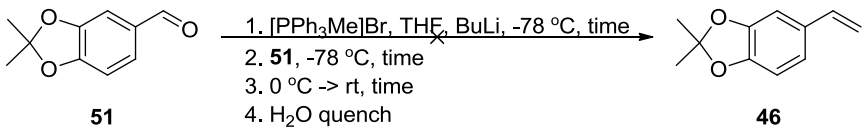


Scheme 3.8 Synthetic attempts towards **46** using single Wittig reaction.

| Trial | 1.Time | 2. Time | 3. Time | Result |
|---|---|---|---|---|
| 1 | 1 hr | 6 hr | 48 hr | Product present in GC-MS, but still very impure ($^1$H NMR) after column chromatography |
| 2 | 0.5 hr | 1 hr | 16 hr | Product decomposed on column, resulting in "smear" TLC |

Table 3.3 Summary of Wittig conditions attempted toward **46**.

On both attempts to prepare this compound, new spots appeared on the TLC during the reaction, but upon aqueous workup and column purification, other spots formed, suggesting that the product **46** is very unstable, or sensitive to oxidation. It is possible that in the presence of radical initiators, or an oxidizing environment, the molecule behaves like styrene and polymerizes into complex polymers, which could explain the "smearing" observed on TLC after column. Alternatively, it may be that, in the presence of acid, as found on silica, the electron-rich alkene is protonated, resulting in a stabilized cation that could undergo addition reactions and the like. Another potential problem could be cyclization through the electron-rich diene, such as a Diels–Alder reaction. Although the correct mass could be detected in GC-MS from trial 1, no $^1$H NMR spectrum could be obtained that contributed significantly to the determination, and in any case, only traces of products could be collected from the column. Although there are

peaks in the alkenyl region of the $^{13}C$ NMR, this is hardly definitive, and can be simply considered a supporting piece of information. There is no doubt that the compound can be prepared, but it is likely highly unstable to typical work up or benchtop conditions.

Finally, it is likely that either the Hiyama or Kumada reactions should be revisited, as they may be able to be optimized for this molecule, and would hopefully require less tedious workup and present fewer workup opportunities for the product to react further. A preparation of a related molecule, with less atom efficiency, but an alkyl "break" between the vinyl and aryl moieties, might prove more stable, as in the case of eugenol, found in nature and easily isolated in the lab. This would entail the exploration of techniques such as a Friedel–Crafts reaction, which might bring up new challenges, but it also holds promise as a viable solution.

#### 3.2.1.3 Summary

The target compound, **45**, has yet to be prepared and tested. In spite of this, a great deal has been learned about the synthetic route that will successfully form it. Numerous reactions have been investigated for this target, and although some did not work, it is likely that with further experimentation a path can be developed. In particular, the optimization of the Kumada reaction holds appeal, for it could provide a quick and cheap avenue to the vinyl-functionalized protected catechol **46**, or a new approach to disconnect the vinyl group from the electron-donating catechol species. If the Rieche reagent became less costly and the Wittig reaction could be improved, that methodology could serve, as well. These reactions must proceed well in order for **45** to ever be a viable additive in

industrial scale coatings, and much work remains to be done. Doubtless this project will be highly valuable to both academia and industry upon completion, and might even help to elucidate the mechanism of catechol binding, with comparative studies using a protected and a non-protected catecholic polysiloxane derivative.

## 3.3 Experimental

### General Procedures

Chemicals were purchased from commercial suppliers and used without further purification. All reactions were conducted in standard, dry glassware and under an inert atmosphere of nitrogen. Evaporation and concentration were carried out with a water aspirator, except in the case of vacuum distillation of trimethylphosphite, where a high vacuum pump was used. Flash column chromatography was performed using 240-400 mesh silica gel obtained from SiliCycle. Thin-layer chromatography (TLC) was carried out with silica gel 60 F254 covered on plastic sheets and visualized by UV light. Melting points were measured on an Optimelt automated melting point system, manufactured by Stanford Research Systems. $^{1}$H NMR and $^{13}$C NMR were measured on a BrukerAvance III 300 MHz spectrometer, except in the case of **49**, which was taken on a BrukerAvance 500 MHz spectrometer. Chemical shifts are reported in ppm downfield from the signal of the internal reference $SiMe_4$. A single bounce diamond ATR accessory was used on a Bruker Alpha IR spectrometer to obtain all IR spectra. High-resolution mass spectrometric (HRMS) analyses were performed on a GTCPremier Micromass instrument (MS Technology) using atmospheric pressure chemical ionization (APCI). Gas

chromatography mass spectra were obtained on an Agilent6890N gas chromatograph using an Aglient 5973 *inert* mass spectrometer. The column was an Agilent J&W DB-5MS, 30m long, 0.5mm diameter, with 0.25 μm film thickness.

**2,2-Dimethylbenzo[*d*][1,3]dioxole-5-carbaldehyde (51).**

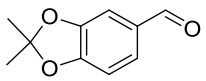

**51**

Compound **47** (1.8119 g, 6.54 mmol) was dissolved in THF (40 mL) and chilled while stirring at -78 °C for 15 minutes. Butyl lithium (5.25 mL, 2.5 M, 13.1 mmol) was added dropwise at -78 °C over 5 minutes, and the reaction left to stir for 30 minutes. Dry DMF (1 mL, 12.9 mmol) was added dropwise at -78 °C over 5 minutes, and the reaction left to stir at -78 °C for 1.5 hours. The reaction was moved from a dry ice-acetone bath to an ice-water bath and warmed to 0 °C for 1.5 hours. Excess butyl lithium was quenched with dropwise addition of water at 0 °C, after which the reaction mixture was concentrated under reduced pressure. The resultant off yellow oil and clear colorless solution was extracted with ethyl acetate. The extractions were combined and washed with water, then dried over $MgSO_4$. Evaporation of ethyl acetate at reduced pressure afforded **51** (1.0285 g, 5.78 mmol, 88%) as a clear yellow oil.

Compound **48** (247.1 mg, 1.65 mmol) was dissolved in $CH_2Cl_2$ (15 mL) and chilled in an ice-water bath to 0 °C. $Cl_2HCOCH_3$ (0.2 mL, 2.26 mmol) and subsequently $TiCl_4$ (0.25 mL, 2.28 mmol) were added, and the reaction left to stir at 0 °C for 30 minutes. The reaction was quenched at 0 °C with dropwise addition of $NH_4Cl$, the separated, and the

organic layer washed with $H_2O$ and dried over $MgSO_4$. Evaporation of solvent afforded **51** (243.6 mg, 13.7 mmol) as a dark yellow oil.$^1$H NMR (300 MHz, $CDCl_3$) δ 9.79 (s, 1H), 7.39-7.35 (dd, *J* = 7.9 Hz, 1.6 Hz, 1H), 7.27-7.24 (d, *J* = 1.7 Hz, 1H), 6.84 (d, *J* = 7.9 Hz, 1H) 1.71 (s, 6H); $^{13}$C NMR (75 MHz, $CDCl_3$) δ 190.43, 153.04, 148.50, 131.44, 128.37, 119.79, 108.18, 106.77, 25.96; FTIR (neat) 3076.94, 2992.31, 2938.19, 2834.55, 2787.98, 2737.07, 2713.06, 2619.72, 1684.88, 1599.06, 1489.96, 1448.67, 1378.14, 1358.26, 1255.25, 1213.23, 1147.79, 1068.71, 979.71, 831.10, 809.00, 783.33 $cm^{-1}$; HRMS (EI, TOF, +eV) *m/z* calculated for $C_{10}H_{10}O_3$ 178.0630, found $M^+$ 178.0639.

**5-Iodo-2,2-dimethylbenzo[*d*][1,3]dioxole (47).**

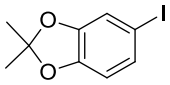

**47**

Compound **48** (9.25 g, 61.6 mmol) was diluted in $CH_2Cl_2$ (300 mL), and then $I_2$ (17.36 g, 67.8 mmol) and $Hg(OAc)_2$ (21.86 g, 68.5 mmol) were dissolved in the solution. The reaction was left to stir at rt for 24 hours. At this time, the reaction solution was filtered through a pad of diatomaceous earth, and the clear pink filtrate concentrated under reduced pressure to yield a white solid in brown solution. The solid was dissolved in MeOH and chilled at −78 °C until thick white solid formed. This was isolated by suction filtration with −78 °C MeOH washes to yield **47** (12.76 g, 46.1 mmol, 75%) as a white solid.$^1$H NMR (300 MHz, $CDCl_3$) δ 7.11-7.07 (dd, *J*= 8.1, 1.7 Hz, 1H), 7.03-7.01 (d, *J*- 1.7 Hz, 1H), 6.53-6.47 (d, *J*= 8.1 Hz, 1H), 1.66 (s, 6H); $^{13}$C NMR (75 MHz, $CDCl_3$) δ 148.57, 147.65, 129.99, 118.78, 117.46, 110.35, 81.47, 25.84; FTIR (pure) 3095.70,

3072.92, 3044.783, 2992.37, 2936.12, 1489.60, 1376.93, 1232.00, 974.70, 863.85, 826.42, 795.82, 653.21, 574.87, 508.55 $cm^{-1}$; HRMS (EI, TOF, +eV) m/z calculated for $C_9H_90_2I$ 275.9647, found $M^+$ 275.9659; M. P. 44.9-46.0 °C.

**2,2-Dimethylbenzo[*d*][1,3]dioxole (48).**

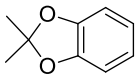

**48**

Catechol (33.1266 g, 0.301 mol) and acetone (29 mL, 0.396 mol) were combined in benzene (120 mL) at rt. To this, $PCl_3$ (11 mL, 0.124 mol) was added dropwise over 30 minutes, and the reaction left to stir at rt over 3 days. This was poured over $K_2CO_3$ (50 g, 0.362 mol) in $H_2O$ (100 mL), and suction filtered to remove solid residue. The filtrate was separated, and the organic layer washed with KOH (15 v/v%) and $H_2O$, then dried over $MgSO_4$. Evaporation under reduced pressure afforded **48** (33.9773 g, 0.226 mol, 75%) as a clear yellow oil. $^1H$ NMR (500 MHz, $CDCl_3$) δ 6.76 (m, 4H), 1.67 (s, 6H). The data are consistent with literature report.[6]

### 3.4 References


1. Feng, J. M. Eng. Thesis. Memorial University, 2014.

2. Ivanov, A. V.; Svinareva, P. A.; Tomilova, L. G.; Zefirov, N. S., *Russ Chem Bull* **2001,** *50*, 919-920.

3. Alacid, E.; Najera, C., *J. Org. Chem.* **2008,** *73*, 2315-2322.

4. Pittelkow, M.; Nielsen, C. B.; Brock-Nannestad, T.; Shau-Magnussen, M.; Christensen, J. B., *Eur. J. Org. Chem.* **2012**, 4931-4936.

5. Shi, J.-P.; Wu, D.-L.; Ding, Y.; Wu, D.-H.; Hu, H.-W.; Lu, G.-Y., *Tetrahedron* **2012,** *68*, 2770-2777.

6. Rathore, R.; Chebny, V. J.; Kopatz, E. J.; Guzei, I. A., *Angew. Chem. Int. Edit.* **2005,** *44*, 2771-2774.

# Chapter 4

# Summary and Future Work

Through the course of this thesis, a series of DTFs, **27** to **31**, has been synthesized using the one-pot olefination reaction, involving in situ generation of phosphonate ester by reacting thione and trialkyl phosphite and subsequent Horner-Wittig reaction with an aldehyde. The resulting yields varied greatly, from 12 to 91%. The low yields are mainly caused by either poor product stability or significant side reactions. These problems often led to difficult or tedious purification tasks, such as the determination of recrystallization conditions, or the use of a series of column purifications to obtain pure products. One the one hand, recrystallization tends to afford highly stable crystals that are resistant to heat, light, and air, on the other hand, the concentrates of column fractions, even if as pure as the crystal according to NMR, tend to decompose rapidly. The exceptions to this are **30** and **31**, which can remain relatively stable in the fridge for several months, but **27**, **28**, and **29** all degrade further, even protected from heat and light, and purged with nitrogen gas. In future work, efforts should be directed toward reaction conditions optimizing recrystallization yields and affording stable products. This would facilitate large scale syntheses, and eventually make DTF compounds useful in practice for applications in materials industries.

The reactivity towards oxidative dimerization of these DTFs was evaluated, and it was observed that, for those that could accomplish the reaction, the yields were again diverse.

The oxidation of **30** afforded **39** in 39% yield after recrystallization, and the crystals, as observed in the DTFs, were stable under benchtop conditions. However, in the oxidation of **27**, the product **36** was obtained in a mere 16% yield, as the compound appeared to degrade over the course of column purification. It may be that these challenges in workup and purification are at least somewhat to blame for the dearth of earlier research around DTF reactivity towards oxidative dimerization, as the compounds are costly to prepare in both time and materials. As can be seen in the oxidation of **28**, while some information can be derived from the experiment, the inability to purify the reaction mixture by either column chromatography or recrystallization after many attempts would be discouraging to anyone exploring similar topics.

From these studies, it is found that oxidative dimerization of DTFs to TTFVs depends on two major and universal effects; that of steric interactions, and that of resonance delocalization.

As observed with the *o*-bromophenyl DTF, previously prepared by a former group member, Stephen Bouzan, the presence of an *ortho* substituent on the aryl moiety affects and modifies the mechanism of dimerization. In that case, it was unclear if the change was due to sterics or the electronic inductive effect of the bromine atom, or a combination of the two. With the addition of the *o*-tolyl DTF, **28**, a pure steric influence was observed, and the mechanism was similarly changed, although not to the same degree. From these experiments, it is clear that sterics do play a role in the mechanism of dimerization, but that induction also influences things, as *o*-tolyl DTF produced a mixture of TTFV and the spiro-product, while *o*-bromophenyl DTF yielded only the spiro-product. The effect of

resonance can be seen in **31**, which fails to dimerize, due to electron delocalization on the DTF radical cation. It is reasonable to state that if the spin-density is not on the vinylidene carbon in predictive DFT calculations, it is highly unlikely that dimerization will occur with that species, and, as a result, the starting material may be lost in the formation of an undesired byproduct. Most certainly, further investigation and the preparation of new model compounds will aid in ascertaining the relative significances of these factors, and allow better prediction of products in future. It may be that *ortho* substitutions should be performed after the preparation of a TTFV to prevent spiro-product formation, or that non-conjugated DTF precursors should be used for TTFV dimerization, followed by reduction to afford the target.

In the preparation of a novel catechol-functionalized polysiloxane, numerous synthetic obstacles were encountered. While there are doubtless other methods available to achieve the target than those explored here, it is essential that the final synthesis be cost-effective for industrial scale processes, and so only the least expensive of methods have been attempted. Furthermore, new approaches to bulk material preparations such as these are much preferred to be environmentally friendly, or "green", prohibiting the use of toxic reagents or the formation of harmful workup wastes.

Furthermore, the instability of the target molecule **46** has been found to be one of the greatest challenges with this synthesis. It may be that the vinyl group can be protonated readily, as it is an electron-rich alkene, resulting in many possible addition reactions. The presence of a diene could trigger cyclization, such as a Diels-Alder reaction, further complicating the reaction or workup mixture. Finally, there is a risk of oxidation or

interaction with any trace radical initiator generating complex polymers or polymer mixtures. It is clear that this molecule, while highly atom efficient, is not a reasonable target for industrial scale preparation, and so new avenues must be considered.

It is possible that, with the addition of an $sp^3$ carbon between the protected catechol and the vinyl groups, the lack of conjugation would allow the vinyl group to be stable, as in the case of the naturally occurring molecule eugenol. This new molecule (compound **52**, Figure 4.1), which should be able to be hydrosilylated, will be useful not just in anticorrosion work, but potentially also in the medical and surface modification fields, as it could be bonded to a target easily using coupling chemistry, and transfer its adhesive qualities to the final product.

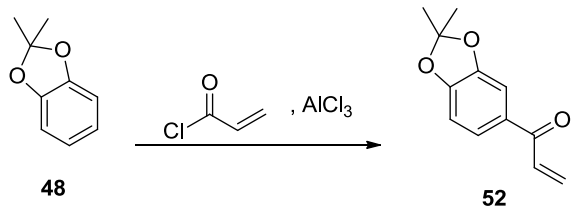


Figure 4.1 New catechol target, compound **52**.

Finally, the preliminary synthesis of a dialkyne linked π-exTTFV (compound **53**, Figure 4.2) has been performed, using the methodology laid out by former group member Dr. Guang Chen.[1] The sole exception to this method was a minor change in the homocoupling catalyst, reported in literature to reduce byproduct formation and generally clean up the reaction.[2]

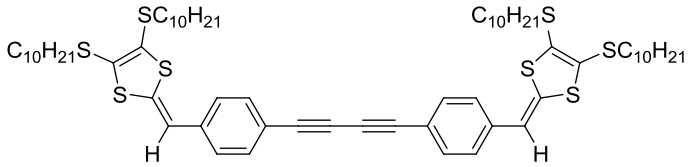


**53**

Figure 4.2 Dialkyne-linked π-exTTFV, compound **53**.

This product was found to be stable under controlled conditions (low temperature, protected from light and air), and preliminary electrochemical investigations show intriguing behaviour. The compound has been sent on to collaborators at Saint Mary's University in Nova Scotia for further study, including more electrochemical analyses and single-molecule layer behaviour. It is anticipated that this compound could serve as a molecular building block for electroactive polymers, with applications in chemical sensors, electrochemical devices, and intelligent materials (e.g. stimuli-responsive materials), to name a few.

## 4.1 References

1. Chen, G.; Mahmud, I.; Dawe, L. N.; Daniels, L. M.; Zhao, Y., *J. Org. Chem.* **2011,** *76,* 2701-2715.

2. Fairlamb, I. J. S.; Bauerlein, P. S.; Masrrison, L. R.; Dickinson, J. M., *Chem. Commun.* **2003**, 632-633.

# Appendix A

**Selected $^{1}H$ and $^{13}C$ NMR Spectra**

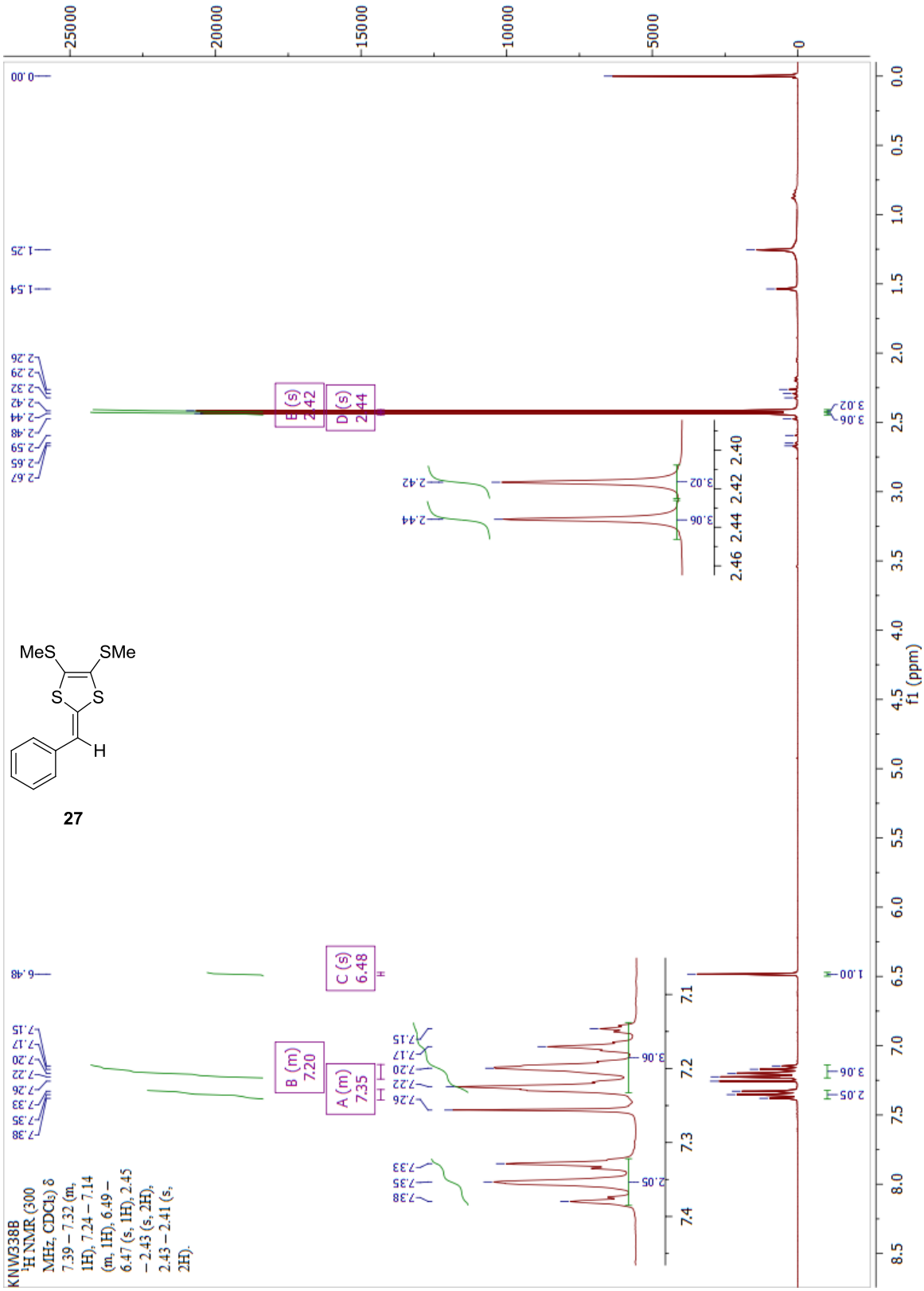
KNW338B
$^1$H NMR (300 MHz, CDCl$_3$) δ 7.39 – 7.32 (m, 1H), 7.24 – 7.14 (m, 1H), 6.49 – 6.47 (s, 1H), 2.45 – 2.43 (s, 2H), 2.43 – 2.41 (s, 2H).
A (m) 7.35
B (m) 7.20
C (s) 6.48
D (s) 2.44
E (s) 2.42
MeS
SMe
S
S
H
27
f1 (ppm)

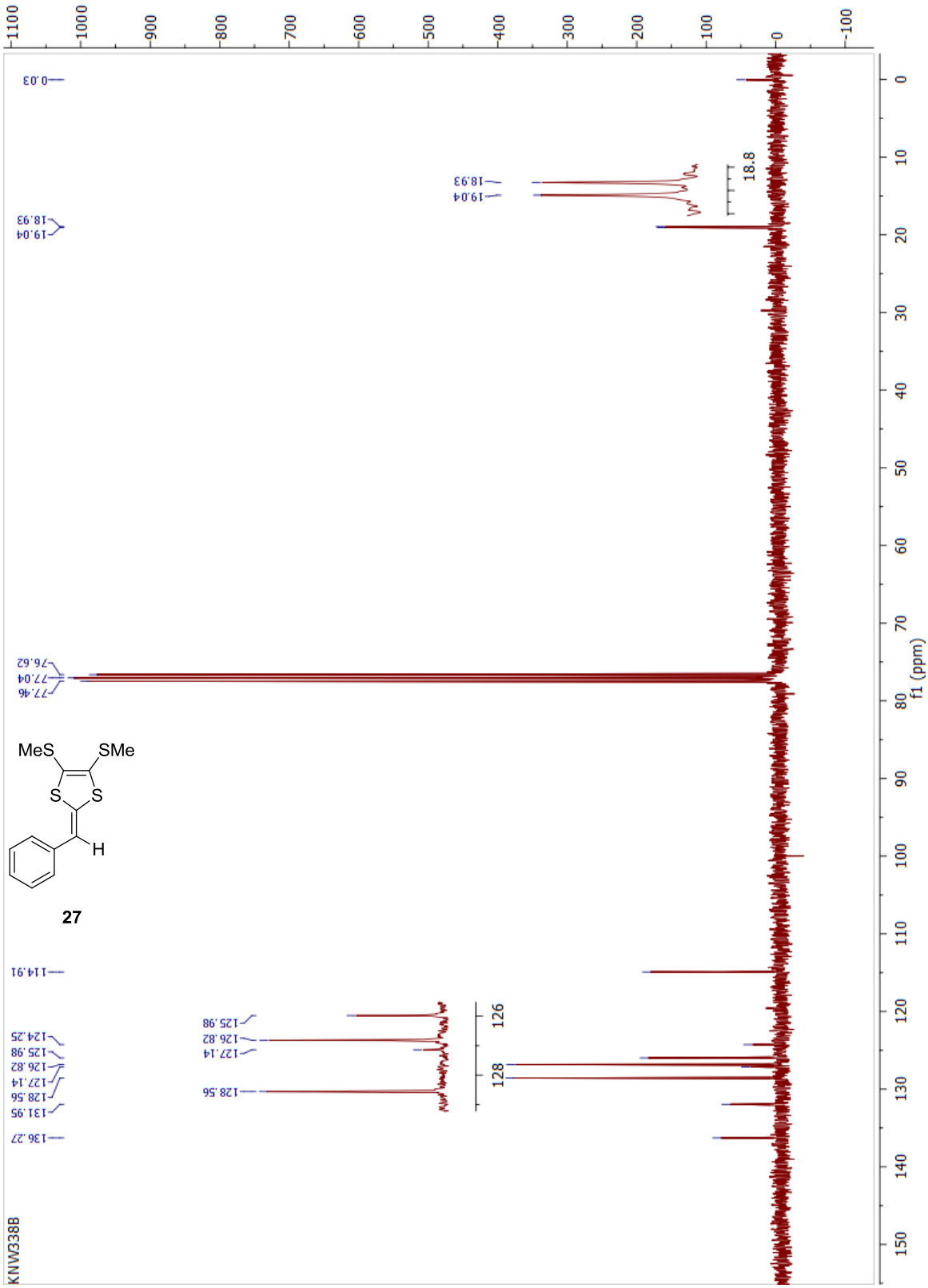
MeS
SMe
S
S
H
27
KNW338B
f1 (ppm)
18.8
126
128

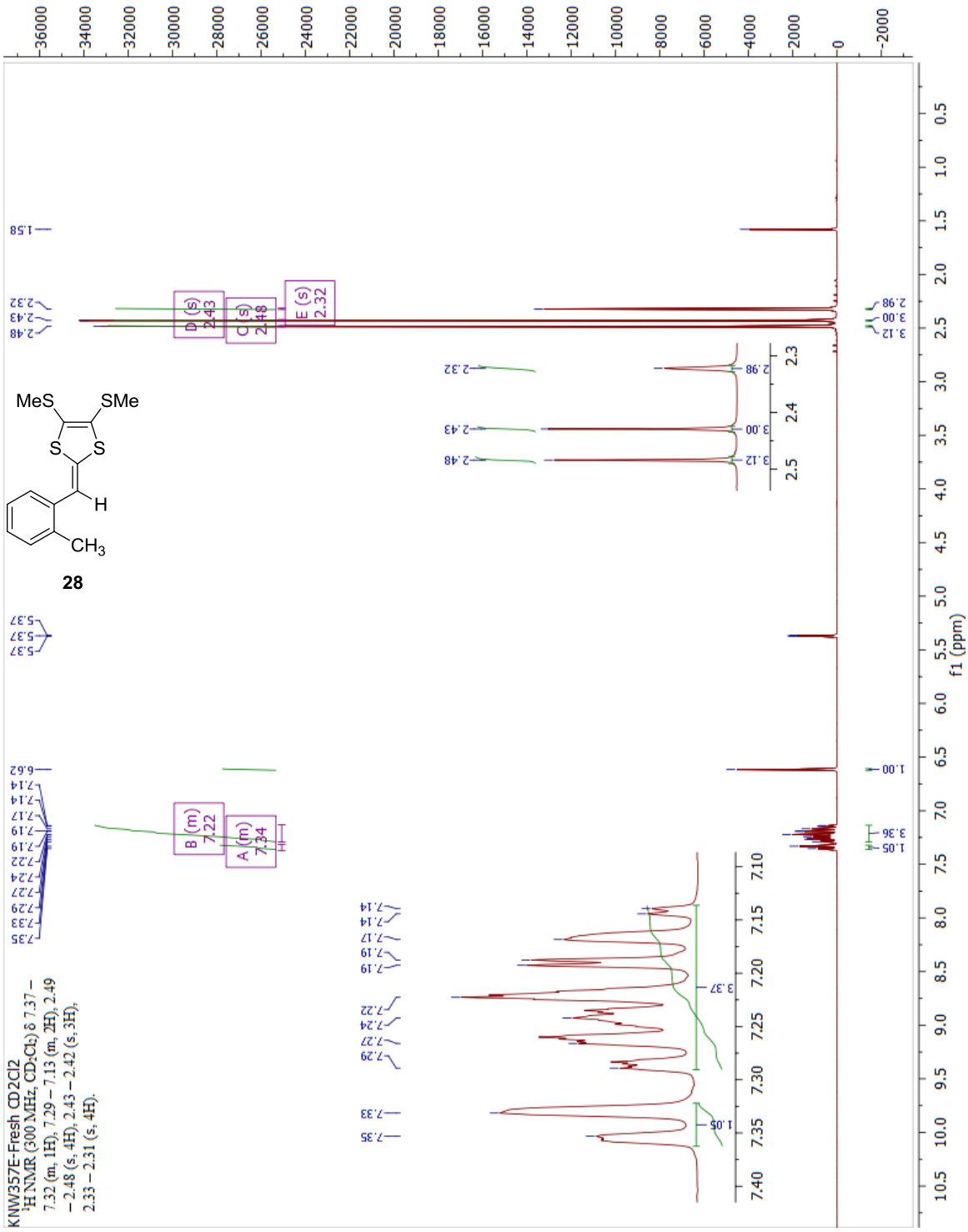
MeS
SMe
S
S
H
CH3
28
KNW357E-Fresh CD2Cl2
1H NMR (300 MHz, CD2Cl2) δ 7.37 – 7.32 (m, 1H), 7.29 – 7.13 (m, 2H), 2.49 – 2.48 (s, 4H), 2.43 – 2.42 (s, 3H), 2.33 – 2.31 (s, 4H).
A (m) 7.34
B (m) 7.22
C (s) 2.48
D (s) 2.43
E (s) 2.32
f1 (ppm)

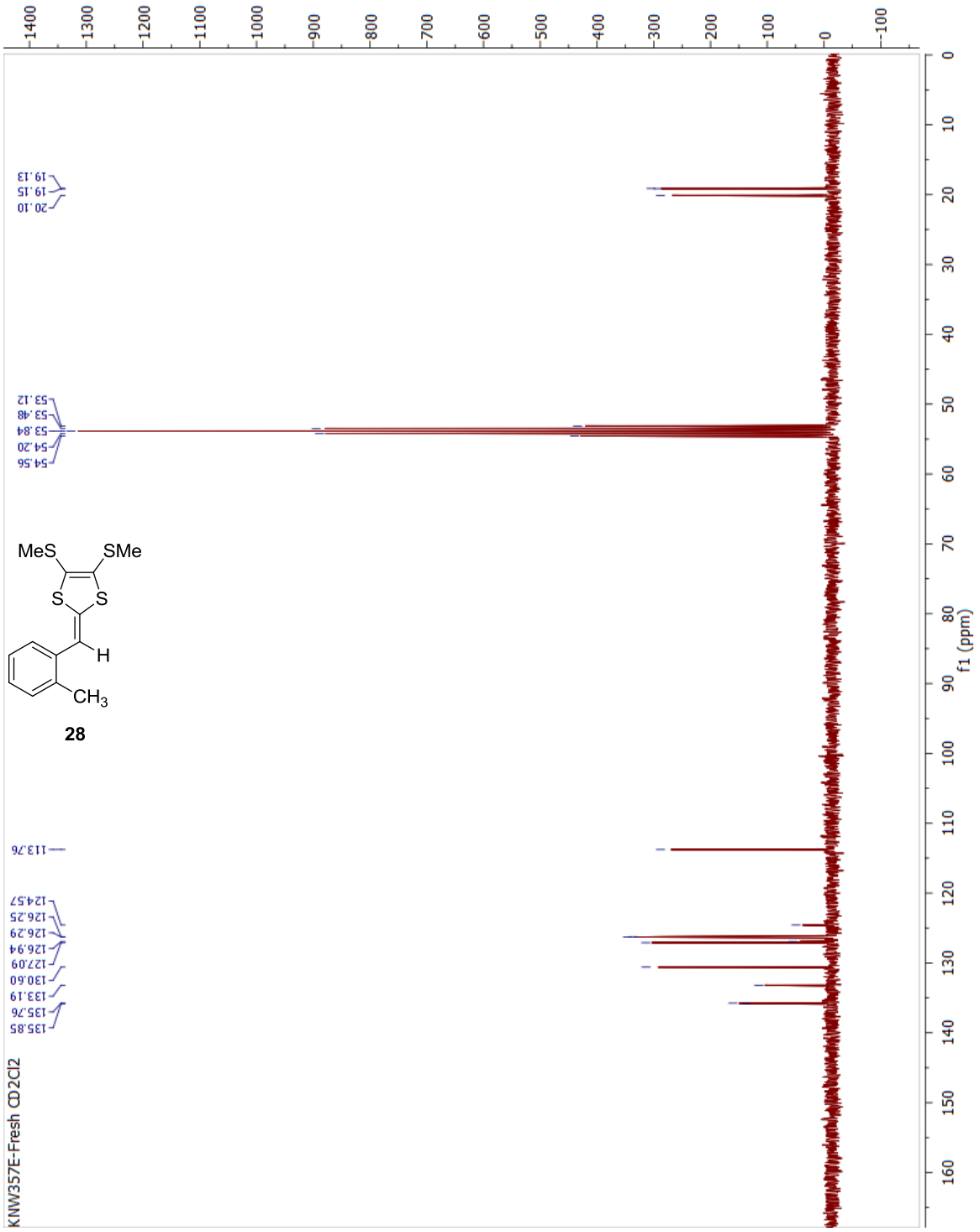
MeS
SMe
S
S
H
CH3
28
KNW357E-Fresh CD2Cl2
f1 (ppm)

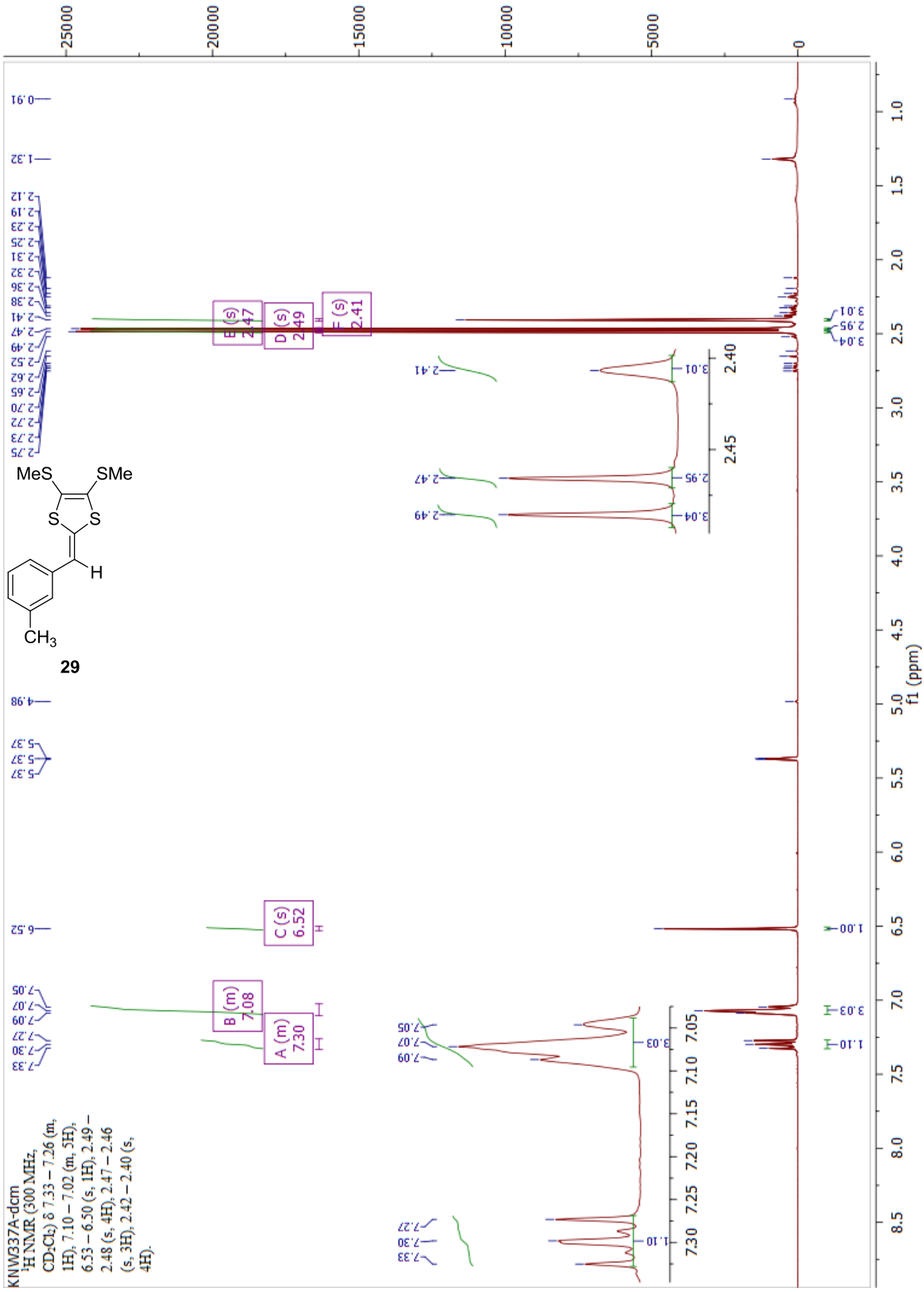
KNW337A-dcm
$^1$H NMR (300 MHz, $CD_2Cl_2$) δ 7.33 – 7.26 (m, 1H), 7.10 – 7.02 (m, 5H), 6.53 – 6.50 (s, 1H), 2.49 – 2.48 (s, 4H), 2.47 – 2.46 (s, 3H), 2.42 – 2.40 (s, 4H).
MeS
SMe
S
S
H
$CH_3$
29
A (m) 7.30
B (m) 7.08
C (s) 6.52
D (s) 2.49
E (s) 2.47
F (s) 2.41
f1 (ppm)

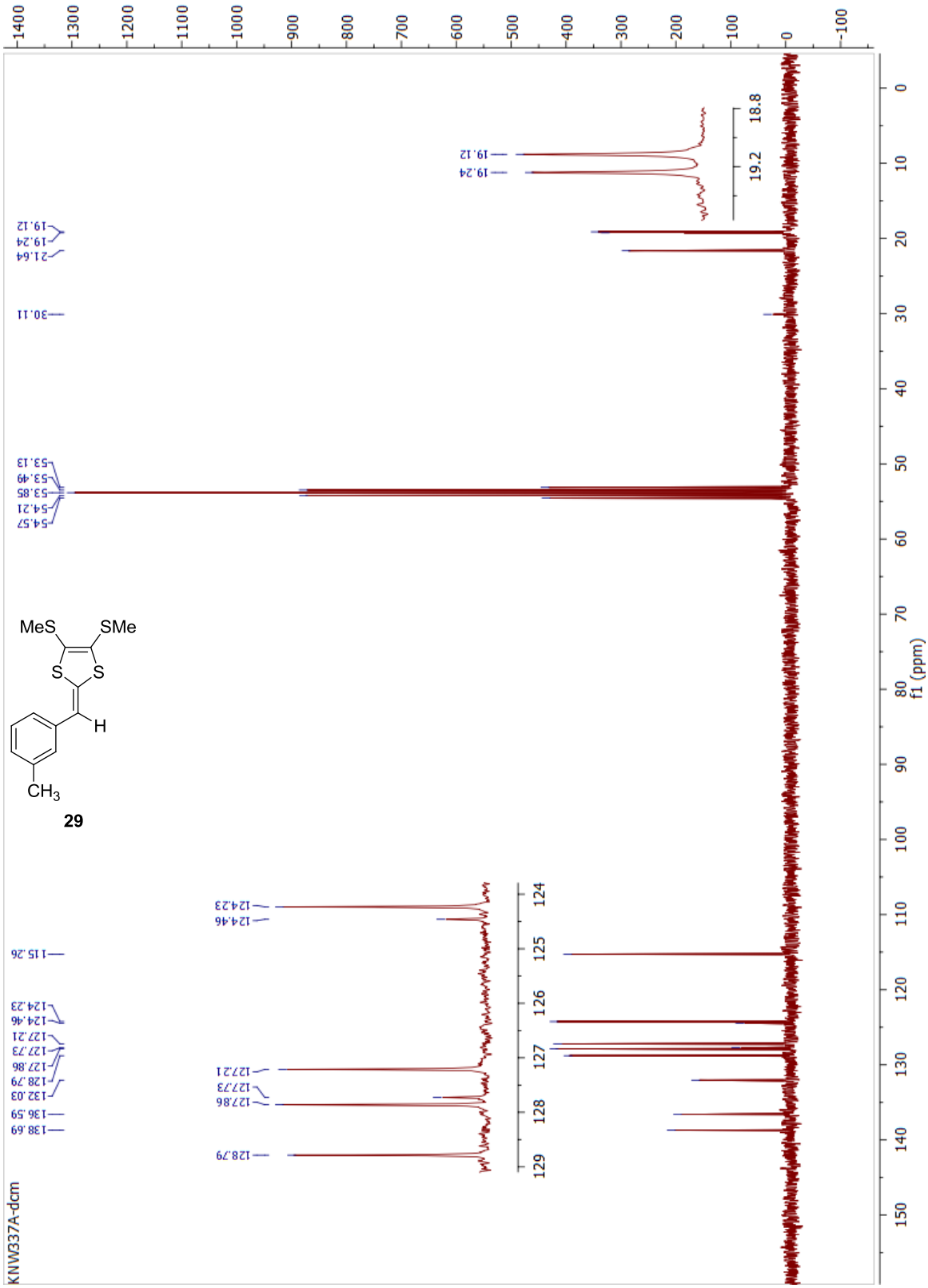
MeS
SMe
S
S
H
CH3
29
KNW337A-dcm
f1 (ppm)
19.12
19.24
21.64
30.11
53.13
53.49
53.85
54.21
54.57
115.26
124.23
124.46
127.21
127.73
127.86
128.79
132.03
136.59
138.69
18.8
19.2

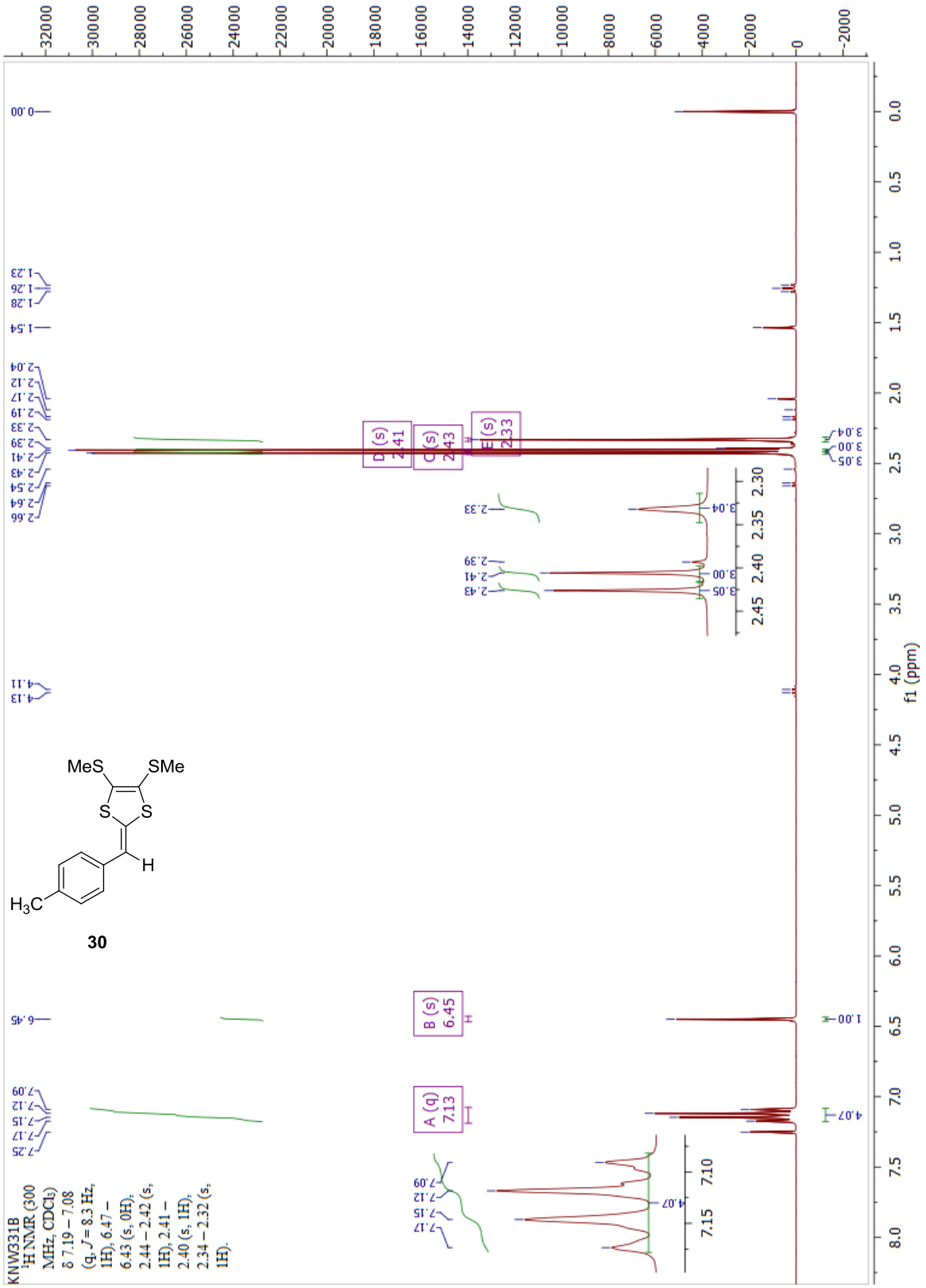
KNW331B
$^1$H NMR (300 MHz, CDCl$_3$)
δ 7.19 – 7.08 (q, J = 8.3 Hz, 1H), 6.47 – 6.43 (s, 0H), 2.44 – 2.42 (s, 1H), 2.41 – 2.40 (s, 1H), 2.34 – 2.32 (s, 1H).
A (q) 7.13
B (s) 6.45
D (s) 2.41
C (s) 2.43
E (s) 2.33
MeS
SMe
S
S
H
H$_3$C
30
f1 (ppm)

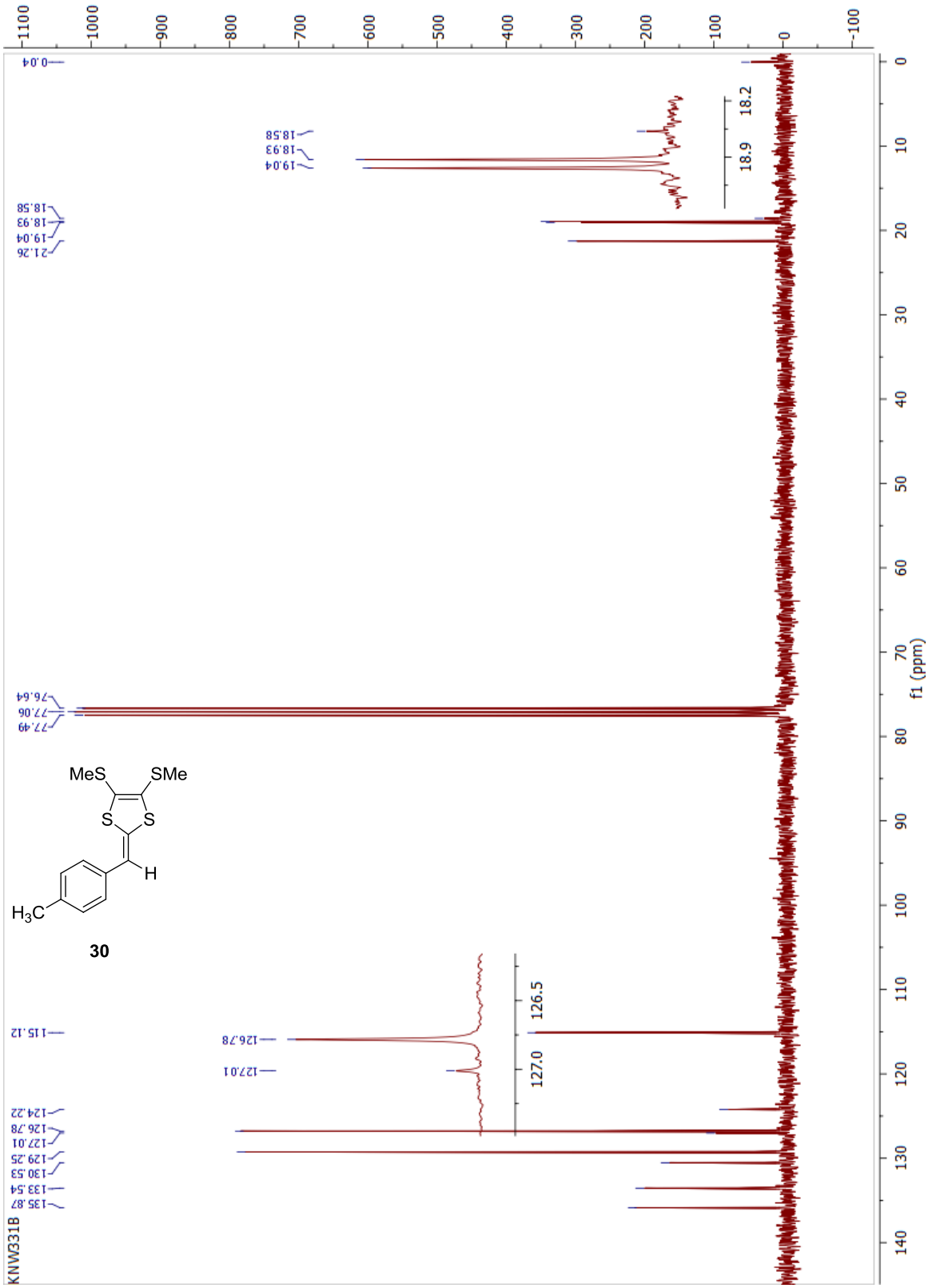
MeS
SMe
S
S
H
H3C
30
KNW331B
f1 (ppm)
18.2
18.9
126.5
127.0

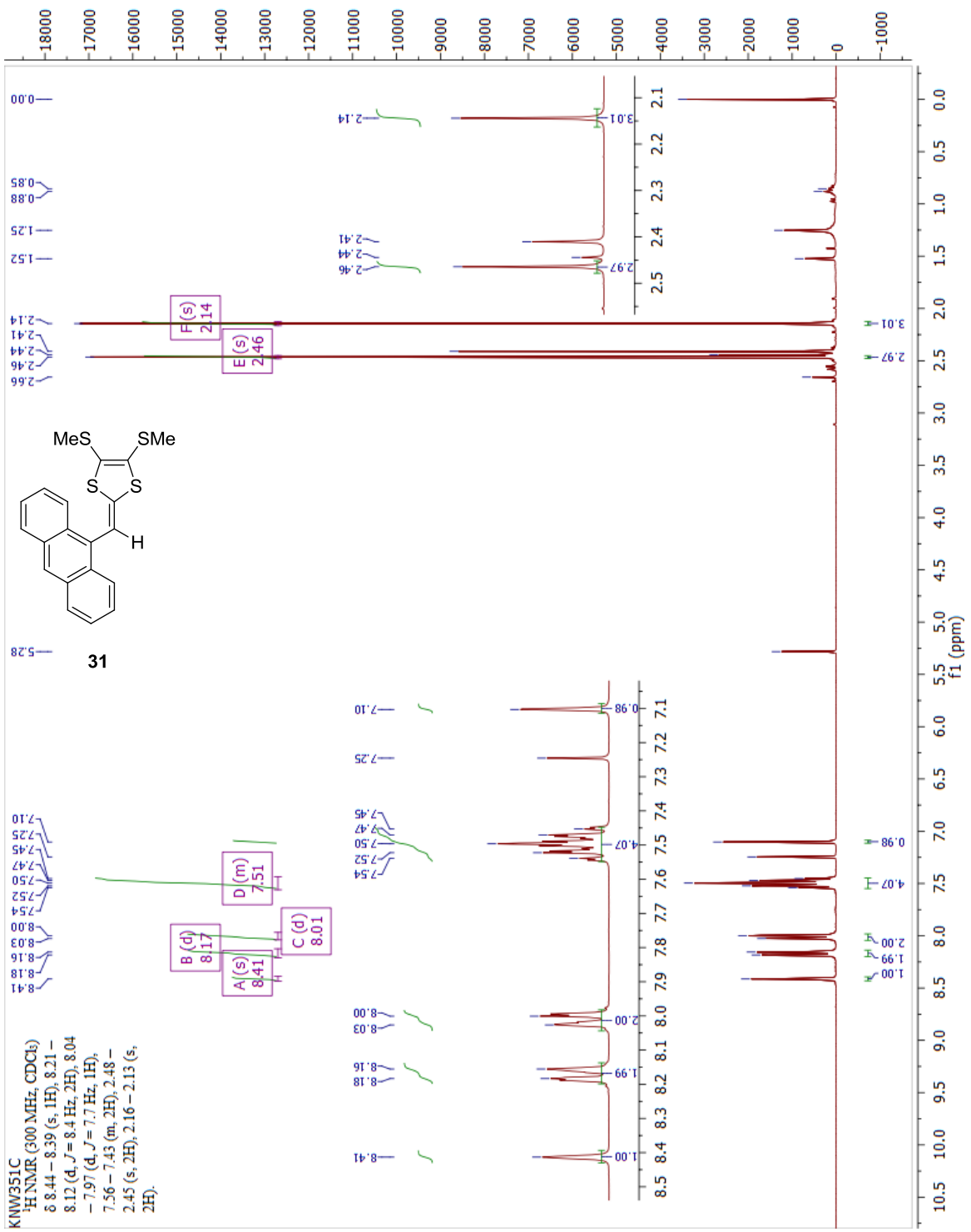
KNW351C
$^1$H NMR (300 MHz, CDCl$_3$)
δ 8.44 – 8.39 (s, 1H), 8.21 – 8.12 (d, J = 8.4 Hz, 2H), 8.04 – 7.97 (d, J = 7.7 Hz, 1H), 7.56 – 7.43 (m, 2H), 2.48 – 2.45 (s, 2H), 2.16 – 2.13 (s, 2H).
MeS
SMe
S
S
H
31
A (s) 8.41
B (d) 8.17
C (d) 8.01
D (m) 7.51
E (s) 2.46
F (s) 2.14
f1 (ppm)

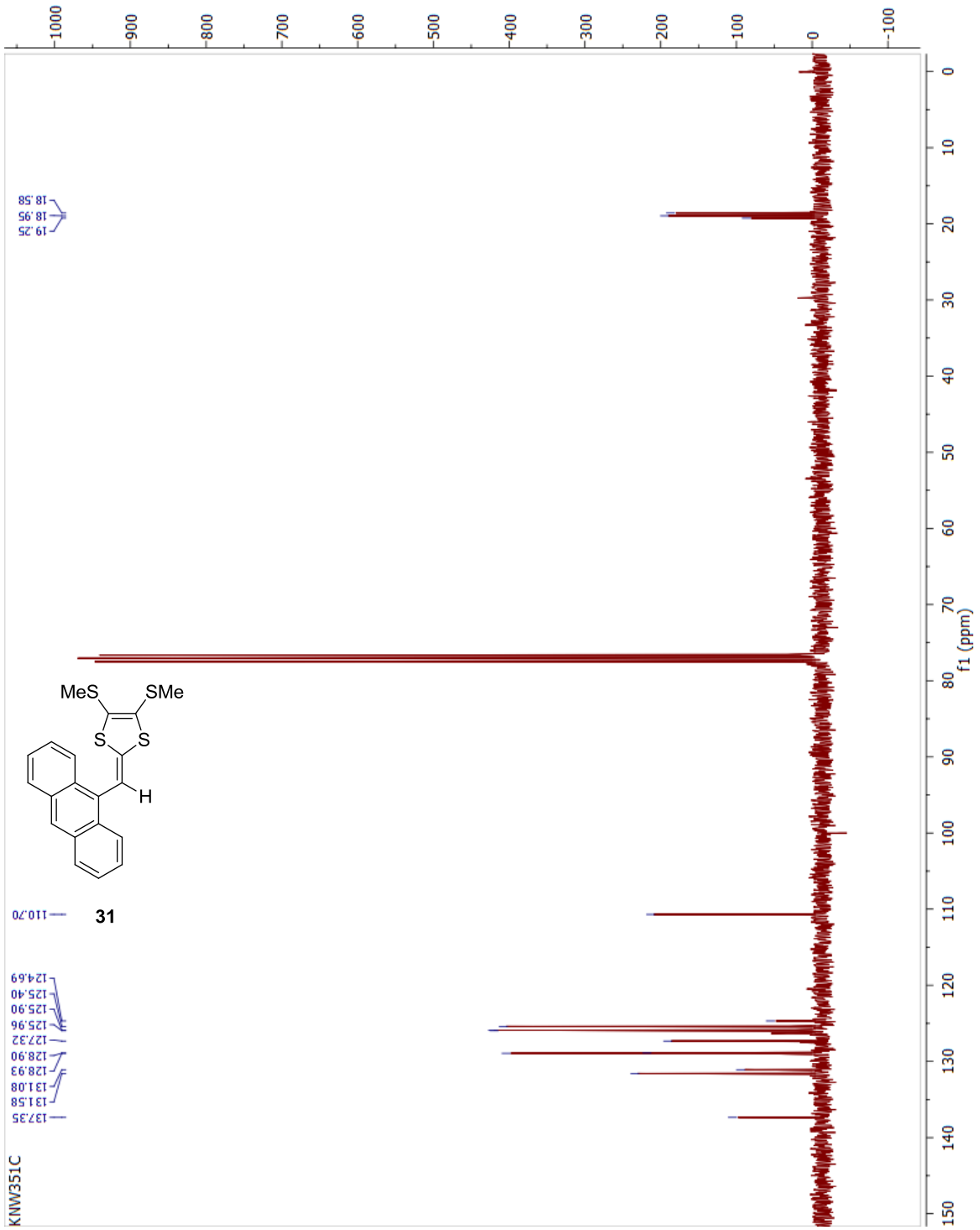
MeS
SMe
S
S
H
31
f1 (ppm)
KNW351C

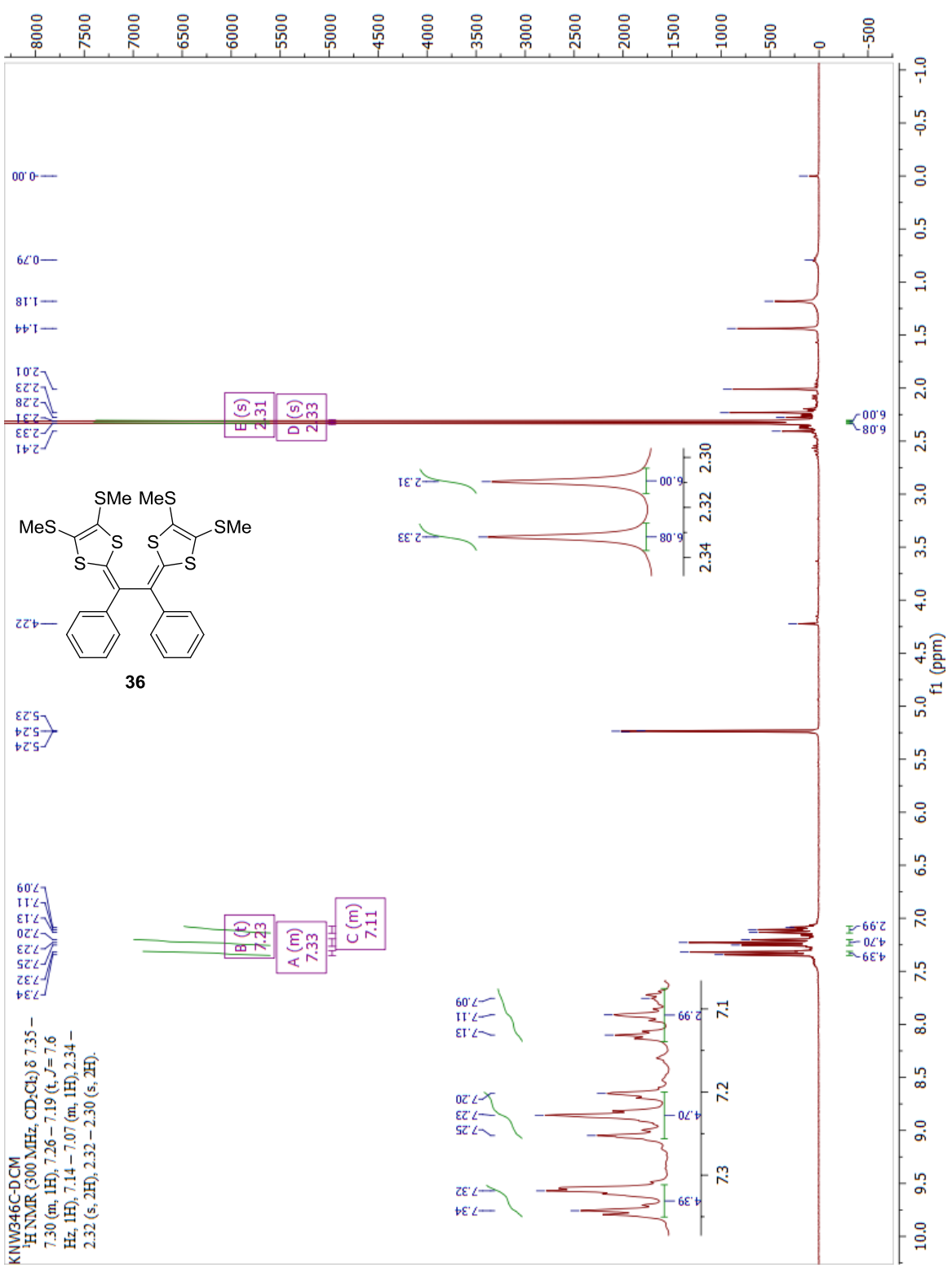
KNW346C-DCM
$^1$H NMR (300 MHz, $CD_2Cl_2$) δ 7.35 – 7.30 (m, 1H), 7.26 – 7.19 (t, J= 7.6 Hz, 1H), 7.14 – 7.07 (m, 1H), 2.34 – 2.32 (s, 2H), 2.32 – 2.30 (s, 2H).
SMe MeS
MeS
S
S
S
S
SMe
36
E (s) 2.31
D (s) 2.33
B (t) 7.23
A (m) 7.33
C (m) 7.11
f1 (ppm)

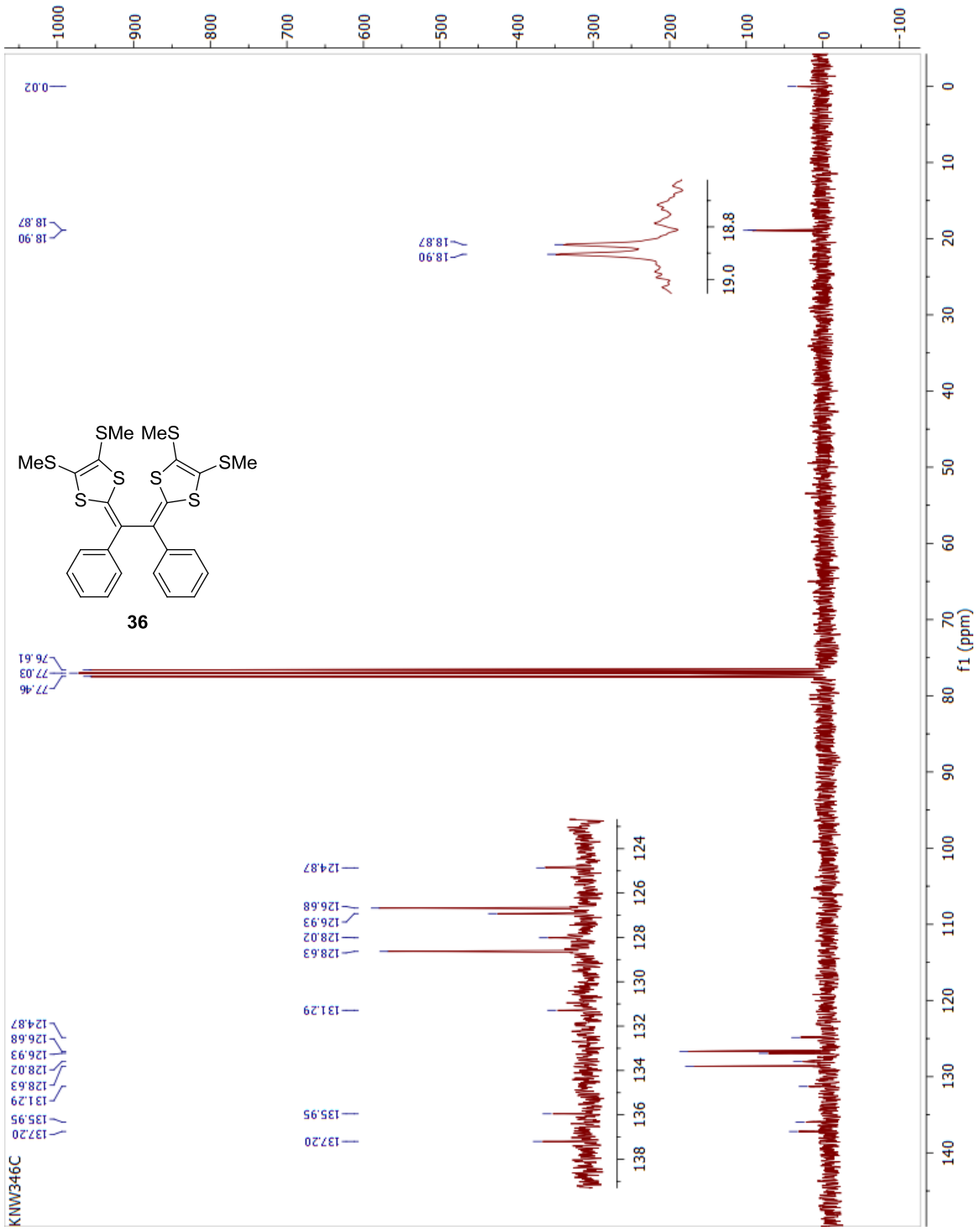
SMe MeS
MeS
S
S
S
S
SMe
36
KNW346C
f1 (ppm)

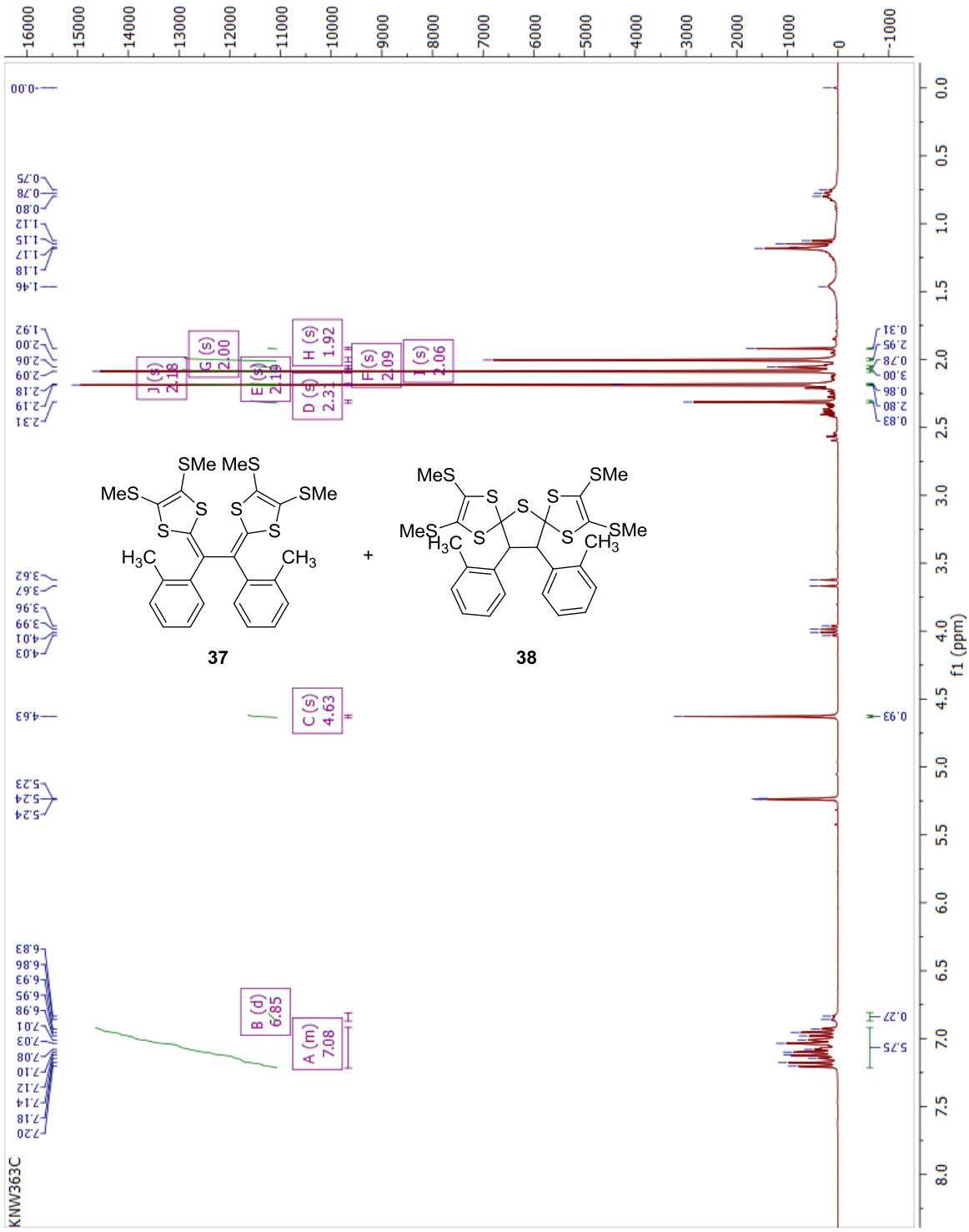
SMe MeS
MeS
SMe
H3C
CH3
37
+
MeS
SMe
MeS
H3C
CH3
38
J (s) 2.18
G (s) 2.00
E (s) 2.19
H (s) 1.92
D (s) 2.31
F (s) 2.09
I (s) 2.06
C (s) 4.63
B (d) 6.85
A (m) 7.08
KNW363C
f1 (ppm)

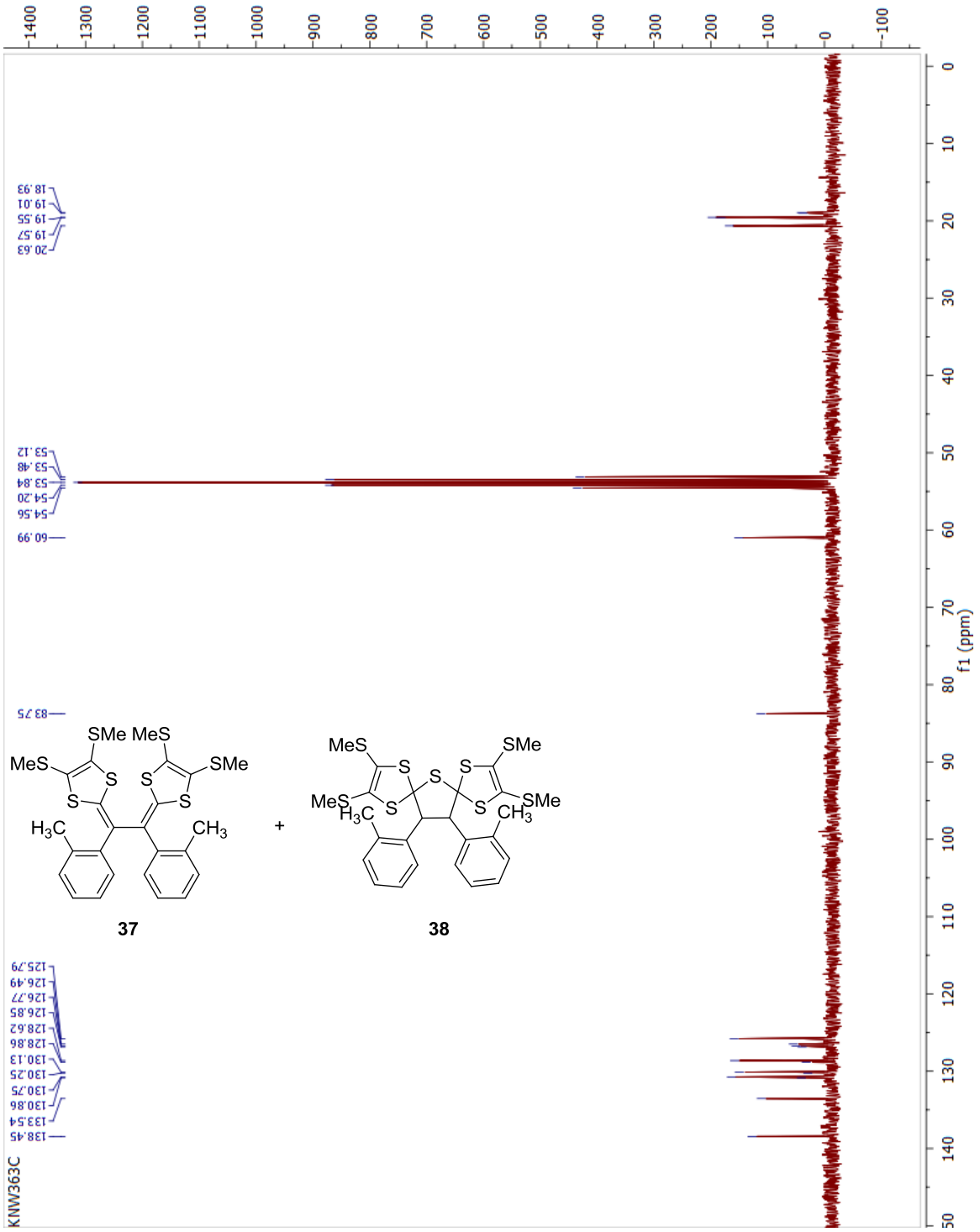
f1 (ppm)
KNW363C
SMe MeS
MeS
SMe
S
H3C
CH3
+
MeS
SMe
H3C
CH3
37
38

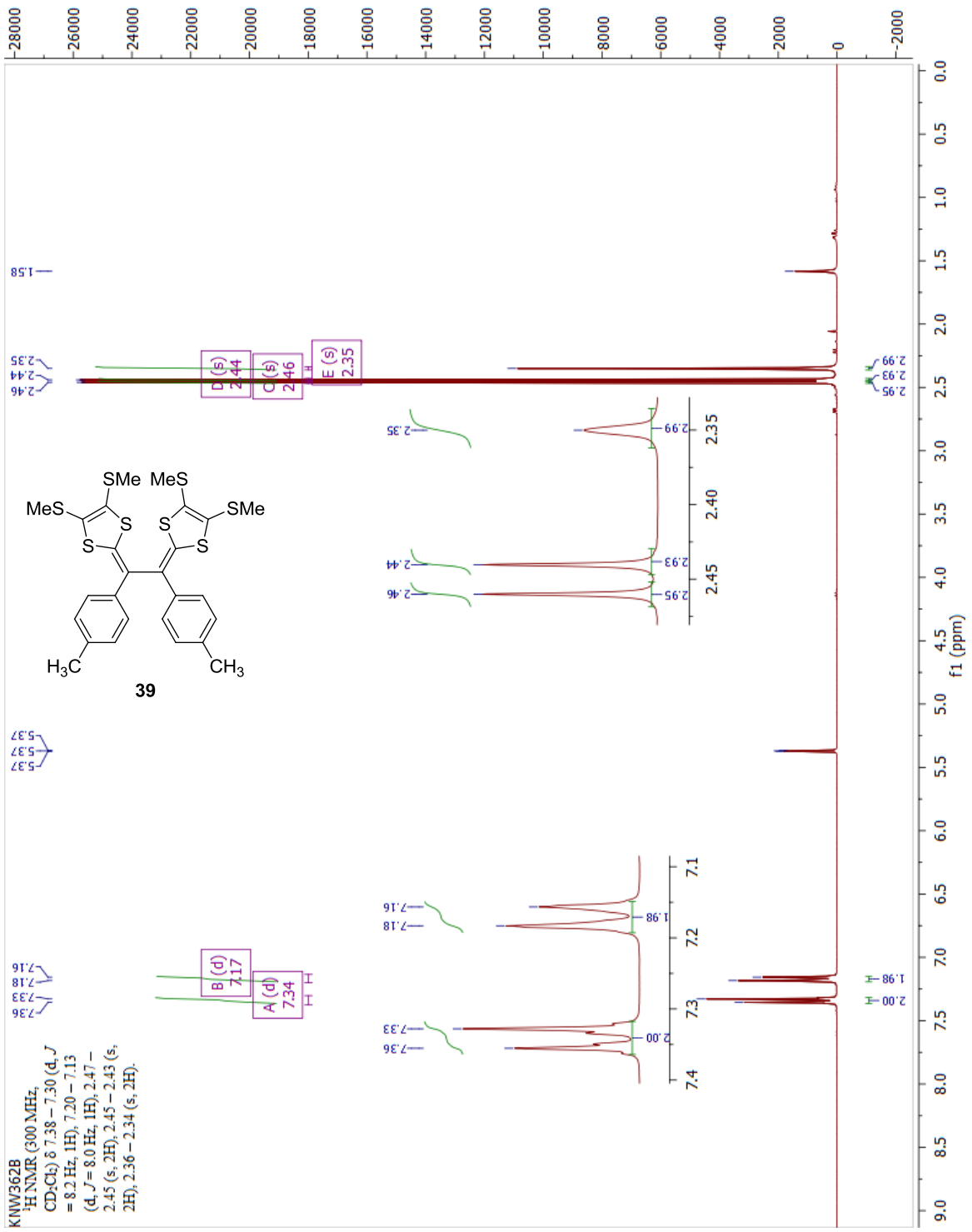
KNW362B
$^1$H NMR (300 MHz, $CD_2Cl_2$) δ 7.38 – 7.30 (d, J = 8.2 Hz, 1H), 7.20 – 7.13 (d, J = 8.0 Hz, 1H), 2.47 – 2.45 (s, 2H), 2.45 – 2.43 (s, 2H), 2.36 – 2.34 (s, 2H).
SMe MeS
MeS
S
S
S
S
SMe
$H_3C$
$CH_3$
39
A (d) 7.34
B (d) 7.17
C (s) 2.46
D (s) 2.44
E (s) 2.35
f1 (ppm)

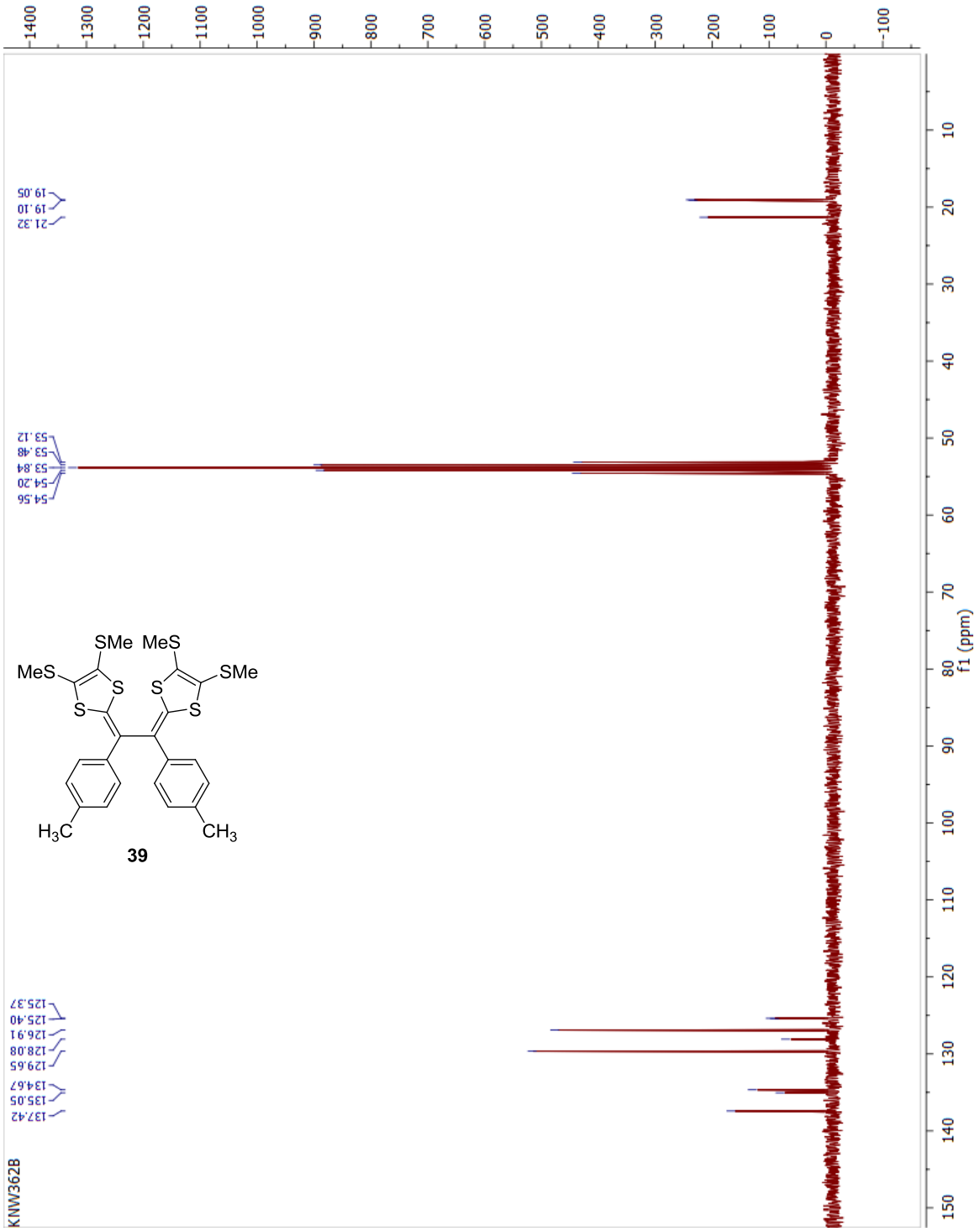
SMe MeS
MeS
SMe
S
S
S
S
H3C
CH3
39
KNW362B
f1 (ppm)

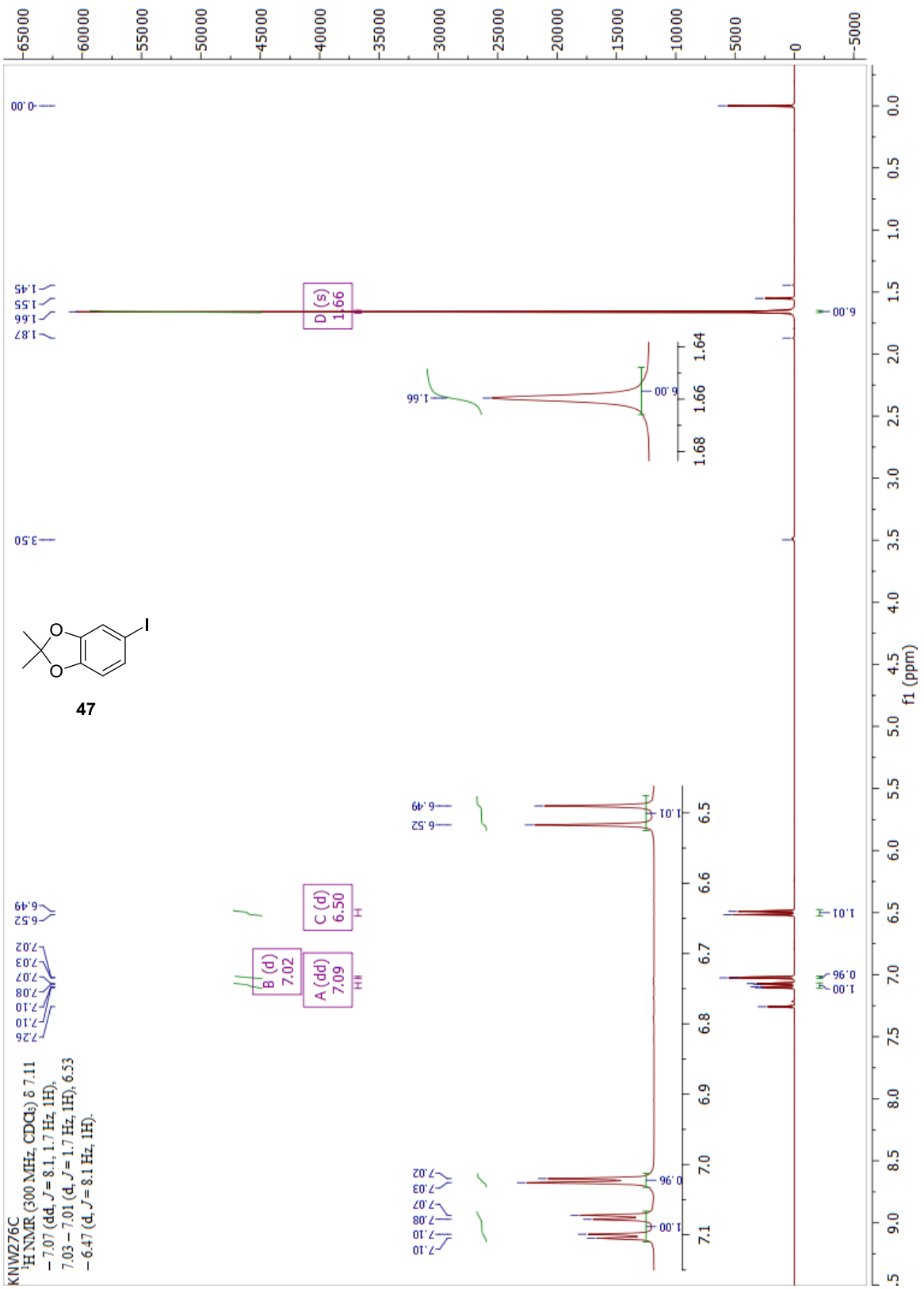
KNW276C
$^1$H NMR (300 MHz, CDCl$_3$) δ 7.11 – 7.07 (dd, J = 8.1, 1.7 Hz, 1H), 7.03 – 7.01 (d, J = 1.7 Hz, 1H), 6.53 – 6.47 (d, J = 8.1 Hz, 1H).
A (dd) 7.09
B (d) 7.02
C (d) 6.50
D (s) 1.66
47
f1 (ppm)

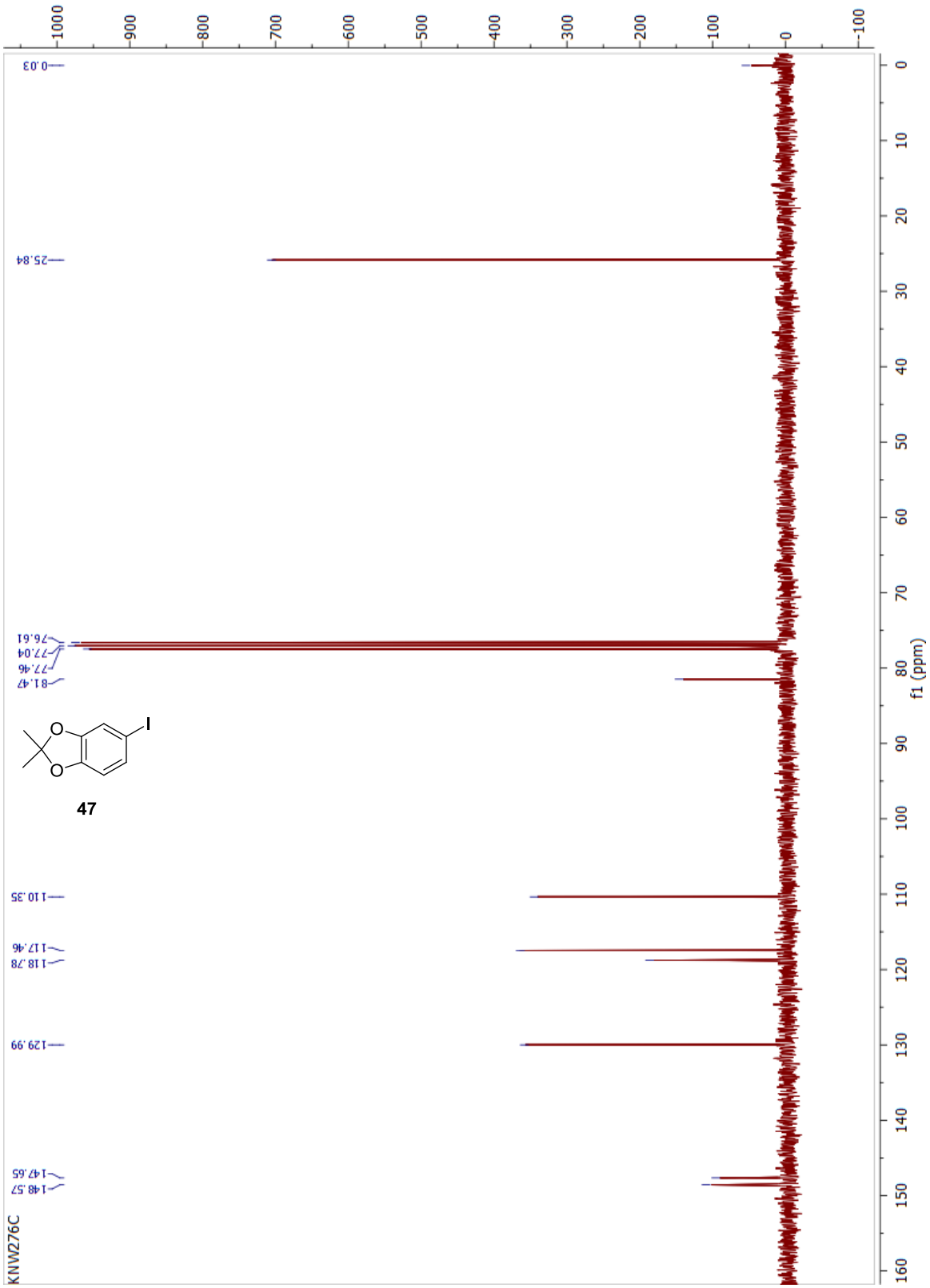
0.03
25.84
76.61
77.04
77.46
81.47
110.35
117.46
118.78
129.99
147.65
148.57
KNW276C
f1 (ppm)
O
O
I

**47**

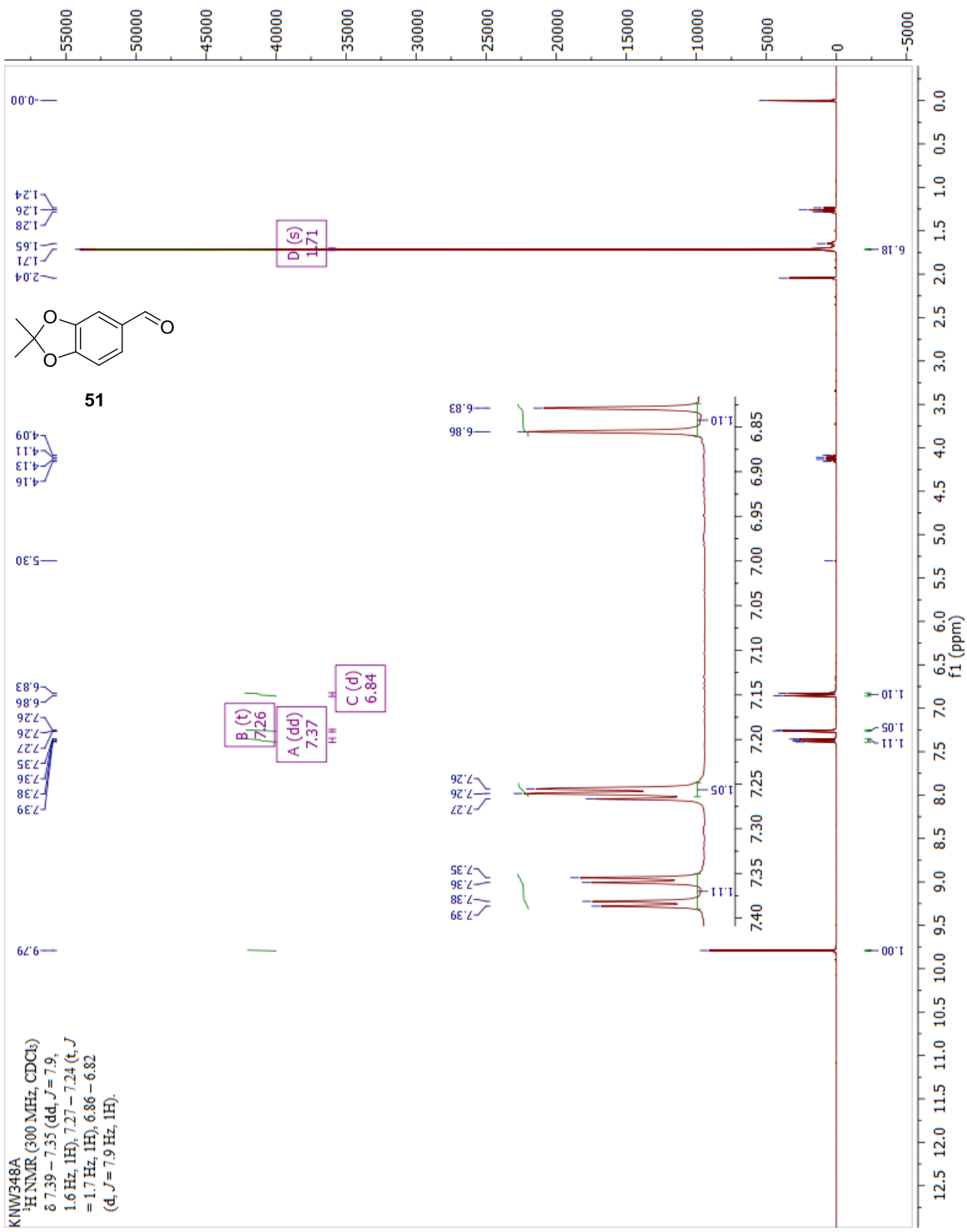
KNW348A
$^1$H NMR (300 MHz, CDCl$_3$)
δ 7.39 – 7.35 (dd, J = 7.9,
1.6 Hz, 1H), 7.27 – 7.24 (t, J
= 1.7 Hz, 1H), 6.86 – 6.82
(d, J = 7.9 Hz, 1H).
D (s)
1.71
B (t)
7.26
A (dd)
7.37
C (d)
6.84
51
f1 (ppm)

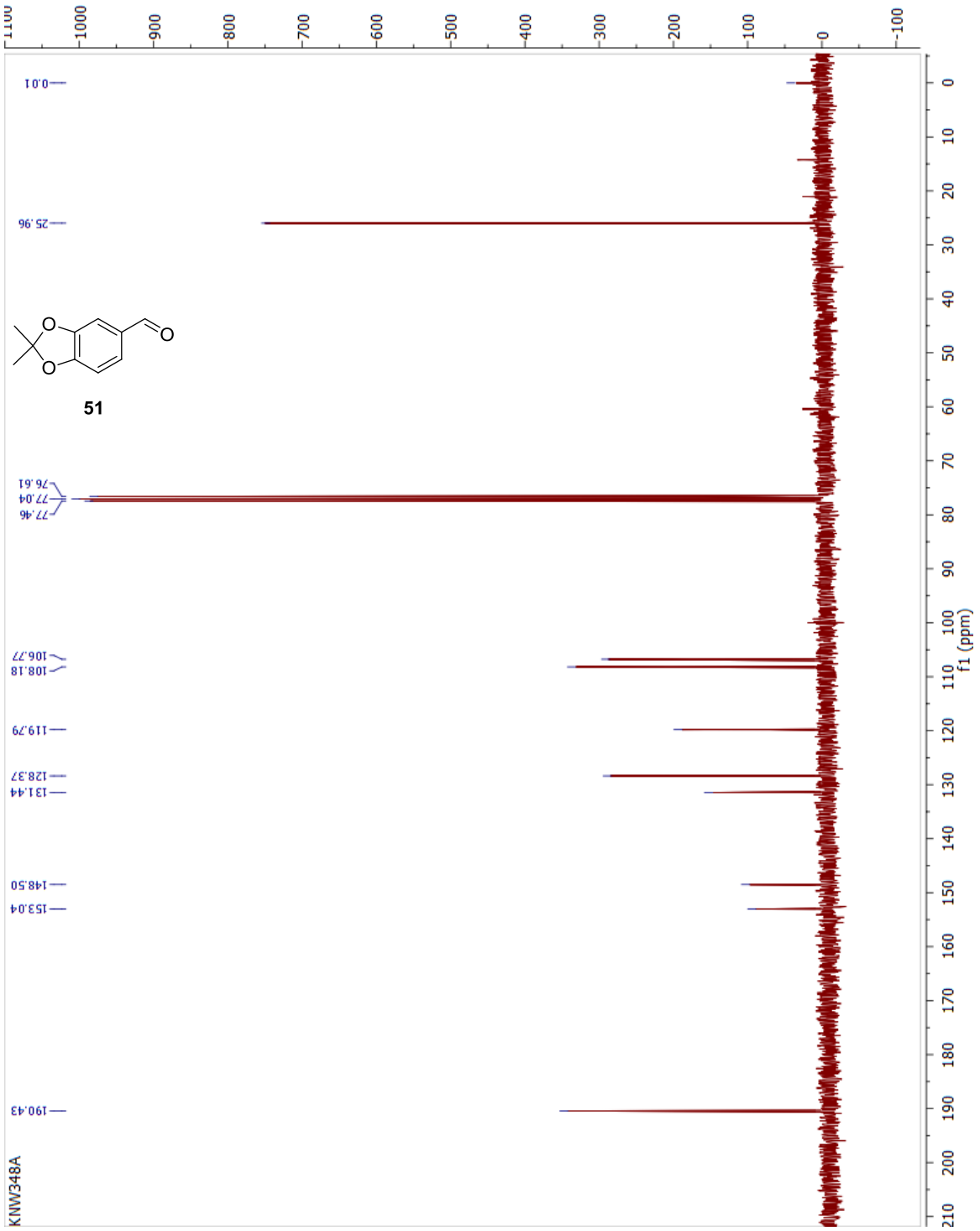
0.01
25.96
77.46
77.04
76.61
106.77
108.18
119.79
128.37
131.44
148.50
153.04
190.43
KNW348A
f1 (ppm)
51